ISSN 0971 - 6203

Journal of Medical Physics

Volume 43 | Issue 1 | January - March 2018

Full text at www.jmp.org.in

PubMed

Association of
Medical Physicists of India
An Affiliate of Indian National Science Academy
and
International Organization for Medical Physics
www.ampi.org.in

Medknow

Wolters Kluwer

Versa HD.

Powered by high definition dynamic radiosurgery.

Versa HD™ with Monaco® gives you the clinical flexibility of high definition dynamic radiosurgery (HDRS) and conventional RT in a single platform. HDRS means you can deliver stereotactic treatments within standard RT time slots, regardless of anatomy or complexity. And, with advanced image guidance tools and up to 5x less transmission to non-targeted regions, you have assurance of end-to-end precision.

Discover how Versa HD can help you meet operational efficiencies while achieving better outcomes for patients.

elekta.com/VersaHD

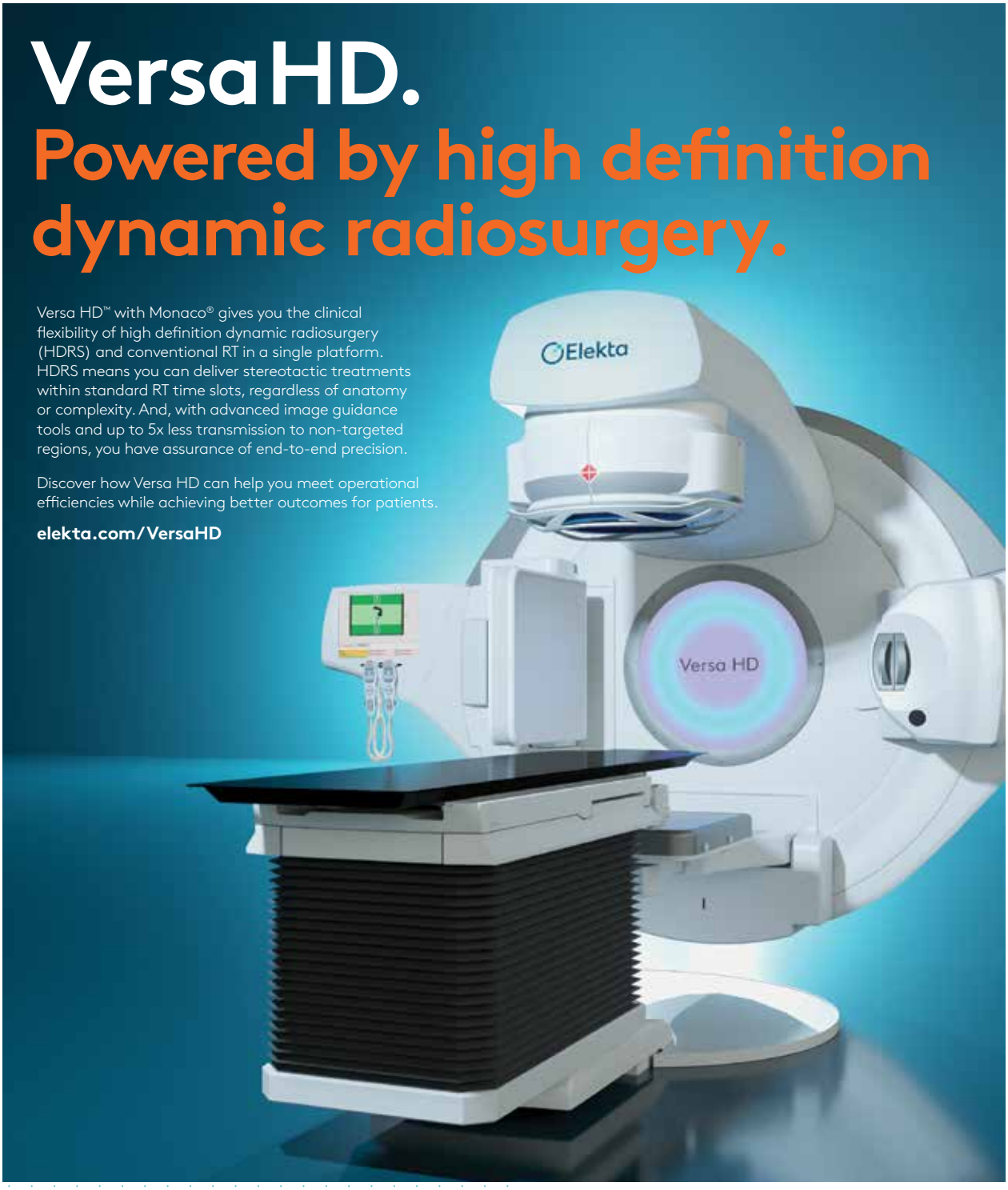

Elekta

Focus where it matters.

Nueclear
NATIONWIDE NETWORKED

PET-CT Scans, Now Made Simple & Affordable

Are you a Diagnostic Centre?

- Do you dream of PET-CT ?
- Does the high cost of PET-CT machine worry you ?
- Does the high cost of FDG deter you ?

We have a franchise model for PET-CT solutions

Powered By

Thyrocare®

Think Thyroid. Think Thyrocare.

PREFERRED CITIES - All air connected cities in India and GCC

For Franchisee Enquiries

Give a missed call on: 9702 566 333 | **WhatsApp/Mobile No.:** 922 319 4040
Landline No.: 022 - 4128 9999 / 4128 2888 | www.nueclear.com | petct@nueclear.com

Film is a ~~hassle~~. *snap*

GafChromic introduces FilmQA-PRO Verification Software for IMRT QA.

You know that film gives you a more complete picture than electronic arrays. What's more, emerging techniques like SRS and RapidArc™ are better suited to film because film lets you shoot from any angle. But film may feel hard to work with and time-consuming. All that changes. Now FilmQAPro™ 3.0 is taking full advantage of what we've built into GafChromic™ film. One-scan analysis lets you do calibration and plan verification simultaneously. So you eliminate variables, and post-exposure growth no longer gets between you and your results. You get answers in minutes. And multi-channel dosimetry ensures the integrity of your measurement. Finally, software that makes film easy. With help from FilmQAPro 3.0, the future is film.

GAFCHROMIC® Films for Radiotherapy:

(1) Gafchromic® EBT3 and EBT3-1417 (2) Gafchromic® RTQA2-1010 (3) Gafchromic® RTQA2-111

Let's take care.

Exclusively distributed in India by:

LATESTECH INTERNATIONAL

GafChromic

17-G/319, Vasundhara, Ghaziabad-201012, INDIA
Telephone: 0120-2881252 Fax: 91-120-2881179
Mob: 09873278842 Email: latestech@rediffmail.com

ROSALINA INSTRUMENTS

FARMER TYPE CHAMBER FAR 65-GB

Preliminary Data Sheet

APPLICATIONS

- Absolute dosimetry in radiation therapy
- Photons and High Energy Electrons.
- Traditional chamber construction for absolute dosimetry in x-rays
- Standard reference detector for reference dosimetry and scientific applications

FEATURES

- Air ionisation chamber
- Chamber with graphite wall, for all applicable radiation conditions
- Non waterproof
- Vented through waterproof sleeve
- Guarded upto 15 mm from base
- Supplied with individual factory calibration certificate and user's guide (Provisional)

MATERIAL

- Outer electrode Graphite **(1.82 g/cm^3)**
- Inner electrode Aluminium **(2.70 g/cm^3)**
- Build-up cap for ^{60}Co Delrin **(1.42 g/cm^3)**

ACTIVE DIMENSIONS

- Volume (nominal) **0.65 cm^3**
- Total active length **23.1 mm**
- Inner diameter of cylinder **6.2 mm**
- Wall thickness 0.4 mm
- Diameter of inner electrode **1.0 mm**
- Wall thickness of build-up cap for ^{60}Co **3.9 mm**

CABLE AND CONNECTOR

- Connector type **TNC triaxial**
- Cable length **1.40 m**

OPERATIONAL DATA

- Leakage current **<± 10 x 10^{-15} A**
- Sensitivity **21 x 10^{-9} C/Gy**
- Radiation quality (e^-) **1.3 Mev - 50 MV**
- Polarising voltage **+ 300 V**
- Reference point w/o build-up cap **13 mm from the distal end of the chamber**
- Reference point with build-up cap **17 mm from the distal for ^{60}Co end of the build-up cap**

127, Bussa Udyog Bhavan,
T.J Road, Sewri (W)
Mumbai - 400 015.
India

91 22 24166630
support@rosalina.in
www.rosalina.in

5 Year Warranty

MADE IN INDIA

DOSEVIEW™ 3D

PREMIUM QUALITY
AFFORDABLE PRICE

PRECISION REDEFINED

INTUITIVE SOFTWARE • WIRELESS INTERFACE

Wi Fi

STANDARD IMAGING®

ADVANCING RADIATION QA™

ROSALINA INSTRUMENTS

QA BEAMCHECKER™ PLUS

- **Wire-free operation**
- **Automatic energy detection**
- **Integrated build-up beyond dmax for all energies**
- **Unique "flip" feature**
- **Easy to use software**

The QUICK FLIP

Photon to electron with no additional build-up

The new ***QA BeamChecker Plus*** from Standard Imaging is a reliable and uncomplicated device for daily quality assurance testing of linear accelerator output.

With wire-free technology, integrated build-up and automatic determination of energy, technicians can quickly complete daily QA procedures, and physicists have access to powerful data, trending and analysis.

ROSALINA INSTRUMENTS

127, Bussa Udyog Bhavan, Tokershi Jivraj Road, Sewri, Mumbai - 400 015. INDIA
Tel : 91 22 24166630 / 24173493 Fax : 91 22 66627766
E-mail support@rosalina.in www.rosalina.in

ROSALINA INSTRUMENTS

RENTRANT WELL CHAMBER

BDS 1000 BRACYTHERAPY DOSIMETRY SYSTEM

BRACHYTHERAPY SOURCE CALIBRATION

The BDS 1000 Well Chamber is air vented chamber, Highly accurate for low dose rate and high dose rate brachytherapy. Source holders are available for most existing sources as well as custom made source holders.

Calibrations Available	^{60}Co ^{192}Ir and/or LDR radionuclides from various manufacturers as requested
Active Volume	240 cm^3
Connector	TNC triax (standard) Other Optional
Range	10 U to 80 MU 0.01 mCi to 20 Ci
Cable	5 ft, 1.5 m
Bias voltage	± 300 volts, typical
Leakage	Less than 25 fA
Stability	0.2% (Reproducibility over 2 years)
Response	± 0.5% over 25 mm at center of axis

5 Year Warranty

MADE IN INDIA

Preliminary Data Sheet

127, Bussa Udyog Bhavan T.J Road, Sewri (W) Mumbai - 400 015. INDIA
Tel : 91 22 241 66630, E-mail : support@rosalina.in www.rosalina.in

ROSALINA INSTRUMENTS

SURE DOSE Universal Radiation Dosimeter

We Make The Things That Make Indian Medical Physicist Proud

Cutting edge Indian technology, high calibre engineering expertise, decades of experience, devotion and total commitment to the nation.

Innovative Leadership in Radiation Oncology and Medical Physics

Farmer type ionisation chambers
Electro Meters
Specialized phantoms
IGRT Dosimetry
Absolute Dosimetry
Relative Dosimetry
VMAT Dosimetry
INVIVO Dosimetry

www.rosalina.in

STANDARD IMAGING®
ADVANCING RADIATION QA™

ROSALINA INSTRUMENTS

Exradin W1 Scintillator FFF - Small Field Dosimetry

The Exradin W1 Scintillator is a near-water equivalent detector that achieves paramount precision by significantly decreasing beam disturbance.

Minimize Beam Perturbation and Corrections

The unprecedented characteristics of the W1 Scintillator closely mimic water, easing data collection by negating many measurement corrections required with other detectors.

- Near water equivalence (within 5% of physical density)
- Linear dose response
- Dose rate independence
- Energy independence within the MV range
- Minimal temperature dependence

Ideal for Measurement and Characterization of Small Fields

1mm spatial resolution makes the W1 a perfect tool for stereotactic radiosurgery (SRS) and stereotactic body radiation therapy (SBRT) QA. This includes compatibility with the Lucy 3D QA Phantom and use in the following systems:

- Gamma Knife®
- CyberKnife®
- BrainLab®
- Varian®
- Elekta®
- TomoTherapy®

Automatically Correct for Cherenkov Effect

Pair the W1 Scintillator with the SuperMAX Electrometer to effectively eliminate Cherenkov effect without the need for extraneous hand calculations.

Consistent, Convenient Setup

Integration with the Exradin Scintillator Calibration Slab and solid water phantoms allows for easy, repeatable measurements.

PTW

Knowing what responsibility means

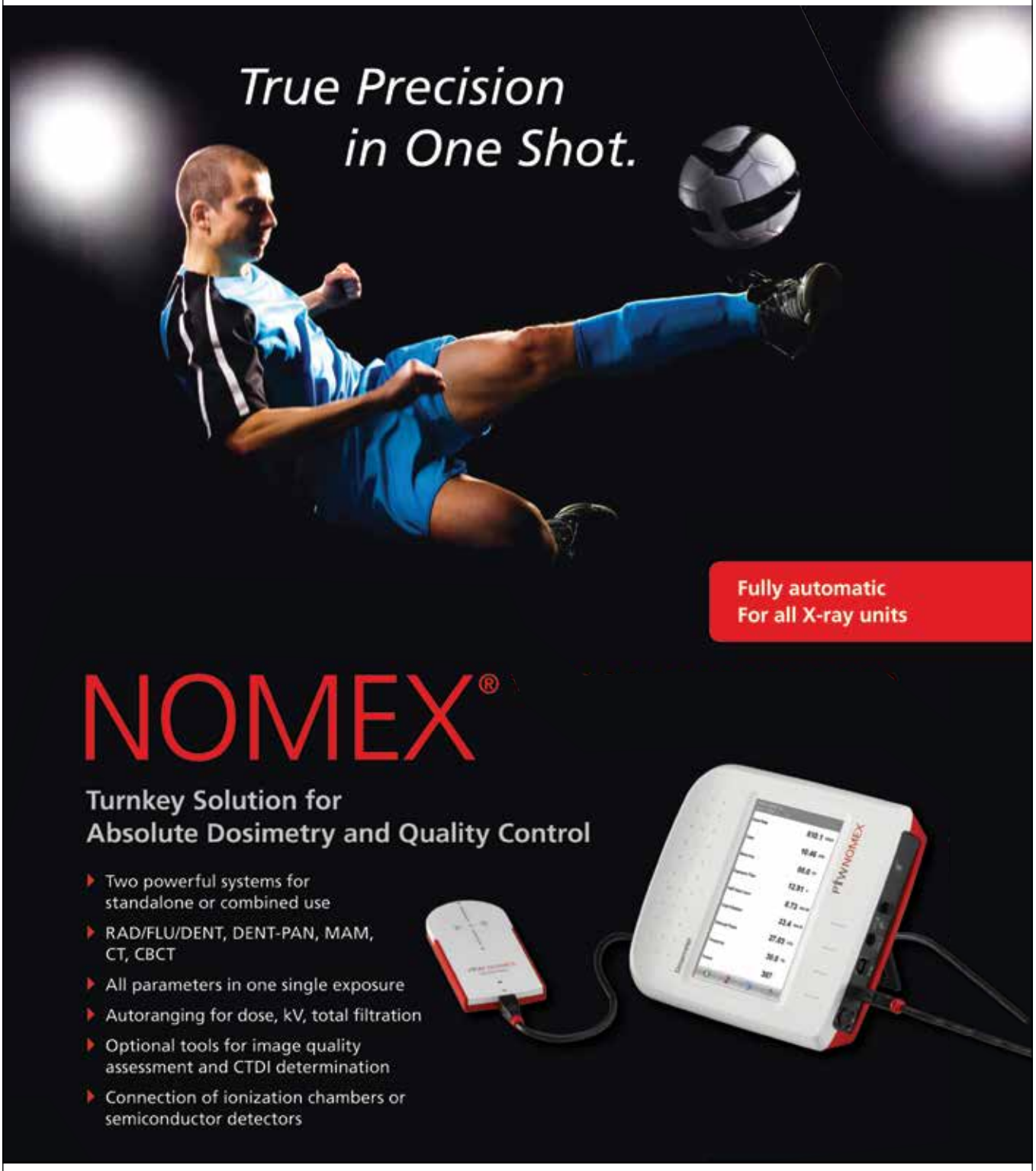

PTW DOSIMETRY INDIA PVT.LTD

ACE Towers, 2nd Floor, 73/75, Dr. Radhakrishnan Road, Mylapore, Chennai - 600 004.
Ph : 044 - 4207 9999 Telefax : 044 - 4207 2299 E-mail : info@ptw-india.in Web : www.ptw-india.in

Print ISSN: 0971-6203, E-ISSN: 1998-3913

Journal of Medical Physics

(Incorporating AMPI Medical Physics Bulletin)

Editorial Board - 2018

Association of Medical Physicists of India

(Regd. No. 421/1976 GBBSD, Public Trust F 4238)
(An affiliate of the Indian National Science Academy & The International Organization for Medical Physics)
C/o Radiological Physics & Advisory Division, BARC
CT & CRS Building, Anushaktinagar, Mumbai - 400094, ● Website: www.ampi.org.in

The Association of Medical Physicists of India (AMPI) is a professional but a non-profit making / non-governmental organization, devoted to serving the needs of the country in the field of Medical Physics. Its membership is open to science graduates, engineers and physicians interested in the application of physics to medical and biological sciences. Medical Radiation Physicists, Radiation Safety Officers, Radiological and Hospital Physicists, Radiation Oncologists and Radiologists form the main group of the association. It publishes this quarterly journal. The association is having about 1200 active members. The journal is provided to its members and also to the libraries of almost all leading Cancer Centres in the country on a very nominal subscription. Other than publishing Journal of Medical Physics, the association holds a national/ international conference every year to exchange information among its members. The association also supports advanced training of Medical Physicists by offering Travel Fellowships. For public awareness, publication of articles related to medical physics and radiation safety in newspapers and periodicals is encouraged. The association also works towards worldwide exchange of information on medical physics.

The College of Medical Physics of India (CMPI) is an autonomous wing of AMPI which was established to function as the certifying and accreditation body. Membership of AMPI is prerequisite to appear for CMPI certification examination. A member of AMPI can become member of CMPI only by passing the certification examination. CMPI certification indicates that the holder has acquired, demonstrated, and maintained a minimum standard of knowledge in medical physics and the competence to practice as clinical physicist in Diagnostic Radiology, Radiation Oncology and Nuclear Medicine.

Membership Fee Details (w.e.f. February 07, 2015)

Annual Member	
Indian Resident	INR ₹ 1,280.00
Developing Countries	USD $ 50.00
Other Countries	USD $ 165.00
Life Member	
Indian Resident	INR ₹ 3,615.00
Developing Countries	USD $ 257.00
Other Countries	USD $ 970.00
Institution Member (India)	INR ₹ 4,780.00

AMPI Executive Committee (2015-2017)

President	Prof. Arun Chougule
Vice President	Mr. Balasubramanian Nagappan
Secretary	Dr. Vellaiyan Subramani
Treasurer	Mr. Varadharajan Ekambaram
Members	Dr. Lalit M Aggarwal
	Dr. Atul Tyagi
	Dr. Thayalan Kuppusamy
	Dr. Varatharaj Chandraraj
	Dr. Raghukumar P
	Dr. Arabinda Rath
	Mr. Vinod Pandey
	Mr. Suresh Pangam
	Mr. S Karthikeyan
	Dr. Om Prakash Gurjar
	Dr. Vinod Kumar Dangwal

AMPI Board of Trustees (2015-2017)

Chairman	Mr. Satya Pal Agarwal
Convener	Dr. Pankaj Tandon
Members	Dr. Deepak Deshpande
	Dr. Kamlesh Passi
	Mr. Radhakrishnan Balan Nair

College of Medical Physics of India (CMPI) Board 2015-2017

Chairman	Mr. V. K. Sathiyanarayanan
Vice Chairman	Dr. Tharmar Ganesh
Chief Examiner	Dr. Sunil Dutt Sharma
Registrar	Dr. Dayananda Shamurailtpam
Secretary-Treasurer	Dr. K. J. Maria Das
Members	Dr. Arabinda Kumar Rath
	Dr. Pratik Kumar
	Dr. Jamema Swamidas
	Mr. Raghavendra Holla

JMP H-Index = 13

Journal of Medical Physics

General Information

The journal

The Journal of Medical Physics (known as AMPI Medical Physics Bulletin till 1994) is a quarterly publication of Association of Medical Physicists of India (AMPI). Issues are published quarterly in January, April, July and October. The main objective of the Journal is to serve as a vehicle of communication to highlight all aspects of medical physics. The scope of this journal covers all aspects of the application of radiation physics to health science, mainly radiation therapy, radiodiagnosis, nuclear medicine, radiation dosimetry, radiation standards, quality assurance, calibration and radiation protection. Papers / manuscripts on radiobiology pertaining to cancer therapy also fall within the scope of the journal. Apart from the original research work, papers which are of practical importance to medical physicists e.g., those dealing with practices (performance and quality assurance tests, clinical investigations and follow-ups with novelty), radiation accidents and emergencies are also published in the journal. Brief manuscripts dealing with the validation of relatively newer concepts may be considered as technical notes or letter to editor. Reviews of publications (e.g., ICRP/ ICRU reports and books related to the scope of the journal) may also find a place in the journal. Manuscripts with no or oblique relevance to the scope may not find place.

Abstracting and indexing information

The journal is registered with the following abstracting partners: Baidu Scholar, CNKI (China National Knowledge Infrastructure), EBSCO Publishing's Electronic Databases, Exlibris – Primo Central, Google Scholar, Hinari, Infotrieve, National Science Library, ProQuest, TdNet

The journal is indexed with, or included in, the following: DOAJ, EMBASE/ Excerpta Medica, Emerging Sources Citation Index, Index Copernicus, Indian Science Abstracts, IndMed, Pubmed Central, Scimago Journal Ranking, SCOPUS

Information for Authors

Copies of the journal are provided free of cost to the AMPI members.

There are no page charges for JMP submissions. However, there are charges for color reproduction of photographs. Please check http://www.jmp.org.in/contributors.asp for details.

All manuscripts must be submitted online at www.journalonweb.com/jmp.

Subscription Information

A subscription to Journal of Medical Physics comprises 4 issues. Prices include postage. Annual Subscription Rate for non-members-

Annual Subscription Rates

Print	Personal	Institutional
India (INR)	1700.00	2800.00
Abroad (USD)	130.00	260.00
Online only		
India (INR)	1400.00	2200.00
Abroad (USD)	100.00	210.00
Print + Online		
India (INR)	2100.00	3500.00
Abroad (USD)	160.00	330.00
Single Issue		
India (INR)	581.00	925.00
Abroad (USD)	46.00	86.00

For mode of payment and other details, please visit www.medknow.com/subscribe.asp.

Claims for missing issues will be serviced at no charge if received within 60 days of the cover date for domestic subscribers, and 3 months for subscribers outside India. Duplicate copies cannot be sent to replace issues not delivered because of failure to notify publisher of change of address.

The journal is published and distributed by Wolters Kluwer India Private Limited. Copies are sent to subscribers directly from the publisher's address. It is illegal to acquire copies from any other source. If a copy is received for personal use as a member of the association/society, one cannot resale or give-away the copy for commercial or library use. The copies of the journal to the members of the association are sent by ordinary post. The editorial board, association or publisher will not be responsible for non receipt of copies. If any member/subscriber wishes to receive the copies by registered post or courier, kindly contact the publisher's office. If a copy returns due to incomplete, incorrect or changed address of a member/subscriber on two consecutive occasions, the names of such members will be deleted from the mailing list of the journal. Providing complete, correct and up-to-date address is the responsibility of the member/subscriber.

Please send change of address information to subscriptions@medknow.com.

Advertising policies

The journal accepts display and classified advertising. Frequency discounts and special positions are available. Inquiries about advertising should be sent to Wolters Kluwer India Private Limited, advertise@medknow.com.

The journal reserves the right to reject any advertisement considered unsuitable according to the set policies of the journal.

The appearance of advertising or product information in the various sections in the journal does not constitute an endorsement or approval by the journal and/or its publisher of the quality or value of the said product or of claims made for it by its manufacturer.

Annual Advertisement Tariffs

1. Back cover (Color) - ₹ 66,000
2. Back Inside cover (color) - ₹ 50,000
3. First Page (Color) - ₹ 54,000
4. Front Inside cover (color) - ₹ 54,000
5. Full page B/W - ₹ 28,000
6. Full page color - ₹ 36,000
7. Gate Fold Cover - ₹ 102,000
8. Art-Card (Back2Back) - ₹ 87,000

Copyright

Permissions

For information on how to request permissions to reproduce articles/information from this journal, please visit www.medknow.com.

Disclaimer

The information and opinions presented in the Journal reflect the views of the authors and not of the Journal or its Editorial Board or the Publisher. Publication does not constitute endorsement by the journal. Neither the Journal of Medical Physics nor its publishers nor anyone else involved in creating, producing or delivering the Journal of Medical Physics or the materials contained therein, assumes any liability or responsibility for the accuracy, completeness, or usefulness of any information provided in the Journal of Medical Physics, nor shall they be liable for any direct, indirect, incidental, special, consequential or punitive damages arising out of the use of the Journal of Medical Physics. The Journal of Medical Physics, nor its publishers, nor any other party involved in the preparation of material contained in the Journal of Medical Physics represents or warrants that the information contained herein is in every respect accurate or complete, and they are not responsible for any errors or omissions or for the results obtained from the use of such material. Readers are encouraged to confirm the information contained herein with other sources.

Editorial Office
Dr. A. S. Pradhan
Editor-in-Chief
Journal of Medical Physics,
Association of Medical Physicists of India (AMPI)
C/o Radiological Physics & Advisory Division,
Bhabha Atomic Research Centre,
CTCRS, Anushaktinagar, Mumbai - 400094, India.
E-mail: editor@jmp.org.in / Website: www.jmp.org.in

Published by
Wolters Kluwer India Private Limited,
A-202, 2nd Floor, The Qube,
C.T.S. No.1498A/2 Village Marol, Andheri (East),
Mumbai - 400 059, India.
Phone: 91-22-66491818
Print at Website: www.medknow.com

Printed at
Dhote Offset Technokrafts Pvt. Ltd., Jogeshwari, Mumbai, India

Journal of Medical Physics

Volume 43 - Issue 1 - January-March 2018

Contents

Contents (Contd...)

PhD Thesis Reviews

News

Reviewers List, 2017

Journal of Medical Physics on Web

http://www.journalonweb.com/jmp

The Journal of Medical Physics now accepts articles electronically. It is easy, convenient and fast. Check following steps:

1 Registration

- Register from http://www.journalonweb.com/jmp as a new author (Signup as author)
- Two-step self-explanatory process

2 New article submission

- Read instructions on the journal website or download the same from manuscript management site
- Prepare your files (Article file, First page file and Images, Copyright form & Other forms, if any)
- Login as an author
- Click on 'Submit new article' under 'Submissions'
- Follow the steps (guidelines provided while submitting the article)
- On successful submission you will receive an acknowledgement quoting the manuscript ID

3 Tracking the progress

- Login as an author
- The report on the main page gives status of the articles and its due date to move to next phase
- More details can be obtained by clicking on the ManuscriptID
- Comments sent by the editor and reviewer will be available from these pages

4 Submitting a revised article

- Login as an author
- On the main page click on 'Articles for Revision'
- Click on the link "Click here to revise your article" against the required manuscript ID
- Follow the steps (guidelines provided while revising the article)
- Include the reviewers' comments along with the point to point clarifications at the beginning of the revised article file.
- Do not include authors' name in the article file.
- Upload the revised article file against New Article File - Browse, choose your file and then click "Upload" OR Click "Finish"
- On completion of revision process you will be able to check the latest file uploaded from Article Cycle (In Review Articles-> Click on manuscript id -> Latest file will have a number with 'R', for example XXXX_100_15R3.docx)

Facilities

- Submission of new articles with images
- Submission of revised articles
- Checking of proofs
- Track the progress of article until published

Advantages

- Any-time, any-where access
- Faster review
- Cost saving on postage
- No need for hard-copy submission
- Ability to track the progress
- Ease of contacting the journal

Requirements for usage

- Computer and internet connection
- Web-browser (Latest versions - IE, Chrome, Safari, FireFox, Opera)
- Cookies and javascript to be enabled in web-browser

Online submission checklist

- First Page File (rtf/doc/docx file) with title page, covering letter, acknowledgement, etc.
- Article File (rtf/doc/docx file) - text of the article, beginning from Title, Abstract till References (including tables). File size limit 4 MB. Do not include images in this file.
- Images (jpg/jpeg/png/gif/tif/tiff): Submit good quality colour images. Each image should be less than 10 MB) in size
- Upload copyright form in .doc / .docx / .pdf / .jpg / .png / .gif format, duly signed by all authors, during the time mentioned in the instructions.

Help

- Check Frequently Asked Questions (FAQs) on the site
- In case of any difficulty contact the editor

Original Article

Monte Carlo Investigation of Photon Beam Characteristics and its Variation with Incident Electron Beam Parameters for Indigenous Medical Linear Accelerator

Subhalaxmi Mishra[1,5], P. K. Dixit[2,5], T. Palani Selvam[1,5], Sanket S. Yavalkar[3], D. D. Deshpande[4]

[1]Radiological Physics and Advisory Division, Bhabha Atomic Research Centre, [2]Radiological Safety Division, Atomic Energy Regulatory Board, [3]Technology Innovation Department, Society for Applied Microwave Electronics Engineering and Research, Mumbai, [4]Department of Medical Physics, Tata Memorial Hospital, [5]Homi Bhabha National Institute, Training School Complex, Anushaktinagar, Mumbai, India

Abstract

Purpose: A Monte Carlo model of a 6 MV medical linear accelerator (linac) unit built indigenously was developed using the BEAMnrc user code of the EGSnrc code system. The model was benchmarked against the measurements. Monte Carlo simulations were carried out for different incident electron beam parameters in the study. **Materials and Methods:** Simulation of indigenously developed linac unit has been carried out using the Monte Carlo based BEAMnrc user-code of the EGSnrc code system. Using the model, percentage depth dose (PDD), and lateral dose profiles were studied using the DOSXYZnrc user code. To identify appropriate electron parameters, three different distributions of electron beam intensity were investigated. For each case, the kinetic energy of the incident electron was varied from 6 to 6.5 MeV (0.1 MeV increment). The calculated dose data were compared against the measurements using the PTW, Germany make RFA dosimetric system (water tank MP3-M and 0.125 cm^3 ion chamber). **Results:** The best fit of incident electron beam parameter was found for the combination of beam energy of 6.2 MeV and circular Gaussian distributed source in X and Y with FWHM of 1.0 mm. PDD and beam profiles (along both X and Y directions) were calculated for the field sizes from 5 cm × 5 cm to 25 cm × 25 cm. The dose difference between the calculated and measured PDD and profile values were under 1%, except for the penumbra region where the maximum deviation was found to be around 2%. **Conclusions:** A Monte Carlo model of indigenous linac (6 MV) has been developed and benchmarked against the measured data.

Keywords: Beamnrc, dosxyznrc, egsnrc code system, linear accelerator, measurement, monte Carlo

Received on: 13-10-2017 **Review completed on: 21-12-2017** **Accepted on: 02-01-2018**

Introduction

Linear accelerator (linac) has several advantages in comparison to telecobalt units.[1-5] Department of Science and Technology, Government of India, has entrusted the responsibility of development of indigenous linac to one of its constituent units, Society for Applied Microwave Electronics Engineering and Research (SAMEER) under Jai Vigyan National Science and Technology Mission. Due to its development under indigenous technology, the machine has the potential of delivering cost-effective radiotherapy treatments in India. The linac unit is named as Siddharth and is capable of producing photon beam energy of 6 MV. Details can be found at https://www.sameer.gov.in/linearaccelerators.

Benchmarking of photon beams generated from radiotherapy equipment are extensively carried out with the help of Monte Carlo radiation transport simulations.[6-13] The first step of dose calculation using Monte Carlo code is to develop the Monte Carlo beam model for the linac. Tuning of the incident electron beam parameters is an important task to benchmark the calculated dose data against the measured data.[14-17] Detailed studies by Sheikh–Bagheri and Rogers[14] showed that optimum tuning of the beam energy and its width can be performed by using PDD and in-air off-axis factors. A study by

Access this article online

Quick Response Code:

Website: www.jmp.org.in

DOI: 10.4103/jmp.JMP_125_17

Address for correspondence: Subhalaxmi Mishra, Radiological Physics and Advisory Division, Bhabha Atomic Research Centre, Safety and Environment Group, Mumbai - 400 09, Maharashtra, India.
E-mail: b.subwu@gmail.com

How to cite this article: Mishra S, Dixit PK, Selvam TP, Yavalkar SS, Deshpande DD. Monte Carlo investigation of photon beam characteristics and its variation with incident electron beam parameters for indigenous medical linear accelerator. J Med Phys 2018;43:1-8.

Lin *et al*.[18] found that it is possible to tune the beam width by the 10 cm × 10 cm beam profile measured in a water phantom. Verhaegen and Seuntjens[19] identified suitable electron beam width based on larger fields and shallower depths. Recently, Sangeetha and Surekha[20] used EGSnrc code system[21] to simulate Varian 600 C/D linac of photon energy 6 MV (for both with flattening filter and without flattening filter). Several studies on determination of incident beam parameters are reported in the literature.[15,22-29]

The purpose of the present study is to develop Monte Carlo model of 6 MV Siddharth linac unit using the Monte Carlo-based BEAMnrc user-code[30] of the EGSnrc[21] Monte Carlo code system and benchmark this model against the measured data. The calculated dose data are based on the DOSXYZnrc user code[31] of the EGSnrc code system.[21] In the study, simulations were carried out for different incident electron beam parameters.

Materials and Methods

Simulation of medical linear accelerator (Siddharth)

The geometry of the linac unit was simulated based on the manufacturer's detailed information using the BEAMnrc user code[30] of the Monte Carlo-based EGSnrc code system.[21] In this study, different components of the treatment head such as target, primary collimator, flattening filter, monitor chamber, mirror, and secondary collimator were modeled. Figure 1 shows the display of linac modeled in the present study using the BEAMnrc user code.[30] In this simulation, the z-axis is taken along the beam axis, and the origin is taken at the front face of the target.

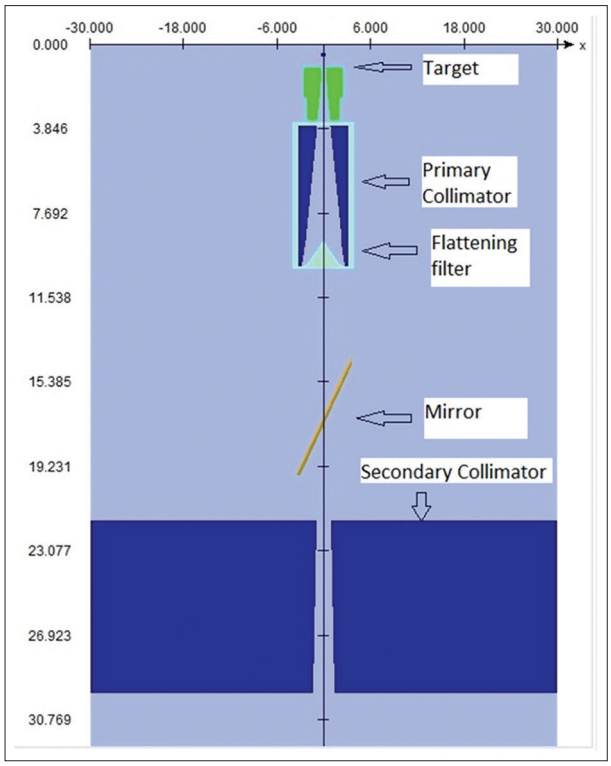

Figure 1: Detailed head structure of Siddharth medical linear accelerator. The dashed line is the Z-axis, with the positive X direction to the right and the Y direction coming out of the page. The origin is on the target surface at position 0. The linac head consists of six main component modules including the target, primary collimator, flattening filter, ion chamber, mirror, and secondary collimator

Incident electron beam parameters

Incident electron parameters play an important role in the dose distributions. To identify appropriate electron parameters, following three cases were studied. For each case, the kinetic energy of the incident electron was varied from 6 to 6.5 MeV (0.1 MeV increment).

Case 1

As per the manufacturer's specification, the electron beam is a point and divergent with a half-angle of 14°. The source is positioned on Z-axis and 4 mm above the target [Figure 2]. The radius of the beam at the target is 1 mm.

Case 2

In this case, the incident electron beam is a circular parallel beam with a diameter of 2 mm [Figure 3]. The electron beam is incident in the XY plane.

Case 3

In this case, the beam is circular, and the spatial distribution of electrons is defined by a Gaussian intensity distribution [Figure 4]. The Full Width Half Maximum (FWHM) of the incident beam is considered to be 1 mm in both X and Y directions.

BEAMnrc and DOSXYZnrc simulations

The Monte Carlo simulations were done in two steps. To identify the incident electron beam parameters, initial simulations were carried out for 10 cm × 10 cm field size and depth of 10 cm. In the first step, phase space file for each of the above cases was scored at 100 cm from the target using the BEAMnrc user-code.

In the BEAMnrc simulations, the electron transport cutoff (ECUT) and photon transport cutoff (PCUT) energies were set to 0.7 and 0.01 MeV, respectively. Secondary electron production cutoff (AE) and bremstrahlung production cutoff (AP) values were set to 0.521 and 0.01 MeV, respectively. Range rejection was turned on with ESAVE value of 0.7 MeV in the target and 2 MeV in other components of the linac.[14] The number of histories for Monte Carlo calculation was set 6×10^9 particles.

In the second step, the phase space data from aforementioned simulations served as the source for the simulations using the DOSXYZnrc user code. This user code is capable of performing 3D absorbed dose calculations in Cartesian coordinates in the water phantom. In DOSXYZnrc, the water phantom size was 50 cm × 50 cm × 50 cm and the phase space source was positioned on the water surface, i.e. at Z = 100 cm. Figure 5 represents the voxel phantom set up in the DOSXYZnrc simulations. The water phantom was divided into a number of voxels. For high-dose gradients regions, small voxel sizes were adapted.[32] For central axis PDD simulation, up to a depth of 2 cm, absorbed dose was scored in voxel dimension of 1.0 cm × 1.0 cm × 0.05 cm and for depths from

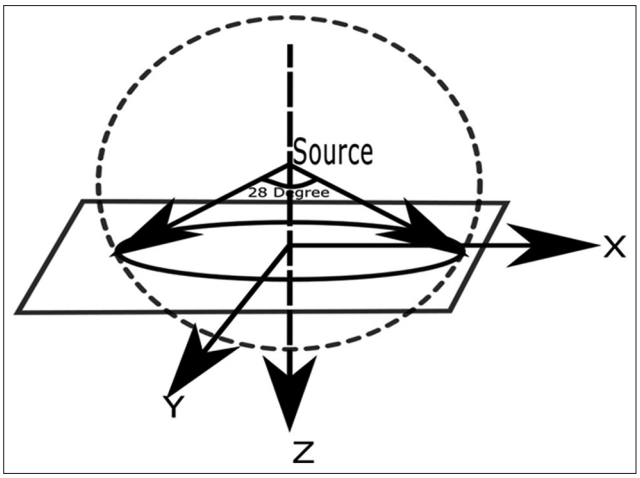

Figure 2: Point divergent source on Z-axis (Case 1) showing the electron beam divergence angle which is the half angle of the circular field at the point of incidence (14^{o}) and the directions of X, Y and Z axes. The beam is centered on the Z axis

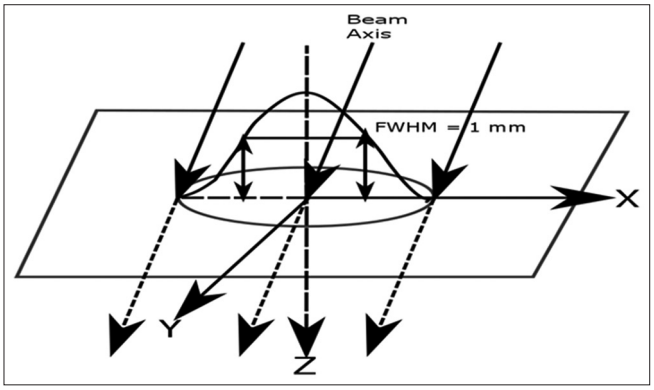

Figure 4: Circular Beam with Gaussian distributions in X and Y (Case 3). The shape of the circle is defined by FWHM (1 mm) of the Gaussian intensity distributions in the X-and Y-directions respectively

2 to 25 cm, voxel dimension of 1.0 cm × 1.0 cm × 0.1 cm were considered. The beam profiles (both X and Y directions) were calculated at three different depths such as d_{max} (1.5 cm), 5 cm and 10 cm. For beam profile simulations, different voxel dimensions were chosen for the shoulder, penumbra, and flattened regions. For example, for dose profile simulation in X-direction for a field size of 10 cm × 10 cm voxel dimensions of 0.1 cm × 1.0 cm × 0.1 cm (from −4.0 to +4.0) for flattened region and 0.05 cm × 1.0 cm × 0.1 cm for shoulder and penumbra regions (from −7.5 to −4.0 and +7.5 to +4.0) were used. The EGSnrc parameters set for DOSXYZnrc simulation were ECUT = AE = 0.521 MeV, PCUT = AP = 0.01 MeV.

All the simulations utilized PRESTA-II electron step length algorithm. Up to 6 × 10^{9} particle histories were followed in the simulation. The statistical uncertainties associated with the absorbed dose values were <0.5%.

Measurement of photon beam dosimetric parameters

Dose measurements were carried out by a PTW MP3 Water Scanning System and ionization chamber (Semiflex 0.125 cm^{3}).

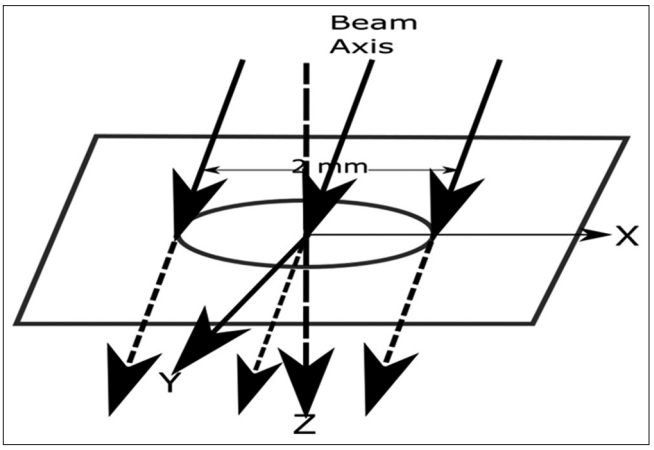

Figure 3: Parallel Circular Beam (Case 2) showing the beam diameter (2 mm) measured perpendicular to the beam central axis and the directions of X, Y and Z axes. The beam is along the Z-axis

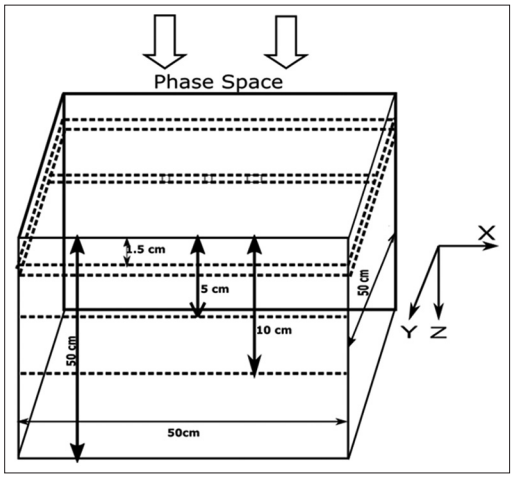

Figure 5: The voxel water phantom of dimension 50 cm × 50 cm × 50 cm used for DOSXYZnrc simulation. The size of voxels set for PDD and beam profile calculations (for 10 cm × 10 cm field size) are also shown

The measurements were performed with 1 mm resolution for both PDD and beam profiles. Field sizes considered were from 5 cm x 5 cm to 25 cm x 25 cm at a SSD of 100 cm. Beam profiles were measured at three different depths, i.e. depth of maximum dose (d_{max}), 5 cm and 10 cm for both X and Y directions. The overall uncertainty in the dose measurement using the water phantom scanning system is estimated up to a maximum value of 2%. This uncertainty is attributed to positioning inaccuracy of the chamber up to 1 mm and fluctuations of chamber and electrometer, air pressure, and temperature during the time frame of one scan.

Results and Discussion

Incident electron beam characteristics

Analysis of central axis percentage depth dose (PDD) data for 10 cm × 10 cm suggests that for a given incident electron beam energy, PDD is almost insensitive to the incident electron beam parameters. PDD values also do not differ significantly

with the investigated incident electron beam energies of 6–6.5 MeV. The relative difference between the calculated depth-dose distributions (10 cm × 10 cm field size) for beam energies 6 and 6.5 MeV was <1.5%. The PDD values at a depth of 10 cm, %dd (10), for a field size of 10 cm × 10 cm, corresponds to the beam quality.[33] Figure 6 presents the %dd (10) values for the investigated electron beam energies which have Gaussian distribution (FWHM = 1 mm). As the energy increases, there is a marginal increase in the value of %dd (10). The same trend was observed for the cases 1 and 2. For the incident electron beam energy of 6.2 MeV (Gaussian with FWHM = 1 mm), the calculated value %dd (10) is 66.3% which is in close agreement with the measured value of 67% carried out in the present study. The overall conclusion is that for the incident electron beam energy of 6.2 MeV, irrespective of the cases investigated (cases 1–3), the agreement between the calculated PDD values and the measurements is <1%.

However, the beam profiles are sensitive to the incident electron beam parameters. Figure 7a presents the comparison of Monte Carlo-calculated profile in X-direction for incident electron beam energies 6.0, 6.2, 6.5 MeV and measured data for a field size of 10 cm × 10 cm and at a depth of 10 cm for point divergent source (case 1). Figure 7b and c present the above comparison for the parallel circular beam (case 2) and Gaussian distribution (case 3), respectively. It was observed that beam profile horns were reduced as the incident electron beam energy increases. Lower energy beams produce horns at the edge of the radiation field while higher ones correspond to flat profiles. An energy difference of 0.1 MeV causes a dose difference at the edge of the field by about 1%. Above discussion demonstrates that the dose profile resulting from 6.2 MeV of electrons with Gaussian distribution (case 3) provides optimum agreement with the measurements. Figure 7d compares the investigated cases with incident electron beam energy of 6.2 MeV with measured data.

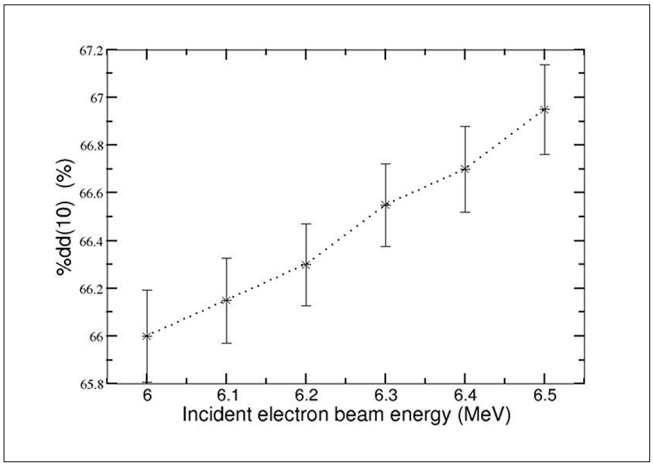

Figure 6: Comparison of percent depth dose value at a depth of 10 cm, %dd (10), in water, Monte Carlo-calculated values for various incident electron beam energies and measurement for a field size of 10 cm × 10 cm

For all the investigated cases, beam parameters such as left penumbra (LP), right penumbra (RP), beam flatness and beam symmetry were investigated. Table 1 presents these parameters analyzed from the calculated beam profiles of all the investigated electron beam parameters for the field size of 10 cm × 10 cm. Measured data are also included for comparison. For case 1, both RP and LP were <6 mm which is less than the measured values of 6.9 mm. Beam symmetry and flatness were observed to be higher than the measured as well as the tolerance values (103% and 106%) as quoted by the IEC protocol.[34] For case 2, both RP and LP were <5.5 mm which is less than the measured values of 6.9 mm. Beam flatness was observed to be higher than the measured as well as the tolerance values. However, beam symmetry was within the acceptable range for all the beam energies. For case 3, all the parameters such as RP, LP, symmetry, and flatness were in good agreement with the measured values at beam energy 6.2 MeV with the Gaussian distribution.

Figures 6 and 7 and Table 1 demonstrate that Monte Carlo calculations using the incident electron beam energy of 6.2 MeV with Gaussian distribution (FWHM = 1 mm) produce dose distributions which agree with the measurements. Table 2 presents the incident electron beam parameters concluded by the other investigators which result in dose distribution comparable to the measurements.

Measured and calculated photon beam dosimetric characteristics

Further Monte Carlo simulations were carried out for other field sizes such as 5 cm × 5 cm, 15 cm × 15 cm, 20 cm × 20 cm and 25 cm × 25 cm for a mono-energetic electron beam of kinetic energy 6.2 MeV with the Gaussian distribution of FWHM = 1 mm. PDDs were calculated for depths from 0 to 25 cm, and beam profiles (both X and Y directions) were calculated at three different depths of d_{max} (1.5 cm), 5 cm and 10 cm for the above field sizes. The calculated PDD and beam profiles for all the above field sizes were compared with the measured data and a good agreement was found.

The dose difference between the calculated and measured PDD values were under 1% for all the investigated field sizes. Both Monte Carlo-calculated and measured depth of d_{max} was found to be at 1.52 cm for a field size of 10 cm × 10 cm. The differences between calculated and measured values were <1% in the tail region and <0.5% in the superficial depth region for all the investigated field sizes. Calculated and measured PDD values are shown in Figures 8-10 for field sizes of 5 cm × 5 cm, 10 cm × 10 cm and 25 cm × 25 cm, respectively.

For beam profiles, the difference between calculated and measured dose values was <1%, except for the border points where the maximum deviation between calculated and measured dose values were found to be around 1.8%. Table 3 presents the comparison of Monte Carlo-calculated and measured beam profile parameters such as LP, RP,

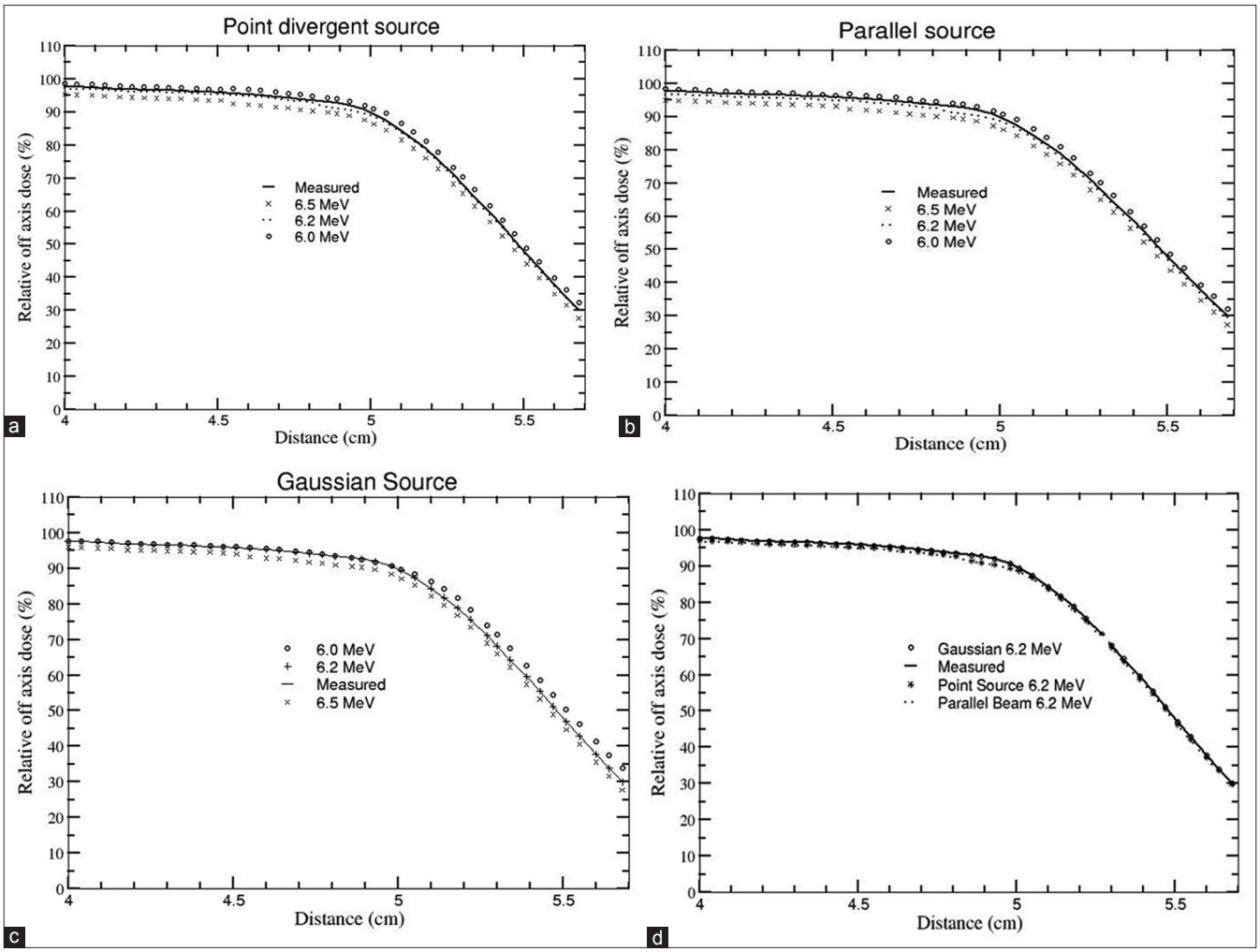

Figure 7: Comparison of Monte Carlo-calculated beam profiles and measured values for incident electron beam energies 6.0, 6.2, 6.5 MeV and measured data for a field size of 10 cm × 10 cm and at a depth of 10 cm (a) Point divergent source placed on the Z-axis (b) parallel circular beam (c) circular beam with Gaussian distributions. (d) Comparison of Monte Carlo-calculated beam profiles of all the investigated radial intensity distributions for incident electron beam energy 6.2 MeV and measured data

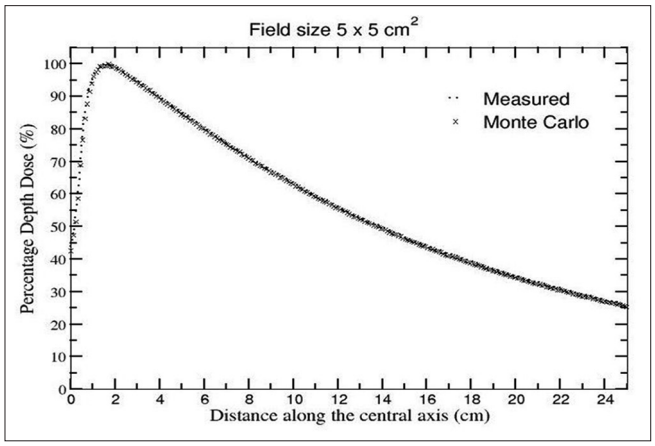

Figure 8: Comparison of Monte Carlo-calculated and measured percentage depth dose values for a field size of 5 cm × 5 cm

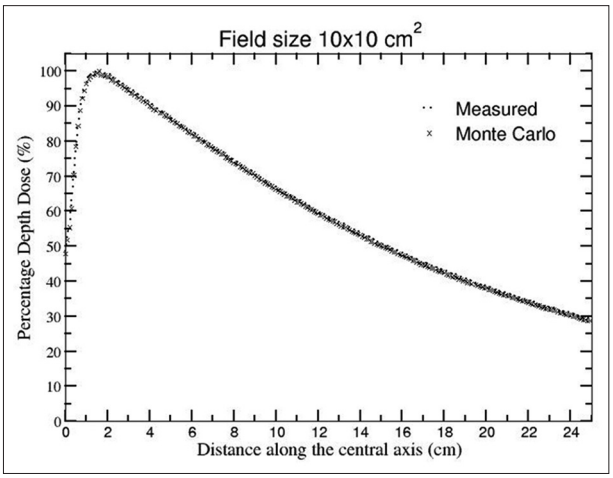

Figure 9: Comparison of Monte Carlo-calculated and measured percentage depth dose values for a field size of 10 cm × 10 cm

flatness, and symmetry for all the investigated field sizes. Monte Carlo-calculated values were found to be in excellent agreement with the measured values for the field sizes.

Calculated and measured X-profiles and Y-profiles for all the investigated field sizes at a depth of 10 cm are presented in

Table 1: The parameters analyzed from the beam profiles for all the combinations of incident electron beam parameters along with the measured parameters for a field size of 10 × 10 cm^2 and at a depth of 10 cm

Electron energy (MeV)	Gaussian source				Point source				Parallel beam source				Measured data			
	LP (mm)	RP (mm)	Flatness (%)	Symmetry (%)	LP (mm)	RP (mm)	Flatness (mm)	Symmetry (mm)	LP (mm)	RP (mm)	Flatness (mm)	Symmetry (%)	LP (mm)	RP (mm)	Flatness (%)	Symmetry (%)
6	6.5	6.4	106.4	101.2	5.3	5.4	108.1	102.2	5.6	5.7	109.2	103.3				
6.1	6.6	6.7	105.6	101.6	5.4	5.5	108.2	102.1	5.7	5.8	109.4	103.1				
6.2	6.8	6.7	104.6	101.5	5.5	5.6	108.4	102	5.9	5.8	109.5	102.9	6.9	6.8	104.9	101.2
6.3	6.6	6.7	105.7	101.7	5.4	5.5	108.6	102.7	5.7	5.8	109.4	103.2				
6.4	6.5	6.4	106.8	100.9	5.5	5.4	108.5	102.5	5.6	5.7	109.8	103.5				
6.5	6.5	6.6	106.9	101.4	5.3	5.4	108.3	102.8	5.6	5.7	109.9	103.7				

Left penumbra and right penumbra stand for left penumbra and right penumbra, respectively. LP: Left penumbra, RP: Right penumbra

Table 2: Comparison of incident electron beam parameters which resulted in good agreement with the measured dose profiles (published and this study)

Model of 6 MV Linac unit	Electron beam parameter	Reference
Varian 600 C/D	Electron energy - 5.7 MeV Gaussian distribution with FWHM 1.3 mm	[20]
Elekta SL 25	Electron energy - 6.3 MeV Gaussian distribution with FWHM 1.1 mm	[14]
Siemens KD	Electron energy - 6.8 MeV Gaussian distribution with FWHM 3.2 mm	[14]
Elekta synergy	Electron energy - 6.45 MeV Gaussian distribution with FWHM 0.25 mm in Y and 1.0 mm in X plane	[24]
Varian 2100 EX	Electron energy - 6.2 MeV Gaussian distribution with FWHM 1.3 mm	[22]
Clinac 2100 C/D	Electron energy - 6.05 MeV Pencil beam with a diameter of 2 mm	[29]
Present study	Electron energy - 6.2 MeV Gaussian distribution with FWHM 1 mm	-

FWHM: Full Width Half Maximum

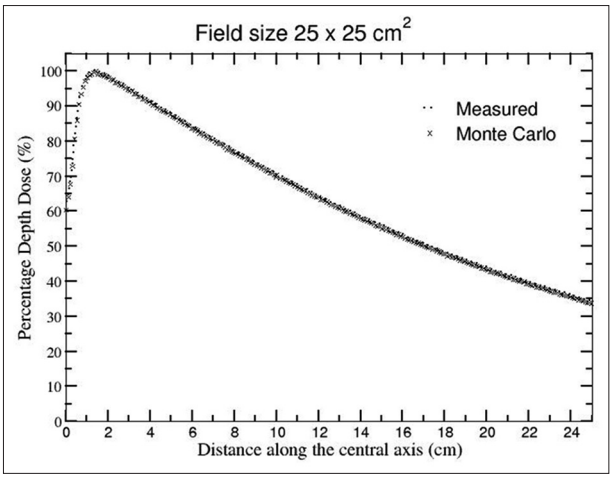

Figure 10: Comparison of Monte Carlo-calculated and measured percentage depth dose values for a field size of 25 cm × 25 cm

Figures 11 and 12, respectively. Statistical uncertainties on the calculated dose values for each voxel were mostly below 0.2% and about 0.7% for regions near field edge.

Conclusions

The indigenous linac unit Siddharth of photon energy 6 MV was simulated using the Monte Carlo-based BEAMnrc code. The dosimetric parameters such as PDD and beam profile were calculated using the DOSXYZnrc user-code of the EGSnrc code system, and the results were compared with the measured data. In the study of the influence of electron beam parameters on photon beam characteristics, five different incident electron beam energies (6-6.5 MeV) and three different type of radial intensity distribution of electron beam (case 1, 2 and 3) were chosen. It was found that the central axis relative depth dose

Table 3: Comparison of Monte Carlo-calculated and measured beam profile parameters such as left penumbra, right penumbra, flatness, and symmetry for the investigated field sizes for incident electron beam energy of 6.2 MeV with a Gaussian distribution of Full Width Half Maximum 1 mm

Field size (cm^2)	Monte Carlo calculated				Measured			
	LP (mm)	RP (mm)	Flatness (%)	Symmetry (%)	LP (mm)	RP (mm)	Flatness (%)	Symmetry (%)
5×5	6.3	6.2	103.2	101.5	6.2	6.4	104.2	101.4
10×10	6.8	6.7	104.6	101.5	6.9	6.8	104.9	101.2
15×15	7.6	7.7	104.2	100.7	7.8	7.7	103.6	102.3
20×20	8.3	8.4	103.5	101.3	8.4	8.5	103.2	101.6
25×25	9.1	9.3	104	103.2	9.2	9.2	103.5	103

Left penumbra and right penumbra stand for the left penumbra and right penumbra, respectively. LP: Left penumbra, RP: Right penumbra

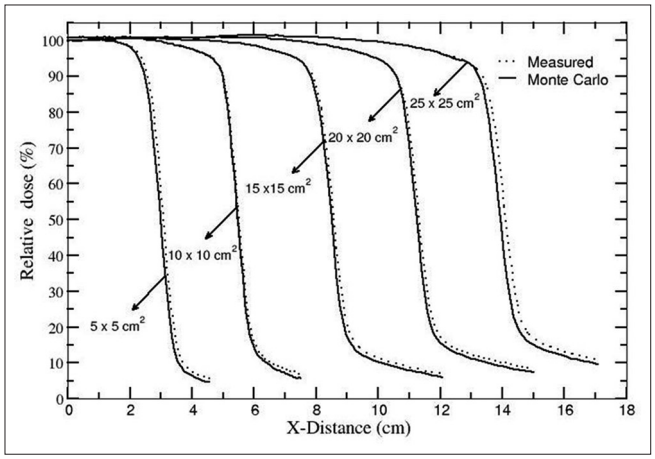

Figure 11: Comparison of Monte Carlo-calculated and measured X-profiles for all the investigated field sizes at a depth of 10 cm

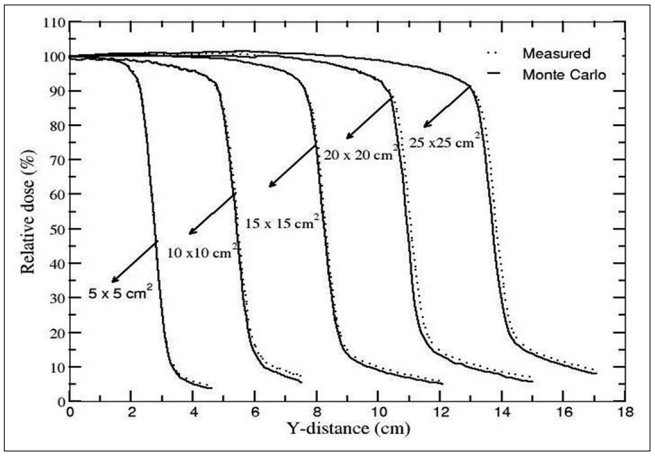

Figure 12: Comparison of Monte Carlo-calculated and measured Y-profiles for all the investigated field sizes at a depth of 10 cm

values, i.e. PDDs are quite insensitive to variations in the electron beam radial intensity distribution. However, the beam profiles are sensitive to the incident electron energy as well as the radial intensity distribution of the incident electron beam. The calculated PDD and lateral beam profiles for 5 cm × 5 cm, 10 cm × 10 cm, 15 cm × 15 cm, 20 cm × 20 cm and 25 cm × 25 cm field sizes were compared with the measured data and a good agreement was found when the calculated dose profiles utilized the combination of incident electron beam energy of 6.2 MeV and the Gaussian distribution with FWHM of 1.0 mm.

Acknowledgment

The authors would like to Dr. D. Datta, Head, Radiological Physics and Advisory Division, Bhabha Atomic Research Centre, and Dr. A. U. Sonawane, Head, Directorate of Regulatory Affairs and Commumnications, Atomic Energy Regulatory Board for their encouragement and support throughout the study. The authors would also like to thank Dr. K. P. Ray, Program Director, SAMEER Mumbai, India for his technical support in the study.

Financial support and sponsorship

Nil.

Conflicts of interest

There are no conflicts of interest.

References

1. Matcalfe P, Kron T, Hoban P. The Physics of Radiotherapy X-Rays from Linear Accelerators. Madison, Wisconsin: Medical Physics Publishing; 1997.
2. Adams EJ, Warrington AP. A comparison between cobalt and linear accelerator-based treatment plans for conformal and intensity-modulated radiotherapy. Br J Radiol 2008;81:304-10.
3. Thwaites DI, Tuohy JB. Back to the future: The history and development of the clinical linear accelerator. Phys Med Biol 2006;51:R343-62.
4. Khan FM. The Physics of Radiation Therapy. 4th ed. Baltimore: Lippincott; 2010.
5. Page BR, Hudson AD, Brown DW, Shulman AC, Abdel-Wahab M, Fisher BJ, *et al.* Cobalt, linac, or other: What is the best solution for radiation therapy in developing countries? Int J Radiat Oncol Biol Phys 2014;89:476-80.
6. Andreo P. Monte Carlo techniques in medical radiation physics. Phys Med Biol 1991;36:861-920.
7. Rogers DW, Faddegon BA, Ding GX, Ma CM, We J, Mackie TR, *et al.* BEAM: A Monte Carlo code to simulate radiotherapy treatment units. Med Phys 1995;22:503-24.
8. DeMarco JJ, Solberg TD, Wallace RE, Smathers JB. A verification of the Monte Carlo code MCNP for thick target bremsstrahlung calculations. Med Phys 1995;22:11-6.
9. Keall PJ, Siebers JV, Arnfield M, Kim JO, Mohan R. Monte Carlo dose calculations for dynamic IMRT treatments. Phys Med Biol 2001;46:929-41.
10. Solberg TD, DeMarco JJ, Chetty IJ, Mesa AV, Cagnon CH, Li AN, *et al.* A review of radiation dosimetry application using the MCNP Monte Carlo code. Radiochim Acta 2001;89:337-55.
11. Fix MK, Manser P, Born EJ, Mini R, Rüegsegger P. Monte Carlo simulation of a dynamic MLC based on a multiple source model. Phys Med Biol 2001;46:3241-57.

12. Das IJ, Kassaee A, Verhaegen F, Moskvin VP. Interface dosimetry: Measurement and Monte Carlo simulations of low-energy photon beams. Radiat Phys Chem 2001;61;593-5.
13. Ma CM, Pawlicki T, Jiang SB, Li JS, Deng J, Mok E, *et al.* Monte Carlo verification of IMRT dose distributions from a commercial treatment planning optimization system. Phys Med Biol 2000;45:2483-95.
14. Sheikh-Bagheri D, Rogers DW, Ross CK, Seuntjens JP. Comparison of measured and Monte Carlo calculated dose distributions from the NRC linac. Med Phys 2000;27:2256-66.
15. Jiang SB, Kapur A, Ma CM. Electron beam modeling and commissioning for Monte Carlo treatment planning. Med Phys 2000;27:180-91.
16. Deng J, Jiang SB, Kapur A, Li J, Pawlicki T, Ma CM, *et al.* Photon beam characterization and modelling for Monte Carlo treatment planning. Phys Med Biol 2000;45:411-27.
17. Mesbahi A, Fix M, Allahverdi M, Grein E, Garaati H. Monte Carlo calculation of Varian 2300C/D linac photon beam characteristics: A comparison between MCNP4C, GEANT3 and measurements. Appl Radiat Isot 2005;62:469-77.
18. Lin SY, Chu TC, Lin JP. Monte Carlo simulation of a clinical linear accelerator. Appl Radiat Isot 2001;55:759-65.
19. Verhaegen F, Seuntjens J. Monte Carlo modelling of external radiotherapy photon beams. Phys Med Biol 2003;48:R107-64.
20. Sangeetha S, Sureka CS. Comparison of flattening filter (FF) and flattening-filter-free (FFF) 6 MV photon beam characteristics for small field dosimetry using EGSnrc Monte Carlo code. Radiat Phys Chem 2017;135:63-75.
21. Rogers DW, Kawrakow I, Seuntjens JP, Walters BR, Mainegra-Hing E. NRC User Codes for EGSnrc. NRCC Report PIRS-702 (revB). Ottawa, ON: National Research Council of Canada; 2010.
22. Keall PJ, Siebers JV, Libby B, Mohan R. Determining the incident electron fluence for Monte Carlo-based photon treatment planning using a standard measured data set. Med Phys 2003;30:574-82.
23. Aljarrah K, Sharp GC, Neicu T, Jiang SB. Determination of the initial beam parameters in Monte Carlo linac simulation. Med Phys 2006;33:850-8.
24. Almberg SS, Frengen J, Kylling A, Lindmo T. Monte Carlo linear accelerator simulation of megavoltage photon beams: Independent determination of initial beam parameters. Med Phys 2012;39:40-7.
25. Tzedakis A, Damilakis JE, Mazonakis M, Stratakis J, Varveris H, Gourtsoyiannis N, *et al.* Influence of initial electron beam parameters on Monte Carlo calculated absorbed dose distributions for radiotherapy photon beams. Med Phys 2004;31:907-13.
26. Pena J, González-Castaño DM, Gómez F, Sánchez-Doblado F, Hartmann GH. Automatic determination of primary electron beam parameters in Monte Carlo simulation. Med Phys 2007;34:1076-84.
27. Bush K, Zavgorodni S, Beckham W. Inference of the optimal pretarget electron beam parameters in a Monte Carlo virtual linac model through simulated annealing. Med Phys 2009;36:2309-19.
28. Fix MK, Stampanoni M, Manser P, Born EJ, Mini R, Rüegsegger P, *et al.* A multiple source model for 6 MV photon beam dose calculations using Monte Carlo. Phys Med Biol 2001;46:1407-27.
29. Björk P, Knöös T, Nilsson P. Influence of initial electron beam characteristics on Monte Carlo calculated absorbed dose distributions for linear accelerator electron beams. Phys Med Biol 2002;47:4019-41.
30. Rogers DW, Walters B and Kawrakow I. BEAMnrc users Manual. PIRS 509(A) Rev. Ottawa, ON: National Research Council of Canada; 2016.
31. Walters B, Kawrakow I, Rogers DW. DOSXYZnrc users Manual. PIRS 794(B) Rev. Ottawa, ON: National Research Council of Canada; 2016.
32. Yani S, Dirgayussa I, Gde E, Rhani MF, Haryanto F, Arif I. The effect of voxel size on dose distribution in Varian Clinac i×6 MV photon beam using Monte Carlo simulation. AIP Conf Proc 2015;1677:040002.
33. Almond PR, Biggs PJ, Coursey BM, Hanson WF, Huq MS, Nath R, *et al.* AAPM's TG-51 protocol for clinical reference dosimetry of high-energy photon and electron beams. Med Phys 1999;26:1847-70.
34. International Electrotechnical Commission- IEC 60977-2. Medical Electrical Equipment – Medical Electron Accelerators – Guidelines for Functional Performance Characteristics. IEC/TR 60977; 2008.

Original Article

A Treatment Planning Method for Better Management of Radiation-Induced Oral Mucositis in Locally Advanced Head and Neck Cancer

Hao Howard Zhang, Warren D. D'Souza

Department of Radiation Oncology, University of Maryland School of Medicine, Baltimore, MD, USA

Abstract

Purpose/Aim: To describe a two-phase intensity-modulated radiation therapy (IMRT) treatment planning approach, that is, promising for reduction of oral mucositis risk in locally advanced head-and-neck cancer. **Materials and Methods:** Ten locally advanced head-and-neck cancer patients who underwent RT were retrospectively collected. Conventional IMRT and volumetric-modulated arc therapy (VMAT) plans were generated for these patients following clinical protocol. Following the first phase of generating conventional IMRT plans, our approach utilized data from Monte Carlo-based kernel superposition dose calculations corresponding to beam apertures (generated from the conventional IMRT plans) and used an exact mathematical programming-based optimization approach applying linear programming (LP) to dose optimization in the second phase. **Results:** Compared with conventional IMRT and VMAT treatment plans, our novel method achieved better preservation of oral cavity (16%–29% lower mean dose, $P < 0.01$), parotid glands (6%–17% lower mean dose, $P < 0.04$), and spinal cord (3-11 Gy lower maximum dose, $P < 0.03$) and lower doses to nonorgan-at-risk/nontarget normal tissues, with the same or better target coverage. **Conclusions:** Our LP-based method can be practically implemented in routine clinical use with a goal of limiting radiation-induced oral mucositis for head-and-neck cancer patients.

Keywords: Head and neck cancer, oral mucositis, radiotherapy, treatment planning

Received on: 10-07-2017 **Review completed on: 10-12-2017** **Accepted on: 02-01-2018**

Introduction

Worldwide, it is estimated that there are approximately 686,000 new head-and-neck cancers (HNCs) diagnosed every year and 375,000 individuals will die annually as a result of the disease.[1] Locally advanced HNC represents one of the most challenging treatment planning scenarios in radiation therapy (RT). Mucositis is among the most common adverse reactions encountered in RT for HNC. Franzese *et al*. reported that 54% of patients treated with volumetric-modulated arc therapy developed ≥grade 2 (G2) oral mucositis.[2] Other studies reported that 73%–100% of patients treated with intensity-modulated RT (IMRT) experienced grade 3/4 mucositis[3,4] and severe oral mucositis occurred in 29%–66% of all patients receiving RT.[5,6]

Oral mucositis is often painful and can significantly affect nutritional intake, mouth care, and quality of life,[7] as well as increase the risk of local and life-threatening systemic infections.[8,9] Patients with oral mucositis are significantly more likely to have severe pain and loss of >5% of pretreatment body weight.[6] In one study, ~16% of patients receiving RT were hospitalized because of mucositis.[10] Moreover, severe oral toxicities can also compromise the delivery of optimal cancer therapy protocols. Trotti *et al*. reported that 11% of patients receiving RT for HNC had unplanned breaks in RT because of severe mucositis.[10] These disruptions in dosing as a result of oral complications can directly affect survivorship. Thus, oral mucositis is a major dose-limiting toxicity of RT to the head and neck region.[8,9,11]

In addition to serious clinical effects, radiation-induced oral mucositis contributes to economic concerns because of costs associated with pain management, liquid diet supplements,

Access this article online

Quick Response Code:

Website: www.jmp.org.in

DOI: 10.4103/jmp.JMP_78_17

Address for correspondence: Dr. Hao Howard Zhang, 22 S Greene St., Baltimore, MD 21201, USA.
E-mail: haozhang@som.umaryland.edu

How to cite this article: Zhang HH, D'Souza WD. A treatment planning method for better management of radiation-induced oral mucositis in locally advanced head and neck cancer. J Med Phys 2018;43:9-15.

gastrostomy tube placement or total parenteral nutrition, management of secondary infections, and hospitalizations.[12] In a retrospective study, oral mucositis was associated with an increase in costs ranging from $1,700 to $6,000 per patient, depending on the grade of mucositis.[5] In summary, mucositis causes statistically significant increases in direct medical costs, averaging ~$3,000 ± $1,000 per treatment episode.[13,14]

Despite the high incidence, associated morbidity, and effects on patient quality of life and economic consequences, no standard RT technique is approved for the prevention of mucositis in HNC.[15] The radiation oncology community has concentrated on studies designed to determine whether altering fractionation schedules can improve cancer control, such as hyperfractionation and concomitant boost fractionation for HNC.[16] However, the incidence of grade 3 or 4 acute mucositis increased by 16%–22% in patients treated with accelerated fractionation or hyperfractionation compared with the conventional schedule.[17]

It has been shown that oral mucositis is correlated with doses received by the oral cavity (e.g., 15, 30, 40, 45, and 50 Gy).[18-21] Cumulative doses to the oral cavity of 32 Gy were associated with acute mucositis, and a dose >39 Gy was associated with longer duration of mucositis.[22] In an attempt to minimize radiation-induced mucositis, Sanguineti *et al*. suggested delivering the smallest possible dose to the oral cavity.[23]

In this research, we provide a treatment plan, that is, promising for reduction of the risk of oral mucositis in locally advanced HNC compared to clinical treatment plans generated using conventional IMRT and VMAT.

Materials and Methods

Data

In this retrospective, institutional review board-approved study, we collected data from 10 patients with locally advanced HNC who had undergone RT in our clinic. Treatment targets included the primary tumor and cervical nodes. A simultaneous integrated boost was employed as the mode of delivery, and the prescribed doses to the primary tumor and high-and low-risk (LR) nodes were 70, 59.4, and 54 Gy, respectively, in 35 fractions. Organs-at-risk (OARs) included the parotid glands, oral mucosa surrounding the oral cavity, brain stem, and spinal cord. We used previously published dose–volume constraints in the optimization process [Table 1].[24]

Treatment plans

Two types of IMRT plans were generated for each patient. The first was generated using the Pinnacle^3 planning system (Philips Healthcare; Fitchburg, WI, USA). The second was generated using our linear programming (LP)-based approach.[25] Although IMRT plans were also generated using the Eclipse planning system (Varian Medical Systems; Palo Alto, CA, USA), both planning systems resulted in comparable IMRT plans. We describe the planning specifics and results for only the Pinnacle^3 planning system in this report.

Conventional intensity-modulated radiation therapy plans

In this work, nine beams were used in IMRT treatment planning. Selected angles were input to the commercial IMRT planning systems. The Pinnacle^3 planning system used a gradient-based optimization approach for conventional IMRT. These plans will be referred to as Pinn IMRT plans.

Linear programming-based intensity-modulated radiation therapy plans

IMRT plans were also generated using an LP-based optimization approach (referred to as LP IMRT).[25] The details of the LP-based approach can be seen from Zhang *et al*.[25] Here, we summarize the approach: The LP-based approach allows for explicit incorporation of dose and dose–volume constraints. An advantage of this approach is that if the problem is feasible and bounded (which is the case for dose optimization problems), formulating and solving it using a linear program guarantees the optimal solution. Our approach employed the principle of segment weight optimization. In the first phase, the Pinn IMRT plan was used to generate an initial set of apertures. These physical apertures were used to initiate a second-phase optimization process that utilized aperture-specific dose calculations to provide input data to an LP-based dose optimization solver. The details of the dose optimization problem are as follows:

$$\text{Minimize } \alpha^{TAR_L}\sum_{j\in T}x_j+\alpha^{TAR_U}\sum_{j\in T}x_j+\alpha^{OAR}\sum_{j\in O}x_j+\alpha^{NOR}\sum_{j\in N}x_j \quad (1)$$

$$\text{subject to } \sum_{i\in\theta}w_iB_{i,j}+x_j\geq b^{TAR_L} \quad \text{for } j\in T \quad (2)$$

$$\sum_{i\in\theta}w_iB_{i,j}\leq x_j+b^{TAR_U} \quad \text{for } j\in T \quad (3)$$

$$\sum_{i\in\theta}w_iB_{i,j}\leq x_j+b^{OAR} \quad \text{for } j\in O \quad (4)$$

$$\sum_{i\in\theta}w_iB_{i,j}\leq x_j+b^{NOR} \quad \text{for } j\in N \quad (5)$$

Table 1: Summary of dose/dose-volume constraints

Left and right parotid mean dose	Oral cavity mean dose	Maximum cord dose	Maximum brainstem dose	Volume of LR PTV receiving ≥59.4 Gy Volume of HR PTV receiving ≥70 Gy Volume of primary PTV receiving ≥75.6 Gy
26 Gy	35-40 Gy	45 Gy	54 Gy	5%

LR: Low-risk, PTV: Planning target volume, HR: High-risk

$$\sum_{i\in\theta} w_i B_{i,j} \le b^{SPC} \quad \text{for } j \in S \tag{6}$$

$$w_i, x_j \ge 0 \tag{7}$$

where i is an index corresponding to beam apertures and j is an index corresponding to voxels over which constraints are specified. The LP dose optimization objective involves minimizing the weighted sum of doses delivered to the voxels that violate the thresholds for dose–volume histogram (DVH) constraints. The treatment volume is divided into region O, including OARs; region T, including the planning target volumes; and region N, which corresponds to normal tissue voxels. In this work, normal tissue is defined as nontarget and non-OAR tissue. Input data include beam aperture-specific dose matrices B corresponding to each delivery aperture. DVH constraints are handled through the introduction of penalty variables that account for target, OAR, and normal tissue underdose and overdose as relevant. $b^{TAR_L}, b^{TAR_U}, b^{OAR}, b^{NOR}$, and b^{SPC} specify the desired dose thresholds for the target, OAR, normal tissue, and any designated region, respectively, at which constraints are desired. $x_j, j \in T$, is a vector of underdoses/overdoses (doses below the prescription level or above a certain level [hot spot] for target voxels) delivered to the target region. The variable $x_j, j \in O$ and $j \in N$ is a vector of overdoses (doses over a certain critical level) delivered to the OARs and normal tissue. S is a subset of O, which corresponds to a special region, such as the spinal cord voxels, in which hard upper-bound dose constraints instead of DVH constraints are specified. w_i is the weight (to be optimized) for aperture i of beam angle set θ. $\alpha^{TAR_L}, \alpha^{TAR_U}, \alpha^{OAR}$, and α^{NOR} are the penalty weights assigned for underdosing, overdosing the target, and overdosing the OARs and normal tissues, respectively. Each type of constraint can be enforced on multiple targets and OARs. Multiple constraints can be enforced on each target and OAR as well.

The dose optimization problem was formulated in the General Algebraic Modeling System (GAMS Development Corporation; Washington, DC, USA);[26] a high-level modeling system for mathematical programming and optimization. The linear program was then solved with an integrated high-performance commercial solver, Parallel CPLEX (IBM; Armonk, NY, USA)[27] on a cluster of 48 Intel 2.4 GHz CPUs available at our clinic.

Volumetric-modulated arc therapy plans

Single-arc and double-arc VMAT plans were generated using the Pinnacle^3 planning system. The Pinnacle^3 planning system adopts a multistep optimization algorithm developed by Bzdusek *et al*. which includes initial segments generation, arc sequencing, machine parameter optimization, and segment weight optimization steps.[28] For each arc, 180 apertures (control points) were used, resulting in 180 apertures for the single-arc (referred to as 1ARC) plans and 360 apertures for the double-arc (referred to as 2ARC) plans. This setting per arc corresponds to the maximum number of apertures available for VMAT from Pinnacle 3.

A summary of the treatment plans generated and their differences are shown in Table 2.

Comparison of plans

We retrospectively tested our approach on data from 10 patients with locally advanced HNC who had undergone conventional RT in our clinic. To compare different treatment plans, we let each approach improve the OAR and normal tissue sparing as much as possible by adjusting weights associated with the individual dose and dose–volume constraints. The adjustments were guided using the best plan obtained from a competing technique as an improvement goal.[29] Each plan was allowed up to 2 h of planning time for improvement.

All plans were normalized so that 95% of the target received at least the prescription dose. Final dose distributions for all plans were compared using a previously validated Monte Carlo-based convolution-superposition dose calculation approach.[30] The dosimetric quality of the plans was compared using DVHs and isodose lines. Dose distributions were compared through the conformity index (CI) and dose gradient index (DGI), defined as:

$$\text{CI} = (\text{prescription isodose volume})/(\text{target volume}) \tag{8}$$

$$\text{DGI} = (50\% \text{ of prescription isodose volume})/(100\% \text{ of prescription isodose volume}) \tag{9}$$

Comparison of delivery efficiency

The delivery efficiency of each technique was compared using the number of apertures, monitor units (MUs), and treatment delivery time for each plan [results shown in Table 3]. A maximum dose rate of 600 MU/min was assumed when calculating delivery time for both IMRT and VMAT. Treatment delivery time was approximated by assuming that the beam off time during transition between successive apertures for a given beam angle in IMRT averaged 0.5 s. The maximum gantry rotation speed was 4.8°/s. For IMRT, the delivery time (in seconds) was calculated as:

Table 2: Summary of treatment plans generated for comparison

	Pinnacle IMRT	VMAT	LP IMRT
Planning system	Pinnacle^3	Pinnacle 3	In-house
Beam arrangement	9 fixed beams	Single or double arcs	9 fixed beams
Input dose calculation	Pencil beam convolution	Pencil beam convolution	Monte Carlo kernel superposition
Optimization method	Gradient-based	Multistep optimization	Linear programming

LP: Linear programming, IMRT: Intensity-modulated radiation therapy, VMAT: Volumetric-modulated arc therapy

Table 3: Comparison of total monitor units, number of apertures, calculated delivery time, conformal index, and dose gradient index

	MU	#Aperture	Time (min)	CI	DGI
1 ARC VMAT	457±73	180	1.3±0.04	3.4±2.2	4.2±1.4
2 ARC VMAT	549±97	360	2.5±0.01	1.9±0.5	3.3±1.2
Pinnacle IMRT	1038±115	269±46	5.1±0.5	2.1±1.2	3.2±2.6
LP IMRT	1152±118	199±44	4.7±0.5	1.4±0.1	3.0±2.4

MU: Monitor unit, CI: Conformal index, DGI: Dose gradient index, 1 ARC VMAT: Single-arc VMAT, 2 ARC VMAT: Double-arc VMAT, IMRT: Intensity-modulated radiation therapy, LP: Linear programming, VMAT: Volumetric-modulated arc therapy

$$\text{IMRT Time} = (\text{Total MUs})/10 + (\text{A} \times 0.5) + \theta_{1,k}/4.8 \qquad (10)$$

where A is the number of apertures and $\theta_{1,k}$ is the distance (in degrees) between the first and last beam. The beam mode-up time for IMRT was ignored for estimating treatment delivery time. Of interest is the fact that individual beam mode-up times are eliminated on the new TrueBeam™ (Varian Medical Systems; Palo Alto, CA, USA) instrumentation. For VMAT delivery, equation (11) was used to obtain the VMAT delivery time: s_l is the actual rotation speed at control point l (recall the spacing between the control points is 2°):

$$\text{VMAT Time} = \sum 2/s_l \qquad (11)$$

where s_l is the actual rotation speed at control point l.

Results

Qualitative dosimetric results are shown as DVH plots [Figure 1] and isodose curves [Figure 2]. Quantitative results were collected at OAR dose constraint setting levels as shown in Figure 3.

Plan dosimetric quality

Figure 1 shows the mean DVHs of the 10 patient records considered in this research. Four approaches were compared, with solid lines representing the two IMRT approaches and dashed lines representing the two VMAT approaches. Primary planning treatment volume, high-risk PTV, and LR PTV DVHs in Figure 1 show that all plans achieved essentially the same target coverage. LP IMRT achieved the best dose uniformity, and 1ARC VMAT resulted in the worst. Pinn IMRT and 2ARC VMAT had similar dose uniformity. The maximum difference between PTV DVHs was <10%.

In comparing OAR sparing across different treatment plans, Figure 1a shows that all four plans achieved similar brainstem sparing. Pinn IMRT and both VMAT plans resulted in the same sparing of the right parotid. LP IMRT spared 15% more of the right parotid than the other three approaches. From oral cavity DVHs shown in Figure 1b, the LP IMRT plan was superior for preserving oral cavity; 20% better than the Pinn IMRT and 2ARC VMAT plans, which were 10% better than the 1ARC VMAT plan. Left parotid sparing was essentially the same (difference <10%) for all four plans, as shown in Figure 1c. For spinal sparing, the 2ARC VMAT plan delivered 10% less maximum dose to spinal cord than the 1ARC VMAT plan [Figure 1d]. LP IMRT delivered 6% and 12% less maximum doses to spinal cord than the Pinn IMRT and 2ARC VMAT plans, respectively.

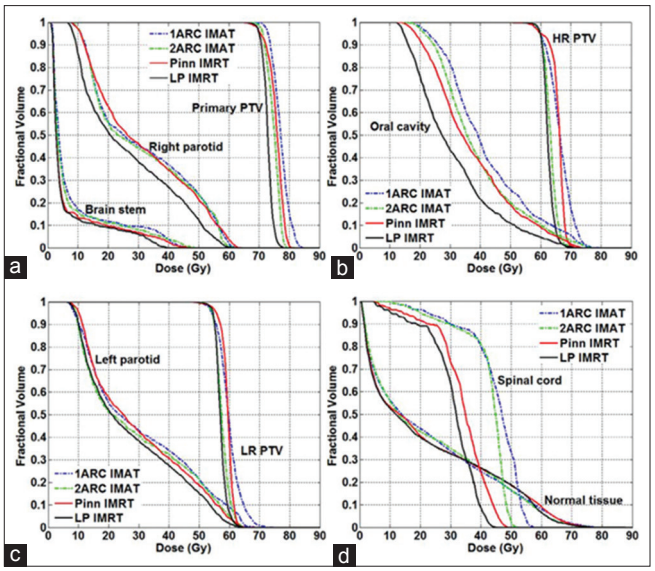

Figure 1: Mean dose–volume histogram comparisons in 10 head-and-neck cases for: (a) Primary planning treatment volume, brain stem, and right parotid; (b) High-risk planning treatment volume and oral cavity; (c) Low-risk planning treatment volume and left parotid; and (d) Spinal cord and normal tissue for intensity-modulated radiation therapy and volumetric-modulated arc therapy plans

Looking at more detailed quantitative results (absolute dose in Gy received by each OAR at constraint setting levels, Figure 3), the LP IMRT plan resulted in 2–5 Gy (6%–17%) lower mean doses for both parotids than the other three plans. For oral cavity mean doses, the LP IMRT plan was 5–11 Gy (16%–29%) lower than the other plans. The maximum spinal cord dose of the LP IMRT plan was 3–11 Gy lower than the other plans.

Figure 2 shows the isodose curves on an axial slice of one of the cases as an example of dose distribution comparison. Only the 1ARC VMAT plans showed hot spots in the primary PTV. The difference in target coverage in isodose curves between the IMRT plans and 2ARC VMAT plan was negligible. LP IMRT plans displayed better OAR sparing for parotids, oral cavity, and spinal cord than the other plans. From the last two columns of Table 3, we observe that the average CI and DGI achieved by the Pinn IMRT and 2ARC VMAT plans were similar. The LP IMRT plan resulted in the lowest average CI and DGI, whereas the 1ARC VMAT plan resulted in the highest.

Paired *t*-tests were conducted to determine whether differences achieved at OAR dose constraint setting levels between different plans were statistically significant [Table 4]. We can see that except for brain stem sparing, the differences between LP IMRT and the other three plans were significant. The tests

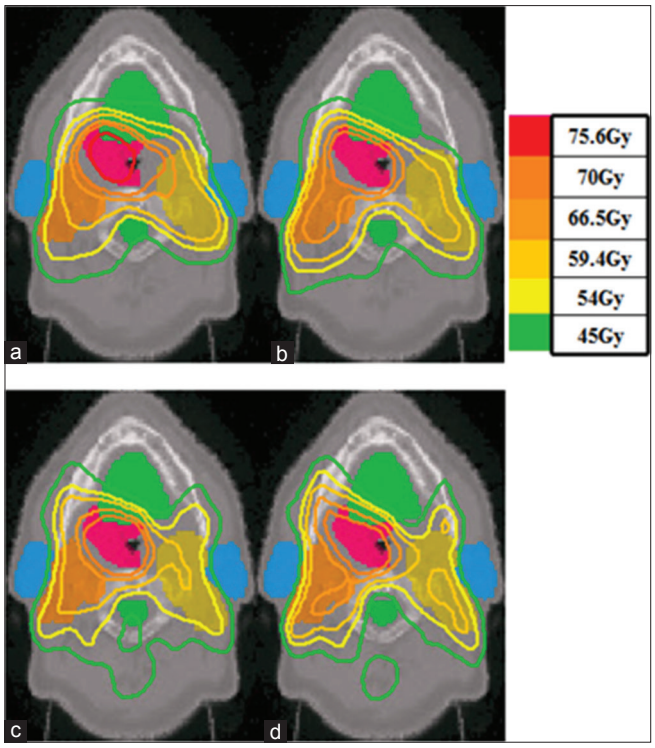

Figure 2: Isodose curves for: (a) Single-arc volumetric-modulated arc therapy plans; (b) Double-arc volumetric-modulated arc therapy plans; (c) Conventional intensity-modulated radiation therapy plans generated by Pinnacle 3; and (d) Linear programming intensity-modulated radiation therapy plans

confirmed the superior preservation of oral cavity and parotid glands achieved by LP IMRT.

Comparison of delivery efficiency

The mean and standard deviation of total MUs, number of apertures, and treatment delivery time for all plans are summarized in Table 3. The 2ARC plans resulted in 20% more MUs than 1ARC plans. LP IMRT plans resulted in 10% more MUs than Pinn IMRT plans. IMRT plans at least doubled the MUs used by VMAT plans. The number of apertures in the IMRT plans was generally between that of the 1ARC VMAT and 2ARC VMAT plans, which were ~180 and ~360, respectively. LP IMRT plans reduced the number of apertures by 25% compared with Pinn IMRT plans. LP IMRT plans resulted in zero weights for a significant number of the Pinn IMRT apertures while improving plan quality. This finding ultimately resulted in 8% shorter calculated LP IMRT delivery times than Pinn IMRT delivery times. 2ARC VMAT delivery times were ~2.5 min shorter than the estimated LP IMRT delivery times.

Discussion

Our results showed that double-arc VMAT plans improved plan quality over single-arc VMAT plans. IMRT plans and double-arc VMAT plans generated by Pinnacle 3 were comparable. However, our LP-based IMRT consistently provided better overall plan quality than both the IMRT and double-arc VMAT

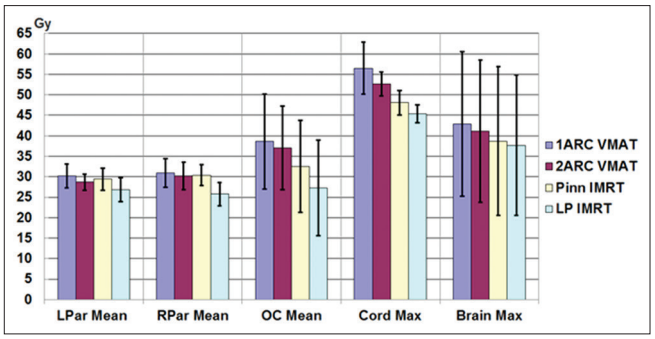

Figure 3: Comparison of doses (in Gy) at constraint levels for intensity-modulated radiation therapy and volumetric-modulated arc therapy plans

plans. The CI and DGI of LP IMRT plans were consistently better than those with other plans. DVHs for normal tissues were better for LP IMRT plans than for VMAT plans.

For locally advanced HNC cases, OARs either sit within the concavity of the targets or are very close to the targets. Mallick and Waldron[31] showed that the rate of oral mucositis is quite high in patients being treated with fields involving the oral cavity. Since VMAT treatment plans deliver radiation through all possible beams around the patient, it is difficult to avoid those fields involving the oral cavity. As our results showed, VMAT plans were not as competitive as IMRT delivery techniques for preserving the oral cavity. It has been shown that most patients who receive >50 Gy to the oral mucosa will develop severe ulcerative oral mucositis.[18] Clinical severity is directly proportional to the radiation dose administered. Shogan *et al*. showed a correlation between oral cavity dose and mucositis when using IMRT.[19] A statistically significant correlation between acute mucositis grade and percentage of volume of oral cavity receiving 15, 30, 40, and 45 Gy was identified. In other studies, a correlation between grade 3+ mucositis and oral cavity doses of 9.5 and 10.1 Gy per week was found.[20,21] Cumulative doses of 32 Gy to the oral cavity were associated with acute mucositis, and a dose >39 Gy was associated with longer duration of mucositis.[22] Delivery of the smallest dose possible to the oral cavity has been suggested to avoid radiation-induced mucositis.[23] As the results show in this work, using any of these dose levels as an evaluation criteria, our LP IMRT approach is the most promising to prevent radiation-induced mucositis.

Clinical comparisons of IMRT and VMAT treatment plans for HNC have reported either similar or better results with VMAT than IMRT.[32-35] Some of these reports did not include oral cavity sparing as the main comparative objective.[32,35] The limitation in the respective IMRT plans was that fewer beams and apertures utilized (e.g., 39 apertures over 5–7 beams by Bertelsen *et al*.[34]) may constrain performance in these plans. Most of the comparisons did not report the number of apertures used. Moreover, to deliver radiation continuously as the gantry rotates around the patient, VMAT requires that successive beam apertures be linked. The link between successive apertures

Table 4: *P* values of paired *t*-test comparing different treatment plans

	Left parotid mean dose	Right parotid mean dose	Oral cavity mean dose	Maximum cord dose	Maximum brainstem dose
1 ARC VMAT versus pinnacle IMRT	0.47	0.55	<0.01	0.01	0.04
2 ARC VMAT versus pinnacle IMRT	0.43	0.82	<0.01	<0.01	0.05
2 ARC VMAT versus 1 ARC VMAT	0.01	0.07	0.17	0.06	0.26
LP IMRT versus pinnacle IMRT	<0.01	<0.01	<0.01	0.03	0.48
LP IMRT versus 1 ARC VMAT	0.01	<0.01	<0.01	<0.01	0.01
LP IMRT versus 2 ARC VMAT	0.04	<0.01	<0.01	<0.01	0.05

1 ARC VMAT: Single-arc VMAT, 2 ARC VMAT: Double-arc VMAT, IMRT: Intensity-modulated radiation therapy, LP: Linear programming, VMAT: Volumetric-modulated arc therapy

is primarily dictated by the physical speed of the multileaf collimator leaves. As a result, the selection of beam apertures in VMAT is constrained by the need to link apertures to their neighbors. This constraint may adversely influence plan quality, which may be the reason that VMAT could not spare the oral cavity better than IMRT plans in this study.

On the other hand, the superior results achieved by our LP IMRT approach were contributed from both accurate dose calculations and exact optimization algorithm. Most commercial planning systems tend to employ fast, but somewhat inaccurate dose calculation algorithms that provide input to the optimization algorithm. The achieved optimal solution differs from the dose distribution obtained when one performs a more accurate dose calculation. Al-Hallaq *et al*. demonstrated that more accurate dose calculation algorithms, such as convolution/superposition or Monte Carlo approaches, are better suited for IMRT in tailoring doses in HNC cases.[36] The dose calculation algorithm utilized in this research is Monte Carlo kernel superposition.[30] The other factor that may influence results is the optimization approach employed, as suggested by Bortfeld and Webb.[37] Most commercial planning systems employ heuristic or local search-based optimization approaches. Exact optimization approaches such as LP guarantee optimal solutions and provide explicit handling of constraints (soft and hard) over target and OAR voxels. Other exact optimization approaches, such as quadratic programming, should also provide similar results. On another note, IMRT and VMAT explore the degrees of freedom in generating conformal plans differently (aperture space vs. angular space, respectively). Our results show that for reducing the risk of oral mucositis in locally advanced HNC, LP IMRT becomes a more promising approach than VMAT. This result is observed despite the decrease in the number of beam apertures employed in the IMRT plans compared with 2ARC VMAT plans. Our work further suggests that when one considers comparisons between IMRT and VMAT using commercial software, on average, it is possible to obtain comparable plans. However, the LP IMRT approach produces substantially improved results.

For locally advanced HNC, many structures in addition to the oral cavity are at risk for complications. We included these as nontarget/non-OAR normal tissues in this research because of concerns about reducing the risk of secondary cancer and complications for those structures. Hall[38] and Suit *et al*.[39] have pointed out that consideration in any radiation technique is the potential for increasing the number of radiation-induced secondary cancers. They noted that the volume of normal tissue exposed to leakage or low doses is directly related to secondary cancers. Guckenberger *et al*. have shown that using multiple arcs increases the spread of low doses to normal tissue.[40] Our results for normal tissue doses are consistent with this finding. In this work, normal tissue dose was explicitly considered in the constraints. This led to the finding that LP-based fixed-field IMRT plans resulted in lower normal tissue doses compared with VMAT plans for all 10 test cases considered.

Our approach is analogous to segment weight optimization, which has been widely used in clinical practice. The limitation of our approach in the current form is that the starting point of the second phase is based on apertures generated from conventional IMRT plans. The quality of our approach could be further improved if a larger pool of high-quality apertures could be considered. This is the goal of next steps in our research. The entire framework as described here can be easily implemented and adapted to practical clinic use.

Conclusions

In addition to clinical evaluations of commercially available planning software, we applied a different optimization approach for fixed-field IMRT: LP-based IMRT. Our results showed that LP-based fixed-field IMRT plans resulted in superior dosimetric quality compared with conventional IMRT and VMAT plans. VMAT plans, however, consistently resulted in the lowest treatment delivery times. LP-based IMRT was the most promising treatment plan, for patients with locally advanced HNC, that preserves oral cavity and parotid glands so that the risk of oral mucositis can be reduced.

Financial support and sponsorship

This work was financially supported in part by a grant NIH/NCI CA130814.

Conflicts of interest

There are no conflicts of interest.

References

1. Stewart BW, Wild CP. World Cancer Report 2014. International Agency for Research on Cancer; 2014.

2. Franzese C, Fogliata A, Clerici E, Franceschini D, Villa E, D'Agostino G, *et al.* Toxicity profile and early clinical outcome for advanced head and neck cancer patients treated with simultaneous integrated boost and volumetric modulated arc therapy. Radiat Oncol 2015;10:224.
3. Van Gestel D, Van Den Weyngaert D, Schrijvers D, Weyler J, Vermorken JB. Intensity-modulated radiotherapy in patients with head and neck cancer: A European single-centre experience. Br J Radiol 2011;84:367-74.
4. Toledano I, Graff P, Serre A, Boisselier P, Bensadoun RJ, Ortholan C, *et al.* Intensity-modulated radiotherapy in head and neck cancer: Results of the prospective study GORTEC 2004-03. Radiother Oncol 2012;103:57-62.
5. Vera-Llonch M, Oster G, Hagiwara M, Sonis S. Oral mucositis in patients undergoing radiation treatment for head and neck carcinoma. Cancer 2006;106:329-36.
6. Elting LS, Cooksley CD, Chambers MS, Garden AS. Risk, outcomes, and costs of radiation-induced oral mucositis among patients with head-and-neck malignancies. Int J Radiat Oncol Biol Phys 2007;68:1110-20.
7. Duncan GG, Epstein JB, Tu D, El Sayed S, Bezjak A, Ottaway J, *et al.* Quality of life, mucositis, and xerostomia from radiotherapy for head and neck cancers: A report from the NCIC CTG HN2 randomized trial of an antimicrobial lozenge to prevent mucositis. Head Neck 2005;27:421-8.
8. Lalla RV, Peterson DE. Oral mucositis. Dent Clin North Am 2005;49:167-84, ix.
9. Treister N, Sonis S. Mucositis: Biology and management. Curr Opin Otolaryngol Head Neck Surg 2007;15:123-9.
10. Trotti A, Bellm LA, Epstein JB, Frame D, Fuchs HJ, Gwede CK, *et al.* Mucositis incidence, severity and associated outcomes in patients with head and neck cancer receiving radiotherapy with or without chemotherapy: A systematic literature review. Radiother Oncol 2003;66:253-62.
11. Lalla RV, Sonis ST, Peterson DE. Management of oral mucositis in patients who have cancer. Dent Clin North Am 2008;52:61-77, viii.
12. Murphy BA. Clinical and economic consequences of mucositis induced by chemotherapy and/or radiation therapy. J Support Oncol 2007;5:13-21.
13. Elting LS, Cooksley C, Garden AS. Clinical Outcomes of Radiotherapy-Induced Oral Mucositis among Patients with Head and Neck Cancers. Abstract #15-096. Proceedings from the 17th MASCC/ISOO International Symposium. Geneva, Switzerland; June 30-July 2, 2005.
14. Peterman A, Cella D, Glandon G, Dobrez D, Yount S. Mucositis in head and neck cancer: Economic and quality-of-life outcomes. J Natl Cancer Inst Monogr 2001;29:45-51.
15. Rosenthal DI. Consequences of mucositis-induced treatment breaks and dose reductions on head and neck cancer treatment outcomes. J Support Oncol 2007;5:23-31.
16. Fu KK, Pajak TF, Trotti A, Jones CU, Spencer SA, Phillips TL, *et al.* A radiation therapy oncology group (RTOG) phase III randomized study to compare hyperfractionation and two variants of accelerated fractionation to standard fractionation radiotherapy for head and neck squamous cell carcinomas: First report of RTOG 9003. Int J Radiat Oncol Biol Phys 2000;48:7-16.
17. Garden AS. Mucositis: Current management and investigations. Semin Radiat Oncol 2003;13:267-73.
18. Epstein JB, Gorsky M, Guglietta A, Le N, Sonis ST. The correlation between epidermal growth factor levels in saliva and the severity of oral mucositis during oropharyngeal radiation therapy. Cancer 2000;89:2258-65.
19. Shogan JE, Bhatnagar A, Heron DE, Smith RP, Andrede RS, Huq MS, *et al*. Dosimetric correlation of oral cavity dose with acute mucositis in patients treated with intensity modulated radiation therapy (IMRT) and chemotherapy. Int J Radiat Oncol Biol Phys 2005;63:S73-4.
20. Sanguineti G, Gunn GB, Parker BC, Endres EJ, Zeng J, Fiorino C, *et al.* Weekly dose-volume parameters of mucosa and constrictor muscles predict the use of percutaneous endoscopic gastrostomy during exclusive intensity-modulated radiotherapy for oropharyngeal cancer. Int J Radiat Oncol Biol Phys 2011;79:52-9.
21. Sanguineti G, Sormani MP, Marur S, Gunn GB, Rao N, Cianchetti M, *et al.* Effect of radiotherapy and chemotherapy on the risk of mucositis during intensity-modulated radiation therapy for oropharyngeal cancer. Int J Radiat Oncol Biol Phys 2012;83:235-42.
22. Narayan S, Lehmann J, Coleman MA, Vaughan A, Yang CC, Enepekides D, *et al.* Prospective evaluation to establish a dose response for clinical oral mucositis in patients undergoing head-and-neck conformal radiotherapy. Int J Radiat Oncol Biol Phys 2008;72:756-62.
23. Sanguineti G, Sosa M, Culp L, Endres E, Bayouth J. Is it feasible to spare part of the mucosa with IMRT and does it matter. Int J Radiat Oncol Biol Phys 2004;60:S517-8.
24. Lee N, Mechalakos J, Puri DR, Hunt M. Choosing an intensity-modulated radiation therapy technique in the treatment of head-and-neck cancer. Int J Radiat Oncol Biol Phys 2007;68:1299-309.
25. Zhang HH, Meyer RR, Wu J, Naqvi SA, Shi L, D'Souza WD, *et al.* A two-stage sequential linear programming approach to IMRT dose optimization. Phys Med Biol 2010;55:883-902.
26. GAMS. Available from: http://www.gams.com. [Last accessed on 2018 Jan 02].
27. IBM CPLEX. Available from: https://www.ibm.com/analytics/data-science/prescriptive-analytics/cplex-optimizer/. [Last accessed on 2018 Jan 02]
28. Bzdusek K, Friberger H, Eriksson K, Hårdemark B, Robinson D, Kaus M, *et al.* Development and evaluation of an efficient approach to volumetric arc therapy planning. Med Phys 2009;36:2328-39.
29. Rao M, Yang W, Chen F, Sheng K, Ye J, Mehta V, *et al.* Comparison of Elekta VMAT with helical tomotherapy and fixed field IMRT: Plan quality, delivery efficiency and accuracy. Med Phys 2010;37:1350-9.
30. Naqvi SA, Earl MA, Shepard DM. Convolution/superposition using the Monte Carlo method. Phys Med Biol 2003;48:2101-21.
31. Mallick I, Waldron JN. Radiation therapy for head and neck cancers. Semin Oncol Nurs 2009;25:193-202.
32. Vanetti E, Clivio A, Nicolini G, Fogliata A, Ghosh-Laskar S, Agarwal JP, *et al.* Volumetric modulated arc radiotherapy for carcinomas of the oro-pharynx, hypo-pharynx and larynx: A treatment planning comparison with fixed field IMRT. Radiother Oncol 2009;92:111-7.
33. Verbakel WF, Cuijpers JP, Hoffmans D, Bieker M, Slotman BJ, Senan S, *et al.* Volumetric intensity-modulated arc therapy vs. conventional IMRT in head-and-neck cancer: A comparative planning and dosimetric study. Int J Radiat Oncol Biol Phys 2009;74:252-9.
34. Bertelsen A, Hansen CR, Johansen J, Brink C. Single arc volumetric modulated arc therapy of head and neck cancer. Radiother Oncol 2010;95:142-8.
35. Doornaert P, Verbakel WF, Bieker M, Slotman BJ, Senan S. RapidArc planning and delivery in patients with locally advanced head-and-neck cancer undergoing chemoradiotherapy. Int J Radiat Oncol Biol Phys 2011;79:429-35.
36. Al-Hallaq HA, Reft CS, Roeske JC. The dosimetric effects of tissue heterogeneities in intensity-modulated radiation therapy (IMRT) of the head and neck. Phys Med Biol 2006;51:1145-56.
37. Bortfeld T, Webb S. Single-arc IMRT? Phys Med Biol 2009;54:N9-20.
38. Hall EJ. Intensity-modulated radiation therapy, protons, and the risk of second cancers. Int J Radiat Oncol Biol Phys 2006;65:1-7.
39. Suit H, Goldberg S, Niemierko A, Ancukiewicz M, Hall E, Goitein M, *et al.* Secondary carcinogenesis in patients treated with radiation: A review of data on radiation-induced cancers in human, non-human primate, canine and rodent subjects. Radiat Res 2007;167:12-42.
40. Guckenberger M, Richter A, Krieger T, Wilbert J, Baier K, Flentje M, *et al.* Is a single arc sufficient in volumetric-modulated arc therapy (VMAT) for complex-shaped target volumes? Radiother Oncol 2009;93:259-65.

Original Article

Comparison of Volumetric Modulated Arc Therapy and Intensity Modulated Radiation Therapy for Whole Brain Hippocampal Sparing Treatment Plans Based on Radiobiological Modeling

Ethan Kendall, Ozer Algan, Salahuddin Ahmad

Department of Radiation Oncology, Peggy and Charles Stephenson Cancer Center, University of Oklahoma HSC, Oklahoma City, OK, USA

Abstract

Introduction: In this article, we report the results of our investigation on comparison of radiobiological aspects of treatment plans with linear accelerator-based intensity-modulated radiation therapy and volumetric-modulated arc therapy for patients having hippocampal avoidance whole-brain radiation therapy. **Materials and Methods:** In this retrospective study using the dose-volume histogram, we calculated and compared biophysical indices of equivalent uniform dose, tumor control probability, and normal tissue complication probability (NTCP) for 15 whole-brain radiotherapy patients. **Results and Discussions:** Dose-response models for tumors and critical structures were separated into two groups: mechanistic and empirical. Mechanistic models formulate mathematically with describable relationships while empirical models fit data through empirical observations to appropriately determine parameters giving results agreeable to those given by mechanistic models. **Conclusions:** Techniques applied in this manuscript could be applied to any other organs or types of cancer to evaluate treatment plans based on radiobiological modeling.

Keywords: Hippocampal sparing treatment, radiobiological modeling, VMAT versus IMRT

Received on: 20-07-2017 **Review completed on:** 29-11-2017 **Accepted on:** 29-11-2017

Introduction

Brain metastases are the most common intracranial tumors in adults and occur in 10%–30% of cancer patients.[1] One of the treatment options for patients with multiple brain metastases is whole-brain radiation therapy (WBRT) which can be combined with radiosensitizers such as motexafin gadolinium, efaproxiral, and temozolomide.[1] Neurological decline may occur in a patient with WBRT treatment causing cerebral edema in the patient within the first few weeks of treatment, symptoms of which include headaches, somnolence, vomiting, nausea, and inability to focus.[2] One to six months after WBRT, subacute encephalopathy may occur, which increases patient headaches, somnolence, and fatigue. Six months after WBRT, patients may experience severe dementia and memory loss. Irradiating hippocampi is thought to be a factor in WBRT-associated cognitive decline because the hippocampi are essential in learning, retrieval of information, and the formation of new memories. One of the ways to reduce cognitive decline is to avoid irradiating the hippocampus when performing WBRT in a process called hippocampal-avoidance WBRT (HA-WBRT).[2] It is possible to create WBRT treatment plans that spare hippocampi with equivalent dose distributions to conventional WBRT treatment plans. The most common delivery techniques for HA-WBRT are intensity-modulated radiation therapy (IMRT) and volumetric-modulated arc therapy (VMAT). VMAT is a subset of IMRT where radiation is delivered in an arc instead of at static angles.

The most common biological metrics used to guide clinical predictions are tumor control probability (TCP) and normal

Access this article online

Quick Response Code:

Website: www.jmp.org.in

DOI: 10.4103/jmp.JMP_85_17

Address for correspondence: Dr. Salahuddin Ahmad, Department of Radiation Oncology, Peggy and Charles Stephenson Cancer Center, University of Oklahoma HSC, 800 NE. 10th Street, OKCC L100, Oklahoma City, OK 73104, USA.
E-mail: salahuddin-ahmad@ouhsc.edu

How to cite this article: Kendall E, Algan O, Ahmad S. Comparison of volumetric modulated arc therapy and intensity modulated radiation therapy for whole brain hippocampal sparing treatment plans based on radiobiological modeling. J Med Phys 2018;43:16-22.

tissue complication probability (NTCP). TCP is the probability of localized tumor control for a given dose distribution, while NTCP is the probability of an undesirable effect from an organ due to radiation. A challenge of radiation therapy is to find a balance of these values to give each patient the optimal treatment by raising TCP as high as possible, while lowering NTCPs as low as possible. Dose-response models for tumors and critical structures are separated into two groups: mechanistic and empirical. Mechanistic models formulate mathematically with describable relationships while empirical models fit data through empirical observations. We may not be able to accurately formulate some biological processes because of their complexity to make mechanistic models, but this is not a challenge for empirical models which simply need to fit data.[3] Dose-volume histogram (DVH) shows how much dose is being received by a structure. It can be used to view physical parameters such as minimum, mean, and maximum dose to calculate TCP and NTCP. Because of limited information in the setting of HA-WBRT, the purpose of our study was to calculate and compare target doses, normal tissue doses, TCP, and NTCP values for treatment plans utilizing IMRT- or VMAT-based on HA-WBRT.

Materials and Methods

Treatment planning for 15 patients was carried out with Varian Eclipse treatment planning system using 3-arc VMAT (Rapid Arc) and 9-field step-and-shoot (S and S) IMRT, both calculated with Anisotropic Analytical Algorithm. From this point in our manuscript, whenever we refer to IMRT, we are referring to S and S IMRT. The planning target volume (PTV) was defined as the whole-brain excluding a uniform three-dimensional 5-mm expansion around the hippocampus. Prescribed doses in all plans were 30 Gy delivered over 10 fractions normalized to a minimum of 95% of the target volume receiving 100% of the prescribed dose. Simultaneous integrated boost or stereotactic boost was not utilized for any of the treatment plans. The radiation therapy oncology group (RTOG) trial 0933 study criteria[4] were followed for contouring and dose-volume constraints. Bilateral hippocampal contours were made on imaging datasets consisting of thin-slice spoiled gradient echo (SPGR) magnetic resonance imaging sequences fused to a treatment planning computed tomography (CT) scan. The PTV was defined as the whole-brain parenchyma excluding the bilateral hippocampal contours plus a 5-mm margin. The variation acceptable criteria for the protocol were used. In brief, these included PTV D2% ≤40 Gy and D98% ≥25 Gy. The hippocampal constraints included a D100% ≤10 Gy and a maximum hippocampal dose of ≤17 Gy. All treatment plans used identical contour sets and a single radiation oncologist reviewed and evaluated all treatment plans. Calculations of statistical significance were performed using Student's paired *t*-test to compare VMAT and IMRT plans. Treatment plans were evaluated based on tumor dose fall off, amount of dose received by normal brain tissue, and critical structures as well as the radiobiological comparison which was the purpose of this manuscript. This study was reviewed by our institutional IRB before initiation.

Equivalent uniform dose

While we strive to give tumors a homogenous dose in radiation therapy, in reality, they are inhomogeneous. To be able to better compare dose distributions, the concept of the equivalent uniform dose (EUD) was conceived. The EUD is the dose, which when homogenously given to a tumor gives, on average, the same number of surviving clonogens as a real clinical dose distribution gives. This opens a numerical way to be able to compare treatment plans from the DVH. Niemierko[5] defined the EUD mechanistically as follows:

$$EUD = \frac{N_f}{D_{ref}}\left(-\frac{\alpha}{\beta} + \sqrt{\left(\frac{\alpha}{\beta}\right)^2 + 4\frac{D_{ref}}{N_f}\left(\frac{\alpha}{\beta} + D_{ref}\right)\frac{\ln A}{\ln SF_2}}\right) \quad (1)$$

where

$$A = \frac{\sum_{i=1}^{n} v_i * p_i * SF_2^{\frac{D_i}{D_{ref}}\frac{\left(\frac{\alpha}{\beta}+\frac{D_i}{N_f}\right)}{\frac{\alpha}{\beta}+D_{ref}}}}{\sum_{i=1}^{n} v_i * p_i}$$

In this formulation, N_f is the number of fractions in the treatment, D_{ref} is the reference dose of 2 Gy, the α/β is the ratio of two radio-sensitivity parameters found in the linear quadratic model explaining the linear and quadratic parts of cell killing, SF_2 is the clonogenic cell survival fraction at a dose of 2 Gy, D_i is the dose being received by each partial volume segment, and v_i and p_i are, respectively, the local volumes and densities of clonogens.

We calculated EUDs for the IMRT and VMAT treatment plans using the formula shown in equation 1. When calculating the EUDs, we varied the values of SF_2 as 0.4, 0.5, and 0.6 while varying the values of the α/β ratio to 2, 6, and 10 for each value of SF_2 to determine appropriate model parameters for the future studies. Our value for N_f was 10 and the value for D_{ref} was 2 Gy. The DVH was divided into 10 partial volume segments each covering 10% of the structure volume. D_i was taken to be an average of the doses being received by the highest and lowest partial volumes. For example, when calculating the dose for the partial volume segment which spans 80% to 90% of the structure volume, we took D_i to be the average of the dose covering 80% of the structure volume and the dose covering 90% of the structure volume.

Niemierko[6,7] also came up with the concept of a generalized EUD (gEUD) with an empirical formula:

$$gEUD = \left(\sum_{i=1}^{n}\left(v_i D_i^a\right)\right)^{\frac{1}{a}} \quad (2)$$

where v_i is the fractional volume irradiated to a dose D_i, and "a" is a unitless tissue-specific parameter that describes the dose-volume effect. As the value of "a" becomes a large negative number, the gEUD leans toward the minimum dose

received by the tissue. When "a = 1," the gEUD is equal to the average dose. As the value of "a" becomes a large positive number, the value of the gEUD leans toward the maximum dose. For tissues which experience serial organ complication, the value of "a" should be a large positive number, for tissues that experience parallel organ complication, the value of "a" should be around 1, and for tumors, the value of "a" should be a large negative number. We also calculated gEUDs using formula shown in equation 2. D_i's were reused from our previous EUD calculation. Because the DVH was divided into 10 equal segments, v_i was kept constant at 0.10. While calculating gEUDs for PTV, we varied our fitting parameter "a" to integers from −1 to −16. For calculating gEUDs for normal tissues, we used fitting parameter "a" equals +7.

Tumor control probability

The TCP is a quantitative measurement of local tumor control which can be calculated from information obtained from a DVH. While values of TCP calculated from formulas may not be the reflection of reality, the relative values calculated for different DVHs are useful. TCPs are calculated[8] with the following mechanistic formula:

$$TCP = e^{-N * SF_2^{\frac{D}{D_{ref}} \frac{\frac{\alpha}{\beta} + \frac{D}{Nf}}{\frac{\alpha}{\beta} + D_{ref}}}} \quad (3)$$

where N is the number of clonogenic tumor cells (assumed in this study to be 4000, 40000, 400000, and 800000), D is EUD, N_f, D_{ref}, SF_2, and α/β are terms explained before. Radiation therapy is traditionally given in many fractions. This is because delivering the dose over time allows killing of maximum clonogenic tumor cells while having the least toxic effect on normal tissues. We calculated TCPs for each combination of N, SF_2, and α/β ratio using the formula shown in equation 3.

Another common way to calculate TCP is with the following empirical formula[7] shown in equation 4.

$$TCP = \frac{1}{1 + \left(\frac{TCD_{50}}{gEUD}\right)^{4\gamma_{50}}} \quad (4)$$

where TCD_{50} is the dose to control the tumor 50% of the time when the tumor is irradiated homogenously, gEUD is the gEUD calculated with formula shown in equation 2, and is a unitless fitting parameter that determines the slope of the dose-response curve. We also calculated values of TCP using the formula shown in equation 4. We varied the value of parameter "a" in equation 2 from -1 to -16 to get values of gEUD. We used a TCD_{50} value[9] of 22.17 Gy and varied γ_{50} to determine value of TCP that agreed the best with our mechanistic model prediction.

Normal tissue complication probability

The NTCP is a quantitative measurement of the probability a dose of radiation will have an undesirable effect on an organ. The following mechanistic formula[10] is used to calculate the NTCP as shown in equation 5.

$$NTCP = \frac{1}{\sqrt{2\pi}} \int_{-\infty}^{t} e^{-\frac{t^2}{2}} dt \quad (5)$$

where

$$t = \frac{D - TD_{50}(\vartheta)}{m * TD_{50}(\vartheta)} \qquad \vartheta = \frac{v}{v_{ref}} \qquad TD(\vartheta) = TD(1) \quad \vartheta^{-n}$$

ϑ is the fraction of the organ irradiated, V_{ref} is the reference volume for TD_{50}, TD_{50} is the tolerance dose to the reference volume which would lead to a 50% complication probability, n is a parameter which determines the volume dependence of the complication probability, and m is a parameter which determines the slope of the complication probability versus the dose curve. Dose-response models are commonly based on linear-quadratic model of cell killing which has two adjustable parameters: α (linear component of cell killing) and β (the quadratic component of cell killing). The α/β ratio is the dose at which the linear and quadratic components of cell killing have equal contributions.[11] The isoeffective dose is a method to account for the effect of fractionations in radiation therapy treatment that takes into account the behavior of early and late-responding tissues. This is calculated with the following formula[12] shown in equation 6 relative to a standard 2 Gy per fractionation scheme usually used in conventional fractionated radiation therapy.

$$EQD_2 = \frac{1 + \frac{D_f}{\alpha/\beta}}{1 + \frac{2}{\alpha/\beta}} \quad (6)$$

where D_f (=3 Gy) has been the fractionated dose used in the present treatment.

We compared the tissue-sparing capabilities of IMRT and VMAT by calculating the NTCPs for various tissues that included among others hippocampus, optical structures, etc., from each of the corresponding treatment plans. We calculated NTCPs using the formula shown in equation 5. Microsoft Excel's normal distribution function was used to calculate NTCPs once *t*-values were calculated with the formula shown in equation 5. Conventional fractionated radiation therapy usually uses doses of approximately 2 Gy/fraction and so typical value of the parameters TD_{50} used to calculate *t*-values are available in the literature[13] for 2 Gy/fraction schemes. However, we used 3 Gy/fraction for treatment in the present study. Using the isoeffective dose value of 1.25 as shown in equation 6, TD_{50} values[13] of brain (since the TD_{50} value of hippocampus is not known) and optical structures of 60 and 65 are modified and values of the parameters TD_{50}, m, and n used to calculate *t*-values are given in Table 1.

Another common method of calculating the NTCP for various tissues is through the following empirical formula[9] shown in equation 7.

$$NTCP = \frac{1}{1 + \left(\frac{TD_{50}}{gEUD}\right)^{4\gamma_{50}}} \quad (7)$$

Table 1: TD_{50}, *m*, and *n* values used to calculate normal tissue complication probability for each critical structure

	Hippocampus	Optic chiasm	Right optic nerve	Left optic nerve
TD_{50}	48	52	52	52
m	0.15	0.14	0.14	0.14
n	0.25	0.25	0.25	0.25

where TD_{50} is the tolerance dose that gives a 50% complication rate, gEUD, and γ_{50} are parameters previously explained. We also calculated NTCPs using the above formula. Modified TD_{50} values shown in Table 1 were used along with a constant γ_{50} value of 3.[14] Secondary to limitations on the availability of hippocampus-specific parameter estimates, the same calculation end point of necrosis that was used for the brain and optic structures were also used for the hippocampus.

Results

All VMAT and IMRT treatment plans met the RTOG trial 0933 criteria. The average EUDs calculated using equation 1 with SF_2 of 0.4, 0.5, and 0.6 and α/β ratios of 2, 6, and 10 for IMRT and VMAT treatment plans ranged from 25.74–29.11 Gy for IMRT to 25.27–28.58 Gy for VMAT treatment plans. In all cases, the average EUD for IMRT was greater than that of VMAT by about 2% ($P \leq 0.02$) as shown in Figure 1. In general, the average EUD increased with the α/β ratio and the SF_2 for both IMRT and VMAT. Examples of typical EUD (with $SF_2 = 0.5$ and $\alpha/\beta = 2$) and gEUD (with a = −11) for the PTV for each patient are shown in Figure 2. The average EUD and gEUD for IMRT was again greater by 2% compared to that for VMAT. Furthermore, we found that the calculated gEUDs of the PTV using equation 2 decreased when the fitting parameter, "a," decreased and the average gEUD was 2% higher in IMRT treatment plans than that of VMAT treatment plans when $-16 \leq a \leq -2$, and 3% when "a" = −1. In all cases, the difference between average IMRT and VMAT gEUDs were statistically significant ($P \leq 0.02$).

The TCPs for both IMRT and VMAT treatment plans were calculated using equation 3 with various SF_2, α/β, and estimated clonogenic cell counts. Figure 3 shows results of a typical TCP calculation with SF_2 of 0.5, α/β ratio of 2, and clonogenic cell counts estimated with CCD of 500 using formula 4. The ratio of average IMRT TCPs to average VMAT TCPs were also found to increase with the increase of SF_2, α/β ratio, and CCD values. We varied the value of γ_{50} in equation 4 and found that the TCP values were most agreeable with results obtained using the formula in equation 3 when $\gamma_{50} = 3.6$. Using equation 4, it was also found that the ratio of average IMRT TCPs over average VMAT TCPs varied from 1.00 to 1.03, as we varied the parameter "a" from −1 to −16. Figure 3 also shows a typical TCP calculation with "a" equals-11, $\gamma_{50} = 3.6$ and $TCD_{50} = 22.17$. Our results show that on the basis of TCP calculations, IMRT performed 2% better than VMAT using equation 3, and 1% better using

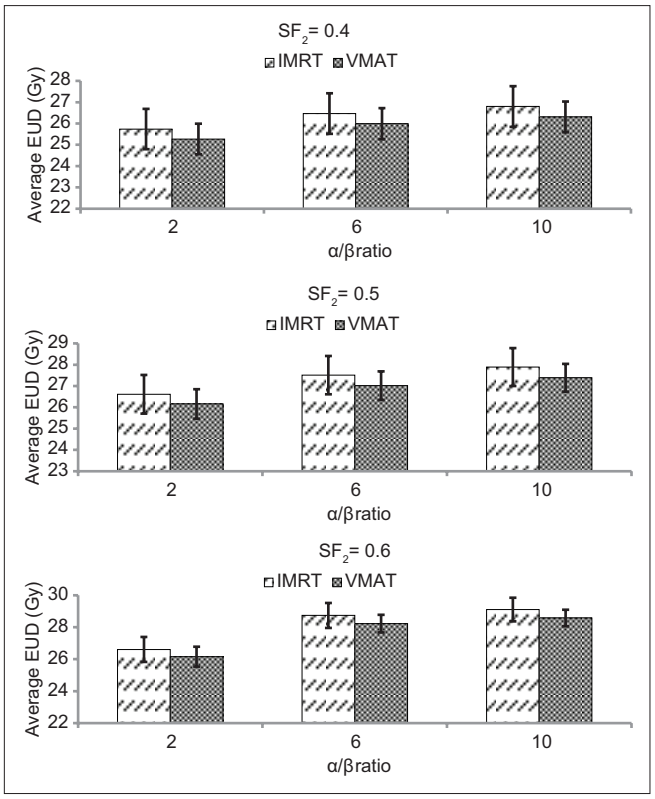

Figure 1: Average equivalent uniform dose for various SF_2 and α/β values for intensity-modulated radiation therapy and volumetric-modulated arc therapy treatment plans. Standard deviation is shown by error bars. All $P \leq 0.02$

equation 4; which again indicated better tumor control in favor of IMRT.

With the mechanistic formula shown in equation 5, NTCPs were calculated for hippocampus, optic chiasm, right optic nerves, and left optic nerves. Specifically, IMRT lowered the NTCP of optic chiasm by a factor of two, right and left optic nerves by a factor of twenty-five but raised the NTCP of hippocampus by a factor of thirty. Figure 4 contains the average gEUDs of critical structures for IMRT and VMAT treatment plans calculated with the formula shown in equation 2. The hippocampus in IMRT treatment plans had a higher gEUD than that of VMAT treatment plans ($P = 0.19$); however, the opposite was true for all the three optical structures ($P < 0.01$) which supports the previous trend obtained using the mechanistic formula. The average NTCPs calculated from gEUDs using equation 7 were greater for IMRT compared to VMAT for the hippocampus by about 27% ($P = 0.13$). The opposite was true for the optical structures, where the NTCPs calculated were lower for IMRT compared to VMAT by about 27% for optic chiasm, 62% for right optic nerve and 56% for left optic nerve ($P < 0.01$). The NTCP values per patient are shown in Figure 5. Figure 6 gives representative examples of dose shown in color-wash superimposed on an axial slice from the treatment planning CT set for both IMRT and VMAT.

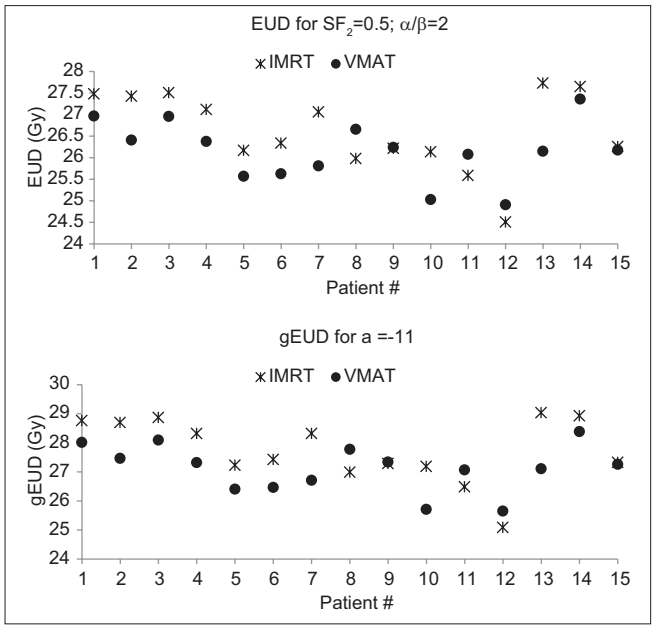

Figure 2: Comparison of intensity-modulated radiation therapy and volumetric-modulated arc therapy treatment plans using formulas for equivalent uniform dose and generalized equivalent uniform dose (generalized equivalent uniform dose). The average equivalent uniform dose for intensity-modulated radiation therapy versus volumetric-modulated arc therapy were 26.61 versus 26.16 and the average generalized equivalent uniform dose was 27.73 versus 27.12, respectively, with $P \leq 0.02$. For both the equivalent uniform dose and the generalized equivalent uniform dose, the ratio of intensity-modulated radiation therapy/volumetric-modulated arc therapy was 1.02

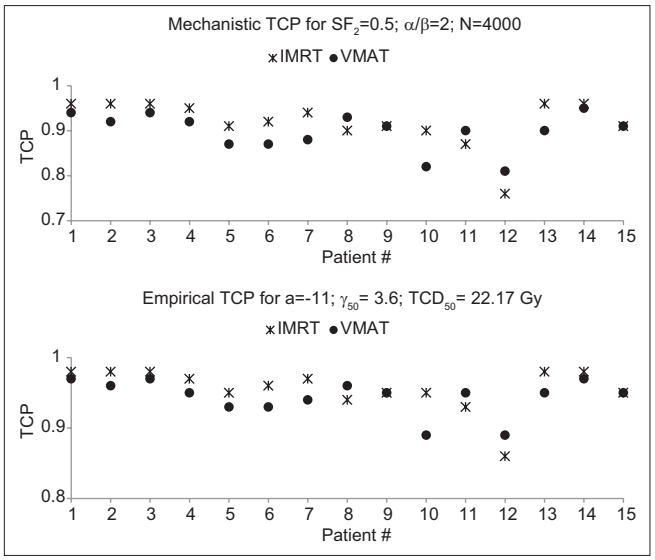

Figure 3: Comparison of tumor control probability values of intensity-modulated radiation therapy and volumetric-modulated arc therapy treatment plans. The average mechanistic tumor control probability was 0.92 for intensity-modulated radiation therapy and 0.90 for volumetric-modulated arc therapy, with an average ratio of intensity-modulated radiation therapy/volumetric-modulated arc therapy of 1.02. For the empirical tumor control probability, these values were 0.95 for intensity-modulated radiation therapy and 0.94 for volumetric-modulated arc therapy, respectively, with an average intensity-modulated radiation therapy/volumetric-modulated arc therapy ratio of 1.01

Discussion

In this manuscript, we estimate TCP, NTCP, and EUD values for IMRT- and VMAT-based treatment planning for hippocampal sparring WBRT. Our analysis suggests that both of these treatment approaches have their advantages. On the basis of TCP calculations, IMRT performed 2% better than VMAT using equation 3 and 1% better using equation 4. Both of these results indicate improved TCP in favor of IMRT-based treatments. Similarly, IMRT-based treatment plans resulted in lower NTCP values for the optic chiasm and optic nerves while higher NTCP parameters were obtained for the hippocampus. These results are consistent with reports suggesting VMAT may be better at sparing the hippocampus while meeting the treatment goals for the PTV.[15,16] Even though the relative difference in NTCP was large, the values for the NTCP's were so small that any rational statement based on this comparison is difficult to make.

In this manuscript, the parameters for empirical TCP and NTCP models were derived by fitting our data to mechanistic models. Values for our mechanistic models were taken from values in literature derived from clinical outcomes and tuned to derive optimal results. While these fitting parameters are not the most optimal, we feel they are appropriate for use. TCP calculations have been utilized for the treatment of brain tumors, both in the setting of stereotactic radiation therapy as well as with standard fractionation radiation therapy.[17-19] The parameters used in our model are consistent with what has been used in these reports. However, there is little information specific to the setting of HA-WBRT with IMRT or VMAT, where the overall dose distribution is more heterogeneous, and our results represent best estimates for this setting. In particular, little information specific to the hippocampus is available. For our NTCP calculations, we used similar parameters for the brain and the hippocampus, while the potential toxicity, as well as the dose at which the toxicity occurs, is very different, both clinically and mechanistically. The toxicity of interest for the hippocampus is the development of neurocognitive function decline which is likely to occur at lower doses than what would be expected for brain necrosis and further studies are necessary to establish $TD_{5/5}$ and $TD_{50/5}$ estimates that are specific for the hippocampus.

Conclusions

HA-WBRT is an effective treatment to the brain with its goal being to provide adequate coverage of the brain parenchyma while reducing the radiation doses to the hippocampus. The linac-based IMRT or VMAT are potential techniques to reduce doses to the hippocampus while treating the brain parenchyma. We found that IMRT treatment plans had a higher TCP than VMAT treatment plans and also had a lower NTCP for the optical structures. For the hippocampus, when the end point for the calculation was necrosis, IMRT plans had higher NTCP values when compared to VMAT treatment

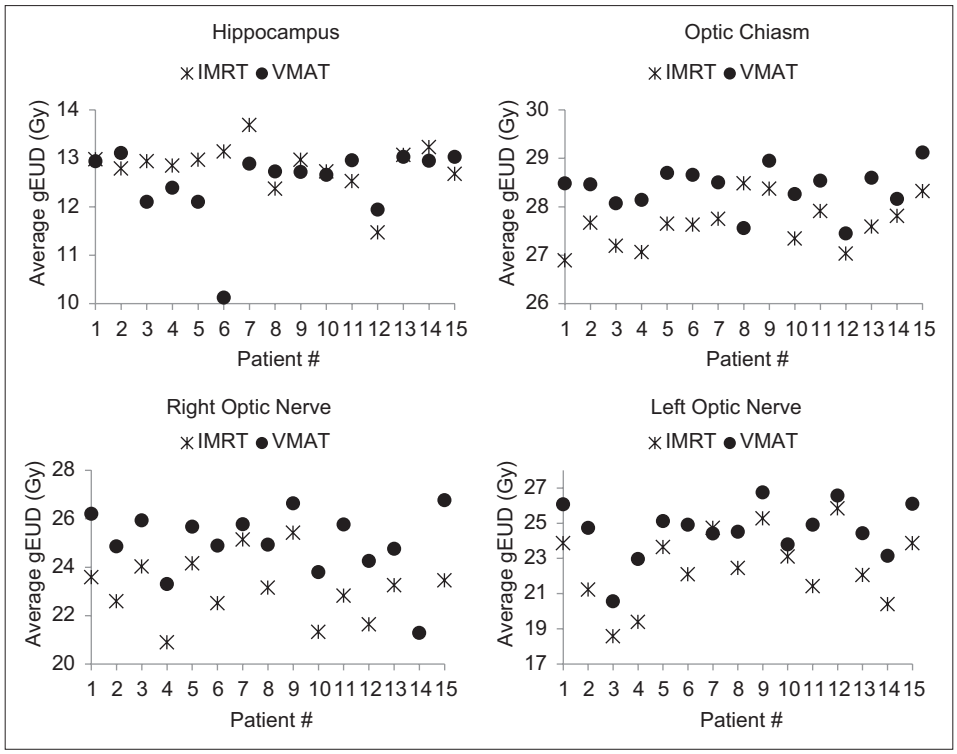

Figure 4: Generalized equivalent uniform doses of critical structures using parameter "a" = +7, for intensity-modulated radiation therapy and volumetric-modulated arc therapy treatment plans. The average generalized equivalent uniform dose in Gy for intensity-modulated radiation therapy versus volumetric-modulated arc therapy for the hippocampus, optic chiasm, right optic nerve, and left optic nerve were, respectively, (12.83 vs. 12.51), (27.64 vs. 28.38), (22.89 vs. 24.98), and (22.52 vs. 24.59)

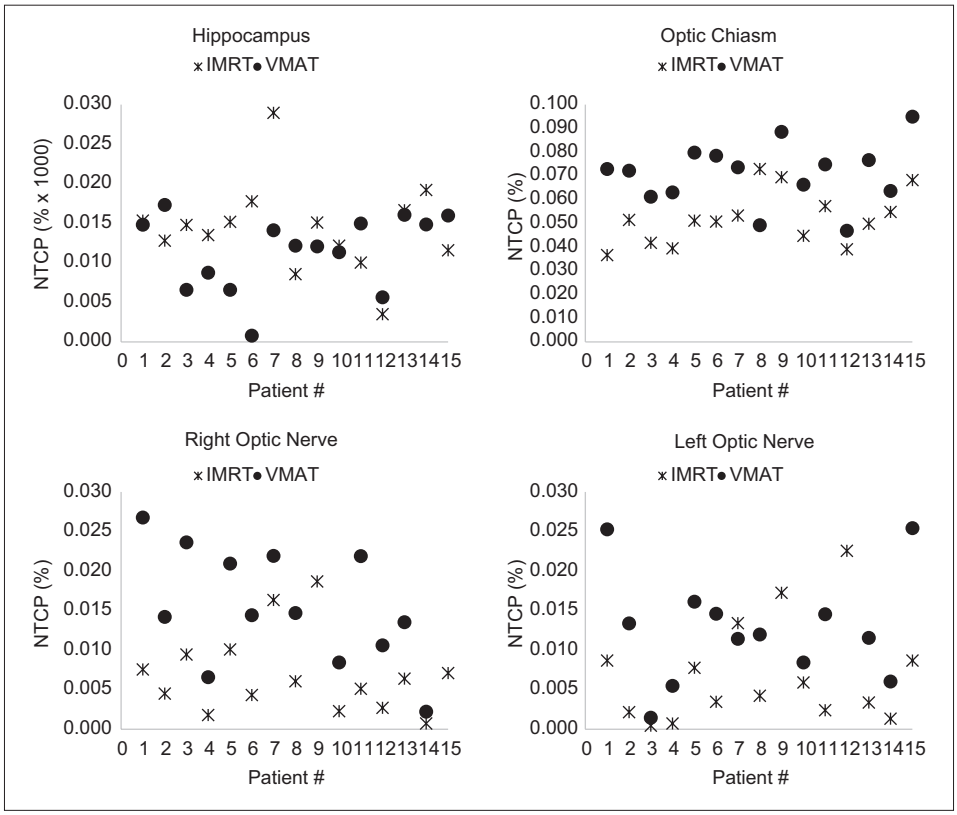

Figure 5: Comparison of normal tissue complication probability values for intensity-modulated radiation therapy and volumetric-modulated arc therapy treatment plans for the hippocampus, optic chiasm, right optic nerve, and left optic nerve

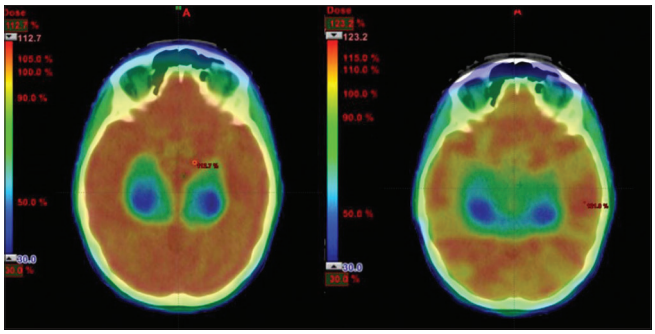

Figure 6: Comparison of typical dose distribution for a patient planned with hippocampal avoidance whole-brain radiation therapy-volumetric-modulated arc therapy (left) and intensity-modulated radiation therapy (right) superimposed on axial slice of planning computed tomography. The volumetric-modulated arc therapy plan has a lower maximum dose than that of the intensity-modulated radiation therapy treatment plan

plans. In this study, we have also found appropriate fitting parameters that can be used in empirical models for EUD, TCP, and NTCP. The concept of isoeffective dose to estimate TD50 for hippocampus and optical structures with 3 Gy per fraction used in this study could be applied to any radiation therapy study for other organs and cancers utilizing different fractionation scheme.

Financial support and sponsorship

Nil.

Conflicts of interest

There are no conflicts of interest.

References

1. Khuntia D, Brown P, Li J, Mehta MP. Whole-brain radiotherapy in the management of brain metastasis. J Clin Oncol 2006;24:1295-304.
2. Marsh JC, Gielda BT, Herskovic AM, Abrams RA. Cognitive sparing during the administration of whole brain radiotherapy and prophylactic cranial irradiation: Current concepts and approaches. J Oncol 2010;2010:198208.
3. Allen Li X, Alber M, Deasy JO, Jackson A, Ken Jee KW, Marks LB, *et al.* The use and QA of biologically related models for treatment planning: Short report of the TG-166 of the therapy physics committee of the AAPM. Med Phys 2012;39:1386-409.
4. Gondi V, Pugh SL, Tome WA, Caine C, Corn B, Kanner A, *et al.* Preservation of memory with conformal avoidance of the hippocampal neural stem-cell compartment during whole-brain radiotherapy for brain metastases (RTOG 0933): A phase II multi-institutional trial. J Clin Oncol 2014;32:3810-6.
5. Niemierko A. Reporting and analyzing dose distributions: A concept of equivalent uniform dose. Med Phys 1997;24:103-10.
6. Niemierko A. A generalized concept of equivalent uniform dose (EUD). Med Phys 1999;26:1101.
7. Gay HA, Niemierko A. A free program for calculating EUD-based NTCP and TCP in external beam radiotherapy. Phys Med 2007;23:115-25.
8. Ahmad S, Vogds BJ, McKenna F, Vlachaki MT. Tumor control probability (TCP) in prostate cancer: Role of radiobiological parameters and radiation dose escalation. J Xray Sci Technol 2009;17:347-54.
9. Okunieff P, Morgan D, Niemierko A, Suit HD. Radiation dose-response of human tumors. Int J Radiat Oncol Biol Phys 1995;32:1227-37.
10. Lyman JT. Complication probability as assessed from dose-volume histograms. Radiat Res Suppl 1985;8:S13-9.
11. Hall EJ, Giaccia AJ. Radiobiology for the Radiologist. Hagerstone, MD: Lippincott Williams & Wilkins; 2012.
12. Metcalfe P, Kron T, Hoban P. The Physics of Radiotherapy X-rays and Electrons. Madison, WI: Medical Physics Publishing Corporation; 2007. p. 450.
13. MacDonald SM, Ahmad S, Kachris S, Vogds BJ, DeRouen M, Gittleman AE, *et al.* Intensity modulated radiation therapy versus three-dimensional conformal radiation therapy for the treatment of high grade glioma: A dosimetric comparison. J Appl Clin Med Phys 2007;8:47-60.
14. Clemente-Gutiérrez F, Pérez-Vara C, Clavo-Herranz MH, López-Carrizosa C, Pérez-Regadera J, Ibáñez-Villoslada C, *et al.* Assessment of radiobiological metrics applied to patient-specific QA process of VMAT prostate treatments. J Appl Clin Med Phys 2016;17:341-67.
15. Wang BH, Hua W, Gu X, Wang XL, Li J, Liu LQ, *et al.* Dosimetric study of different radiotherapy planning approaches for hippocampal avoidance whole-brain radiation therapy (HA-WBRT) based on fused CT and MRI imaging. Australas Phys Eng Sci Med 2015;38:767-75.
16. Rong Y, Evans J, Xu-Welliver M, Pickett C, Jia G, Chen Q, *et al.* Dosimetric evaluation of intensity-modulated radiotherapy, volumetric modulated arc therapy, and helical tomotherapy for hippocampal-avoidance whole brain radiotherapy. PLoS One 2015;10:e0126222.
17. Pedicini P, Fiorentino A, Simeon V, Tini P, Chiumento C, Pirtoli L, *et al.* Clinical radiobiology of glioblastoma multiforme: Estimation of tumor control probability from various radiotherapy fractionation schemes. Strahlenther Onkol 2014;190:925-32.
18. Toma-Dasu I, Sandström H, Barsoum P, Dasu A. To fractionate or not to fractionate? That is the question for the radiosurgery of hypoxic tumors. J Neurosurg 2014;121 Suppl:110-5.
19. Shuryak I, Carlson DJ, Brown JM, Brenner DJ. High-dose and fractionation effects in stereotactic radiation therapy: Analysis of tumor control data from 2965 patients. Radiother Oncol 2015;115:327-34.

Original Article

Interfraction Variations in Organ Filling and Their Impact on Dosimetry in CT Image Based HDR Intracavitary Brachytherapy

Ramya Rangarajan

Department of Radiation Oncology, Government Royapettah Hospital, Chennai, Tamil Nadu, India

Abstract

Aim: Since anatomical and geometric variations occur with every fraction, planning, and dose optimization is necessary for every fraction of high-dose rate intracavitary brachytherapy of carcinoma cervix. In this study, we have tried to quantify the differences in doses to organs at risk (OAR) for each fraction of brachytherapy. **Methods and Materials:** One hundred and seventy computed tomography datasets of cervical cancer patients receiving intracavitary brachytherapy at our institution between January and April 2015 were analyzed. The volumes of the high-risk clinical target volume and OAR contoured were recorded for every insertion. Dose-volume histograms were generated and D90 and D100CTV and D0.1, D1, and D2cc were recorded for bladder, rectum, and sigmoid for each insertion. **Results:** Sixty-one percent had a decrease in bladder volume in the second fraction, 35% had an increase in bladder volume and 4% had no change in bladder volume. There was a strong positive correlation between increase in volume and dose (D2cc), which was statistically significant, $r_s = 0.441$, $P = 0.013$. Nearly 49.4% of patients had an increase in rectal volume during the second fraction. 45.9% had decrease in rectal volume during the second fraction. There was a positive correlation between the increase in volume and dose (D2cc), which was statistically significant, $r_s = 0.393$, $P = 0.010$. About 63.5% of the patients had a decrease in sigmoid volume during the second fraction, whereas 30.6% had an increase in volume and 5.9% had no change in volume. **Conclusion:** First, this study emphasizes the importance of imaging and planning for every fraction of brachytherapy to quantify the exact doses to the target and OAR s. Second, it is important to follow a uniform bladder protocol for every fraction, and adequate bowel preparation is needed for every fraction to minimize the interfraction variations. Finally, it also opens the realm of an adaptive planning strategy in cervical cancers which are known for rapid tumor regression during radiotherapy.

Keywords: Brachytherapy, dosimetry, interfraction variations

Received on: 26-07-2017 **Review completed on: 24-10-2017** **Accepted on: 11-11-2017**

Introduction

Concurrent chemoradiation is the standard of care for locally advanced cervical cancers. External beam radiotherapy is combined with intracavitary brachytherapy to achieve optimal results. High-dose rate intracavitary brachytherapy is commonly practiced worldwide and is usually given in fractionations. The number of fractions varies between different institutions. An EQD2 of 85–90 Gy to D90 to high-risk clinical target volume is recommended for tumors larger than 4 cm at the time of brachytherapy.[1,2] The total dose limit including external beam radiotherapy and brachytherapy for the bladder is 90 Gy EQD2 and 70–75 Gy EQD2 for rectum and sigmoid.

Since anatomical and geometric variations occur with every fraction, planning, and dose optimization is necessary for every fraction.[3-5] Changes in anterior rectal wall dose between two applications were reported by Hoskin *et al*.[3] They found an anterior rectal wall movement between 0 and 22 mm in relation to the surface of the ovoid between the first and second fractions. Since the organ dose variations can have important clinical implications, it is imperative to determine the dose to the target and OAR with every insertion.

In this study, we have tried to quantify the differences in doses to organs at risk (OAR) for each fraction of high-dose rate

Access this article online

Quick Response Code:

Website: www.jmp.org.in

DOI: 10.4103/jmp.JMP_90_17

Address for correspondence: Dr. Ramya Rangarajan, Department of Radiation Oncology, Government Royapettah Hospital, 2B, Maan Sarovar Kalpana Apartments, 37, Hospital Road, Saidapet, Chennai - 600 015, Tamil Nadu, India.
E-mail: ramyarronco@gmail.com

How to cite this article: Rangarajan R. Interfraction variations in organ filling and their impact on dosimetry in CT image based HDR intracavitary brachytherapy. J Med Phys 2018;43:23-7.

intracavitary brachytherapy which arises due to anatomical variations.

Materials and Methods

Case selection

One hundred and seventy computed tomography (CT) datasets of 85 consecutive locally advanced cervical cancer patients receiving intracavitary brachytherapy at our institution between January and April 2015 were analyzed. All patients received external beam radiotherapy dose of 50 Gy to the whole pelvis in 25 fractions along with weekly doses of cisplatin.

Technique

The applicator insertion was performed under general anesthesia in the operating room. A CT-magnetic resonance imaging (CT-MRI) compatible tandem ovoid applicator or a metallic tandem ring applicator was used for the patients. The tandem angle was 30° for the tandem ovoid applicator and 45° for the tandem ring applicator. Different ovoid dimensions ranging from 1.5 to 3 cm were used.

The bladder was catheterized in all patients using a Foley's catheter. Three milliliter of contrast and 4 ml of normal saline was instilled into the Foley's bulb, and the bladder was left to drain. After inserting the applicator and securing its position, vaginal packing with gauze was done with a tandem ovoid applicator. A rectal retractor was used instead of posterior vaginal packing with tandem ring applicator.

Contouring and planning

After the procedure, patients were shifted to CT simulator room (Somatom, Siemens, Erlangen, Germany) and computed tomography scans of the pelvis with 3 mm slices were taken. All CT images were exported to Oncentra planning system (Nucletron, an Elekta company, Stockholm, Sweden). GEC ESTRO GYN working group recommendations[6] were used to contour clinical target volume, bladder, rectum, and sigmoid for all patients. The volumes of the high-risk clinical target volume and OAR contoured were recorded for every insertion. High-dose rate brachytherapy was delivered with ^{192}Ir sources to a dose of 8 Gy to point A given 1 week apart for a total of two fractions. Dose-volume histograms (DVHs) were generated, volume of OARs, D0.1, D1, and D2cc (minimum doses to highest irradiated 0.1cc, 1cc, and 2cc area of OAR) were recorded for bladder, rectum, and sigmoid for each insertion.

Statistical analysis

The statistical analysis was performed using SPSS statistical package version 20 (IBM Corporation, New York, USA). Descriptive statistics such as median, interquartile range, minimum and maximum doses, and volumes were calculated. Spearman's correlation was used to find the correlation between changes in volume and dose. Patients were divided into two cohorts, namely those with an increase in volume in second fraction and those with a decrease in volume in the second fraction and significance of the changes in dosimetry were calculated using the Wilcoxon matched pair test.

Results

Variations in bladder volume and dose

Sixty-one percent had a decrease in bladder volume in second fraction, 35% had an increase in bladder volume, and 4% had no change in bladder volume. For patients with an increase in volume in the second fraction, the median increase in volume was 11 cc. The minimum increase in volume was 1cc and the maximum increase in volume was 127 cc (Range: 126). The median increase in D2cc bladder for the cohort of patients with an increase in volume in the second fraction was 0.90 Gy. For patients with decrease in bladder volume during the second fraction, the median decrease in volume was 9. The maximum decrease in volume during the second fraction was 15 cc (Range- 15). The median decrease in D2cc of the bladder for the cohort of patients with decrease in volume in the second fraction was 0.70 Gy [Table 1].

A Spearman's correlation was done to assess the relationship between increase in bladder volume and the increase in D2cc of the bladder in the second fraction. There was a strong positive correlation between increase in volume and dose (D2cc), which was statistically significant, $r_s = 0.441$, $P = 0.013$. There was a median increase in D2cc of 0.90 Gy in the cohort of patients with increase in bladder volume in the second fraction and this was found to be statistically significant by the Wilcoxon signed rank test ($Z = -4.801$, $P = 0.000$). There was a median decrease in D2cc of 0.70 Gy in the cohort of patients with a decrease in bladder volume in the second fraction and this was found to be statistically significant by the Wilcoxon signed rank test ($Z = -6.333$, $P = 0.000$).

Variations in rectal volume and dose

Nearly 49.4% of patients had an increase in rectal volume during the second fraction. 45.9% had decrease in rectal volume during the second fraction. The median increase in volume for patients with increase in volume in the second fraction was 8.5 cc. The minimum increase in volume was 1 cc and the maximum increase in volume was 54 cc (Range: 53). The median increase in D2cc rectum for the cohort of patients with increase in volume was 0.60 Gy. For patients with decrease in volume in the second fraction, the median decrease in volume was 7 cc. The maximum decrease in volume was 28 cc. The median decrease in dose for patients with decrease in volume during the second fraction was 0.70 Gy [Table 2].

A Spearman's correlation was performed to assess the relationship between increase in rectal volume and the increase in D2cc of the rectum in the second fraction. There was a positive correlation between increase in volume and dose (D2cc), which was statistically significant, $r_s = 0.393$, $P = 0.010$. There was a median increase in D2cc of 0.60 Gy in the cohort of patients with increase in rectal volume in the second fraction and this was found to be statistically significant

by the Wilcoxon signed rank test ($Z = -5.621$, $P = 0.000$) and there was a median decrease in D2cc of 0.70 Gy in the cohort of patients with decrease in rectal volume in the second fraction, which was found to be statistically significant by the Wilcoxon signed rank test ($Z = -5.621$, $P = 0.000$).

Variations in sigmoid dose and volume

Nearly 63.5% of patients had a decrease in sigmoid volume during second fraction, whereas 30.6% had an increase in volume and 5.9% had no change in volume. The median increase in volume for patients with increase in volume in second fraction was 4 cc. The minimum increase in volume was 2 cc and the maximum increase in volume was 13 cc (Range: 11). The median increase in D2cc sigmoid for the cohort of patients with increase in volume was 0.50 Gy. For patients with decrease in volume in second fraction, the median decrease in volume was 2 cc. The maximum decrease in volume was 21 cc. The median decrease in dose for patients with decrease in volume during second fraction was 0.30 Gy [Table 3].

A Spearman's correlation was done to assess the relationship between increase in sigmoid volume and the increase in D2cc sigmoid in second fraction. There was a strong positive correlation between increase in volume and dose (D2cc), which was statistically significant, $r_s = 0.485$, $P = 0.000$. There was a median increase in D2cc of 0.50 Gy in the cohort of patients with increase in sigmoid volume in second fraction and this was found to be statistically significant by the Wilcoxon signed rank test ($Z = -6.318$, $P = 0.000$) and there was a median decrease in D2cc of 0.30 Gy in the cohort of patients with decrease in sigmoid volume in second fraction, which was found to be statistically significant by the Wilcoxon signed rank test ($Z = -4$, $P = 0.000$).

Influence of bladder volume on rectal and sigmoid dosimetry

For the cohort of patients with increase in bladder volume during second fraction, variations in rectal and sigmoid dosimetry were analyzed. For patients with increase in bladder volume in second fraction, there was an increase in mean D0.1cc, D1cc, and D2cc of rectum. The average increase in D0.1cc, D1cc, and D2cc was 0.43 Gy, 0.44 Gy, and 0.40 Gy, respectively. A Spearman's correlation was used to assess the relationship between increase in bladder volume and the increase in D2cc of rectum. There was a positive correlation between increase in bladder volume and increase in D2cc of rectum, which was statistically significant, $r_s = 0.407$, $P = 0.023$.

For the cohort of patients with decrease in bladder volume during second fraction, there was a decrease in mean D1cc and D2cc of rectum. There was an average increase of 0.035 Gy to D0.1cc of rectum. The average decrease in D1cc and D2cc of rectum was 0.002 and 0.11 Gy, respectively. A positive spearman's correlation was found between decrease in bladder volume and decrease in D2cc of rectum, which was statistically significant, $r_s = 0.351$, $P = 0.009$.

Table 1: The median and interquartile range values of volume and dose for the two cohorts of patients with increase in volume in second fraction and decrease in volume in second fraction

Increase in volume in 2nd fraction	Median	Interquartile range
Bladder volume	11 cc	17
D0.1 cc	0.80 Gy	1
D1 cc	0.70	1
D2 cc	0.90	1
Decrease in volume in 2nd fraction	**Median**	**Interquartile range**
Bladder volume	−9 cc	7
D0.1 cc	−1.1 Gy	4
D1 cc	−0.90 Gy	2
D2 cc	−0.70 Gy	3

−: Decrease in volume/dose in second fraction

Table 2: The median and interquartile range values of volume and dose for the two cohorts of patients with increase in volume in second fraction and decrease in volume in second fraction

Increase in volume in 2nd fraction	Median	Interquartile range
Rectal volume	8.5	12.3
D0.1 cc	0.45 Gy	1.7
D1 cc	0.40	1.6
D2 cc	0.60	1.4
Decrease in volume in 2nd fraction	**Median**	**Interquartile range**
Rectal volume	−7 cc	8.5
D0.1 cc	−0.5 Gy	0.9
D1 cc	−0.50 Gy	0.7
D2 cc	−0.70 Gy	0.8

−: Decrease in volume/dose in second fraction

Table 3: The median and interquartile range values of volume and dose for the two cohorts of patients with increase in volume in second fraction and decrease in volume in second fraction

Increase in volume in 2nd fraction	Median	Interquartile range
Sigmoid volume	4 cc	4
D0.1 cc	0.70 Gy	1
D1 cc	0.60 Gy	1
D2 cc	0.50 Gy	0.8
Decreasein volume in 2nd fraction	**Median**	**Interquartile range**
Sigmoid volume	−2 cc	2
D0.1 cc	−0.10 Gy	1.1
D1 cc	−0.30 Gy	1.2
D2 cc	−0.30 Gy	1

−: Decrease in volume/dose in second fraction

For the cohort of patients with increase in bladder volume during the second fraction, the average increase in D0.1cc, D1cc, and D2cc of sigmoid was 0.30 Gy, 0.21 Gy, and 0.09 Gy, respectively. For the cohort of patients with decrease in bladder volume during the second fraction, there was an average increase in D0.1cc, D1cc, and D2cc of sigmoid. The average increase was 0.41 Gy, 0.16 Gy and 0.18 Gy, respectively, to D0.1cc, D1cc, and D2cc of sigmoid. A positive spearman's correlation was found between increase in bladder volume and D2cc of sigmoid but was not statistically significant, $r_s = 0.048$, $P = 0.798$. A negative spearman's correlation was found between decrease in bladder volume and D2cc of sigmoid, which was not statistically significant, $r_s = -0.006$, $P = 0.965$.

Discussion

In the recent years, three-dimensional image-guided brachytherapy[7-10] is slowly replacing the conventional X ray-based, point A-based dose reporting in gynecological brachytherapy. Groupe Européen de Curiethérapie– European Society for Radiotherapy and Oncology has published guidelines on target volume definitions and DVH parameters.[6,11] Organs at risk located in the pelvis are highly distensible organs. The changes in filling of these organs can have a significant impact on the dose delivered to these organs. There are some institutions which follow a fixed bladder protocol and several studies have reported the dosimetric changes arising out of differences in the organ volumes.[12,13]

Interfraction variations in dosimetry can arise as a result of organ deformation, tumor response during treatment and variations in applicator placement. Variations arising due to applicator placement can be minimized by using the same applicator for every insertion and by using rigid/fixed applicators like tandem ring. Imaging modalities with better soft tissue delineation like MRI can be used to assess tumor response during treatment. By following a uniform bladder filling or emptying routine, it is possible to minimize the variations arising due to organ deformation.[14] In the present study, the same type of applicators was used during subsequent fractions for each patient and a standard loading pattern was followed with each insertion.

In a study by Kirsitis *et al*., using TR applicators and MRI imaging, the mean variation in rectal 2cc dose was found to be 3.5 Gy and the mean variation in bladder 2cc dose was found to be 4.2 Gy.[15] They reported that 21% of their patients would have received more doses to the OAR in the second fraction if subsequent imaging was not done for the second fraction. A mean variation of 61% to D2cc bladder was reported by Davidson *et al*.[14] They found a mean variation of 1.7 Gy to D2cc of rectum. In the present series, 35% of the patients had an increase in dose to 2 cc of the bladder in second fraction. A median increase in dose of 0.60 Gy to D2cc rectum was found during the second fraction. Nearly 30.6% of the patients in the present series had an increase in volume of sigmoid during the second fraction and the median increase in dose to sigmoid was 0.50 Gy.

In the present study, more number of patients had decrease in bladder volume during the second fraction; although, all patients were catheterized during the procedure and the bladder was left to drain. Larger filling volumes of OARs expose more of the organs to a higher dose. Here, we found a significant correlation between the organ filling volumes and the corresponding D0.1cc, D1cc, and D2cc doses to OAR. Does that mean that organ volumes should be kept to a minimum to decrease the dose received by these organs?

The present study shows an impact on rectal dosimetry with changes in bladder filling, but there is no significant impact on sigmoid dosimetry. There are some studies which have shown decrease in the small intestine and sigmoid doses when the bladder is distended during brachytherapy.[16] Although a decrease in volumes of OARs led to a decrease in dose during the second fraction, when there is a major organ deformation in successive fractions, there is a high chance of different subvolumes of OAR receiving a high dose.

The limitations of the present study include the retrospective nature and the contouring uncertainties of the organs on CT images. Changes in clinical target volume with every fractionation and the consequent changes in dosimetry were not analyzed in the present study. Since bladder filling seems to have an impact on the OAR dosimetry, future studies should aim to determine the optimal bladder filling protocol to minimize dose to OARs.

Considering the interfraction variations which can occur during intracavitary brachytherapy, it is necessary to repeat imaging before each fraction to accurately quantify doses to the target and OAR. Individualized planning with each insertion helps in accurate estimation of doses to OAR, failing which detrimental effects will be seen in the clinical scenario.

Conclusion

The present study highlights the magnitude of variations in the volumes of organs and the target and the corresponding doses received by them in successive fractions of brachytherapy. First, this study emphasizes the importance of imaging and planning for every fraction of brachytherapy to quantify the exact doses to the target and OARs. Second, it is important to follow a uniform bladder protocol for every fraction, and adequate bowel preparation is needed for every fraction to minimize the interfraction variations. Finally, it also opens the realm of an adaptive planning strategy in cervical cancers which are known for rapid tumor regression during radiotherapy.

Acknowledgment

The authors would like to thank (1) Dr. S. Saravanan, Dr.S. Kalyani, Department of Radiation Oncology, Government Royapettah Hospital. (2) Mrs. Vijayalakshmi, Department of Radiation Oncology, Government Royapettah

Hospital. (3) Mrs. Kumari, Department of Radiation Oncology, Government Royapettah Hospital.

Financial support and sponsorship

Nil.

Conflicts of interest

There are no conflicts of interest.

References

1. Dimopoulos JC, Lang S, Kirisits C, Fidarova EF, Berger D, Georg P, *et al.* Dose-volume histogram parameters and local tumor control in magnetic resonance image-guided cervical cancer brachytherapy. Int J Radiat Oncol Biol Phys 2009;75:56-63.
2. Dimopoulos JC, Pötter R, Lang S, Fidarova E, Georg P, Dörr W, *et al.* Dose-effect relationship for local control of cervical cancer by magnetic resonance image-guided brachytherapy. Radiother Oncol 2009;93:311-5.
3. Hoskin PJ, Cook M, Bouscale D, Cansdale J. Changes in applicator position with fractionated high dose rate gynaecological brachytherapy. Radiother Oncol 1996;40:59-62.
4. Stitt JA, Fowler JF, Thomadsen BR, Buchler DA, Paliwal BP, Kinsella TJ, *et al.* High dose rate intracavitary brachytherapy for carcinoma of the cervix: The Madison system: I. Clinical and radiobiological considerations. Int J Radiat Oncol Biol Phys 1992;24:335-48.
5. Kim RY, Meyer JT, Plott WE, Spencer SA, Meredith RF, Jennelle RL, *et al*. Major geometric variations between multiple high dose rate applications of brachytherapy in cancer of the cervix: Frequency and type of variation. Ther Radiol 1995;195:419-22.
6. Pötter R, Haie-Meder C, Van Limbergen E, Barillot I, De Brabandere M, Dimopoulos J, *et al.* Recommendations from gynaecological (GYN) GEC ESTRO working group (II): Concepts and terms in 3D image-based treatment planning in cervix cancer brachytherapy-3D dose volume parameters and aspects of 3D image-based anatomy, radiation physics, radiobiology. Radiother Oncol 2006;78:67-77.
7. Viswanathan AN, Thomadsen B, American Brachytherapy Society Cervical Cancer Recommendations Committee, American Brachytherapy Society. American Brachytherapy Society consensus guidelines for locally advanced carcinoma of the cervix. Part I: General principles. Brachytherapy 2012;11:33-46.
8. Dankulchai P, Petsuksiri J, Chansilpa Y, Hoskin PJ. Image-guided high-dose-rate brachytherapy in inoperable endometrial cancer. Br J Radiol 2014;87:20140018.
9. Okuma K, Yamashita H, Kobayashi R, Nakagawa K. A study of high-dose-rate intracavitary brachytherapy boost for curative treatment of uterine cervical cancer. J Contemp Brachytherapy 2015;7:128-34.
10. van den Bos W, Beriwal S, Velema L, de Leeuw AA, Nomden CN, Jürgenliemk-Schulz IM, *et al.* Image guided adaptive brachytherapy for cervical cancer: Dose contribution to involved pelvic nodes in two cancer centers. J Contemp Brachytherapy 2014;6:21-7.
11. Haie-Meder C, Pötter R, Van Limbergen E, Briot E, De Brabandere M, Dimopoulos J, *et al.* Recommendations from gynaecological (GYN) GEC-ESTRO Working Group (I): Concepts and terms in 3D image based 3D treatment planning in cervix cancer brachytherapy with emphasis on MRI assessment of GTV and CTV. Radiother Oncol 2005;74:235-45.
12. Adli M, Garipagaoglu M, Kocak Z. Effect of bladder distention on bladder base dose in gynaecological intracavitary high dose rate brachytherapy. Br J Radiol 2009;82:243-8.
13. Kim RY, Shen S, Lin HY, Spencer SA, De Los Santos J. Effects of bladder distension on organs at risk in 3D image-based planning of intracavitary brachytherapy for cervical cancer. Int J Radiat Oncol Biol Phys 2010;76:485-9.
14. Davidson MT, Yuen J, D'Souza DP, Batchelar DL. Image-guided cervix high-dose-rate brachytherapy treatment planning: Does custom computed tomography planning for each insertion provide better conformal avoidance of organs at risk? Brachytherapy 2008;7:37-42.
15. Kirisits C, Lang S, Dimopoulos J, Oechs K, Georg D, Pötter R, *et al.* Uncertainties when using only one MRI-based treatment plan for subsequent high-dose-rate tandem and ring applications in brachytherapy of cervix cancer. Radiother Oncol 2006;81:269-75.
16. Harmon G, Chinsky B, Surucu M, Harkenrider M, Small W Jr. Bladder distension improves the dosimetry of organs at risk during intracavitary cervical high-dose-rate brachytherapy. Brachytherapy 2016;15:30-4.

Original Article

Dosimetric and Radiobiological Evaluation of Patient Setup Accuracy in Head-and-neck Radiotherapy Using Daily Computed Tomography-on-rails-based Corrections

Ines-Ana Jurkovic, Esengul Kocak-Uzel[1], Abdallah Sherif Radwan Mohamed[2], Eleftherios Lavdas[3], Sotirios Stathakis, Nikos Papanikolaou, David C Fuller[2], Panayiotis Mavroidis[4]

Department of Radiation Oncology, University of Texas Health Sciences Center at San Antonio, San Antonio, TX, USA, [1]Department of Radiation Oncology, Istanbul Medipol University, Istanbul, Turkey, [2]Department of Radiation Oncology, University of Texas MD Anderson Cancer Center, Houston, USA, [3]Department of Medical Radiological Technologists, Technological Education Institute of Athens, Greece, [4]Department of Radiation Oncology, University of North Carolina, Chapel Hill, NC, USA

Abstract

Introduction: This study evaluates treatment plans aiming at determining the expected impact of daily patient setup corrections on the delivered dose distribution and plan parameters in head-and-neck radiotherapy. **Materials and Methods:** In this study, 10 head-and-neck cancer patients are evaluated. For the evaluation of daily changes of the patient internal anatomy, image-guided radiation therapy based on computed tomography (CT)-on-rails was used. The daily-acquired CT-on-rails images were deformedly registered to the CT scan that was used during treatment planning. Two approaches were used during data analysis ("cascade" and "one-to-all"). The dosimetric and radiobiological differences of the dose distributions with and without patient setup correction were calculated. The evaluation is performed using dose–volume histograms; the biologically effective uniform dose ($\bar{\bar{D}}$) and the complication-free tumor control probability (P_+) were also calculated. The dose–response curves of each target and organ at risk (OAR), as well as the corresponding P_+ curves, were calculated. **Results:** The average difference for the "one-to-all" case is 0.6 ± 1.8 Gy and for the "cascade" case is 0.5 ± 1.8 Gy. The value of P_+ was lowest for the cascade case (in 80% of the patients). **Discussion:** Overall, the lowest P_1 is observed in the one-to-all cases. Dosimetrically, CT-on-rails data are not worse or better than the planned data. **Conclusions:** The differences between the evaluated "one-to-all" and "cascade" dose distributions were small. Although the differences of those doses against the "planned" dose distributions were small for the majority of the patients, they were large for given patients at risk and OAR.

Keywords: Biologically effective uniform dose, computed tomography-on-rails, dose–volume histogram, radiobiological measures, treatment planning, tumor control

Received on: 12-09-2017 **Review completed on: 18-01-2018** **Accepted on: 18-01-2018**

Introduction

Computed tomography (CT) is the primary imaging mode for planning in radiotherapy (RT). The accuracy of RT depends on many factors, including accurate patient setup during the treatment.[1-3] Positioning uncertainties are the potential source of errors in the radiation therapy that may lead to a dose delivery that is different from the one that was intended to be given originally. For the last few years, the use of image-guided RT (IGRT) tries to reduce the magnitude of uncertainty in patient setup.[4] There are several imaging modalities used for IGRT, one of which is CT-on-rails.[5-7] CT-on-rails gives a complete three-dimensional representation of patient anatomy and enables accurate internal organ delineation and patient setup corrections. Variations in dose delivery stem from setup errors, internal organ motion, and deformation, which can contribute to underdosage of the tumor or overdosage of normal tissue. Those variations may potentially be related to a reduction of local tumor control and an increase of side effects.

Access this article online

Quick Response Code:

Website: www.jmp.org.in

DOI: 10.4103/jmp.JMP_113_17

Address for correspondence: Dr. Panayiotis Mavroidis, Department of Radiation Oncology, University of North Carolina, Chapel Hill, NC, USA.
E-mail: panayiotis_mavroidis@med.unc.edu

How to cite this article: Jurkovic IA, Kocak-Uzel E, Mohamed AS, Lavdas E, Stathakis S, Papanikolaou N, *et al*. Dosimetric and radiobiological evaluation of patient setup accuracy in head-and-neck radiotherapy using daily computed tomography-on-rails-based corrections. J Med Phys 2018;43:28-40.

Dose–volume histograms (DVHs), minimum, maximum, and mean doses, as well as isodose distribution review on the axial slices are the tools that are mainly used in RT plan evaluation. These tools do not take into account the radiobiological characteristics of the organs at risk (OAR) and tumors. Radiobiological measures that have been proposed in the treatment plan evaluation are the biologically effective uniform dose (BEUD) ($\bar{\bar{D}}$) and the complication-free tumor control probability (P_+).[8,9] $\bar{\bar{D}}$ is a concept that assumes equivalency of the different dose distributions when they are causing the same probability of tumor control or normal tissue complication.[10]

The goal of the study is to evaluate the expected clinical impact of dose delivery when setup corrections are taken into account.

Materials and Methods

Ten head-and-neck cancer patients with different tumor locations and sizes were selected for this study. Optimal plans were calculated for the patients' treatment based on their planning CT, and CT-on-rail images were taken in each fraction before the treatment. Three sets of dose distributions were calculated for each patient and compared based on several dosimetric and radiobiological parameters.[10-15]

Treatment planning and computed tomography-on-rails acquisition

Patients' baseline planning was performed on the ADAC Pinnacle Treatment Planning System. An in-room image-guided system with CT-on-rails was used for the daily setup imaging and corrections CT-on-rails system (EXaCT, Varian Oncology Systems, Palo Alto, CA, USA). The online correction was performed before each treatment, to align target volumes. For each fraction, CT-on-rails image sets were taken and the original IMRT contours were overlaid on each daily CT set to acquire and verify the couch corrections needed for the setup adjustments. CT sets taken for each fraction were then used for further analysis. For the "cascade" case, the planning CT was applied to the 1st day of treatment CT-on-rails image set and that way we got the 1st-day results. Then, the 1st-day results were applied to the 2nd-day CT-on-rails image set, the 2nd-day results to the 3rd day, etc. final deformation was then used for the comparison with the planned data. In the "one-to-all" case, the planning CT was applied to all of the CT-on-rail image sets of each patient and the final set was used for further analysis and comparison.

This study evaluates treatment plans based on the expected effect of the patient setup correction (done on the basis of the everyday CT-on-rails) on the dose distribution and plan parameters.

Different sensitive OAR was evaluated for each patient case depending on the area of the treatment [Table 1].

Data registration

In this study, each patient had a reference kilovoltage CT taken that was then used for the development of the treatment plan; this CT is referred to as planning CT. The planning CT images that were exported from the treatment planning system with the corresponding plan dose and structures, for the ten chosen head-and-neck cancer patients, were imported into the Velocity AI (Velocity AI, Velocity Medical Solutions, Atlanta, GA, USA)[16] through the DICOM RT protocol.[17,18] DICOM registration was used to register dose data to the plan CT. For the selected previously delineated and imported structures, DVH data were exported. Next final transformation of the CT-on-rails data set for each of the two studied approaches was imported and registered to the planning CT. CT-on-rails resampled dose data were then registered to the planning CT. For the same previously selected structures, DVHs were calculated and exported. DVH files were then multiplied by the correct number of fractions to get the total dose for each patient [Table 2].

Dosimetric and radiobiological treatment plan evaluation

For the dosimetric evaluation of the treatment plan, DVHs are routinely used together with the mean dose of the dose distribution to the tumor planning target volume (PTV) and tolerance doses of the various tissues. Tolerance doses are usually given as the length of the irradiated portion of structure or fraction (volume) of the organ treated. These data are derived from patient observations and follow the conventional fraction schedule.[19,20] The dose constraints that were used for plan optimization in our study are given in Table 3.

Table 1: Sensitive organs at risks evaluated per patient

Patient#	OARs
1	Mandible, larynx, spinal cord, brainstem, parotids
2	Mandible, larynx, spinal cord, brainstem, parotids
3	Mandible, larynx, spinal cord, brainstem, parotids
4	Mandible, larynx, spinal cord, parotids
5	Mandible, spinal cord, brainstem, parotids
6	Optic chiasm, brainstem, eyes, optic nerves
7	Larynx, brainstem, parotids, right orbit
8	Spinal cord, brainstem, parotids, orbits
9	Brainstem, optic chiasm, parotids
10	Brainstem, optic chiasm, orbits, optic nerves

OAR: Organs at risk

Table 2: Prescription values per patient

Patient#	Number of fractions	Total dose (Gy)
1	33	69.96
2	35	70
3	35	70
4	33	69.96
5	30	60
6	32	64
7	33	70
8	30	60
9	35	70
10	35	70

In this study, linear-quadratic-Poisson model is used to describe the dose–response relations of the tumors and normal tissues:

$$P(D) = \exp\left(-e^{e\gamma - \left(D / D_{50}\right)\cdot\left(e\gamma - \ln\ln 2\right)}\right) \quad (1)$$

where $P(D)$ is the probability to control the tumor or induce a certain injury to a normal tissue that is irradiated uniformly with a dose D. D_{50} is the dose which gives a 50% response, and γ is the maximum normalized dose–response gradient. Parameters D_{50} and γ are organ and type of clinical endpoint specific and can be derived directly from clinical data.[12-14] The response of a normal tissue to a nonuniform dose distribution is given by the relative seriality model which accounts for the volume effect. The dose–response parameters that were used in this study are based on the published data and presented in Table 4.[21] This study is assuming that the 10 patients are of average radiosensitivity, thus characterized by the mean estimates of the radiobiological parameters presented.

Theory for applied methodology

Dosimetric evaluation does not take into account the biological characteristics of the tumor. Different solutions to this problem have been recommended.[22-24] The article by Mavroidis *et al*.[10] generalized the mathematical expressions of D_{eff}[25] and EUD[26] to deal with multiple target or normal tissue cases and introduced the BEUD concept. This is the dose that causes the same tumor control or normal tissue complication probability as the real dose distribution. This allows for the comparison of treatment plans based on the radiobiological endpoints by normalizing dose distributions to a common prescription point and plotting the tissue response probability versus $\bar{\bar{D}}$, which is given from the following analytical formula:

$$P(\bar{D}) = P(\bar{\bar{D}}) \Rightarrow \bar{\bar{D}} = \frac{e\gamma - \ln(-\ln(P(\bar{D})))}{e\gamma - \ln(\ln(2))} \quad (2)$$

The scalar quantity P_+, which expresses the probability of achieving tumor control without causing severe damage to normal tissue, can be estimated from the following mathematical expression:[8]

$$P_+ = P_B - P_{B\cap I} \approx P_B - P_I \quad (3)$$

where P_B is the probability of getting benefit from treatment (tumor control) and P_I is the probability of causing severe injury to normal tissues (complications).

Table 3: Dose constraints for plan optimization for the various head-and-neck structures used for plan comparison

Organ	Data
Spinal cord	Mean <45 Gy, 50 Gy max (0.3 cc)
Brainstem	Mean <54 Gy, 60 Gy max (0.3 cc)
Chiasm	Mean <50 Gy, 54 Gy max (up to 55-60 Gy) (0.3 cc)
Optic nerves	Mean <54 Gy, 60 Gy max (0.3 cc)
Oral cavity	Mean <45 Gy
Larynx	Mean <40 Gy (up to<50 Gy)
Parotids	One parotid mean <15-20 Gy, both mean <25-26 Gy
Mandible	Max 70 Gy or V75 <1 cc, max 66 Gy

Table 4: Summary of the model parameter values used. The α/β was assumed to be 3 Gy for normal tissues and 10 Gy for the targets

Structure	D_{50} (Gy)	γ	s	Endpoint
PTV	51.0	7.5	-	Control
Spinal cord	57.0	6.7	1.00	Cervical myelopathy
Parotid gland	46.0	1.8	0.01	Xerostomia
Mandible	70.3	3.8	1.00	Marked limitation of joint function
Brainstem	65.1	2.4	1.00	Necrosis infarction
Brain	60.0	2.6	0.64	Necrosis infarction
Larynx	78.8	4.8	0.66	Cartilage necrosis
Esophagus	62.3	2.0	0.11	Clinical stricture/perforation
Oral cavity	70.0	3.0	0.50	Mucositis
Thyroid	90.0	2.0	0.1	Radiation-induced hypothyroidism
Unspecified normal tissue	65.0	2.3	1.00	Necrosis

PTV: Planning target volume

Statistical analysis

The different dose distributions of the study were radiobiologically evaluated using the radiation sensitivities of the tumors and OARs involved to calculate the probabilities of benefit and injury, as well as the values of complication-free tumor control probability P_+ and $\bar{\bar{D}}$.

Statistical analysis is done for P_+ clinical delivered values for the three cases – one-to-all, cascade, and planed values. Nonparametric statistical tests were used since they have no assumptions regarding distribution of underlying populations or variance. In view of the fact that our sample size is rather small (n = 10), several nonparametric tests for small samples were performed on the calculated data:

- The Mann–Whitney U-test
- The sign test
- The Wilcoxon signed-rank test
- The Kendall tau rank correlation coefficient.

The Mann–Whitney U-test is used to decide whether or not there is a difference between the two groups. The groups compared were one-to-all versus planned values, cascade versus planned values, and one-to-all versus cascade values. The sign test was used to determine whether planned and CT-on-rails calculated data are different. The most accurate nonparametric test for paired data is the Wilcoxon signed-rank test. With this test, we test our null hypothesis that when it comes to calculated P_+ values, CT-on-rails data will produce worse results than the planned data. The Kendall tau rank correlation coefficient is used for nonparametric data and is used to measure the degree of correspondence between sets of rankings where the measures are not equidistant.

Results

Graphical evaluation of the different plans

In Figure 1 (patient 9 example) and in Appendix Figures 1 and 2, the treatment plans are compared in terms of the DVH and BEUD of benefit ($\bar{\bar{D}}_B$). The dose–response curves of each target and OAR, together with the corresponding P_+ curves, are presented for the individual patients and plans. The dose–response curves are normalized to the $\bar{\bar{D}}_B$, which is forcing the response curves of the PTV (P_B) of the evaluated cases to coincide.

In Appendix Figures 1 and 2, more qualitative description of the comparison is presented. For most of the cases, it is shown that the treatment plan is satisfying plan objectives. In most cases, OAR is spared very well apart from a few that are located close to the PTV, left parotid for patient 1, larynx for patient 2, right parotid for patient 3, mandible for patients 4 and 5, left optic nerve for patient 6, right parotid for patient 7, optic chiasm for patient 9, and optic nerves for patient 10.

Overall, the cascade case, when it comes to the PTV coverage, followed the plan values more closely than the one-to-all case, which is also visible from the plots in Appendix Figures 1 and 2. Plotting the curves of P_B, P_I, and P_+ of the three cases (plan, one-to-all, and cascade) on the same diagram shows that the corresponding curves of the PTVs (P_B) for the three cases coincide. In this situation, the response curves of the OAR (P_I) determine the difference in the plans that are compared, i.e., which case is superior from the radiobiological point of view. In these plots, P_+ is also used as an objective that depicts the quality of the cases being compared.

Quantitative summary of the dosimetric and radiobiological metrics

The values obtained for structures based on their tolerance doses [Table 3] are listed in Appendix Table 1. Based on those values, the differences between the planned and case values were calculated. In Appendix Tables 1-3, the quantitative summary of the physical and biological comparisons is presented. The values (per patient and case) that represent the highest P_+ and the lowest P_I are highlighted in bold.

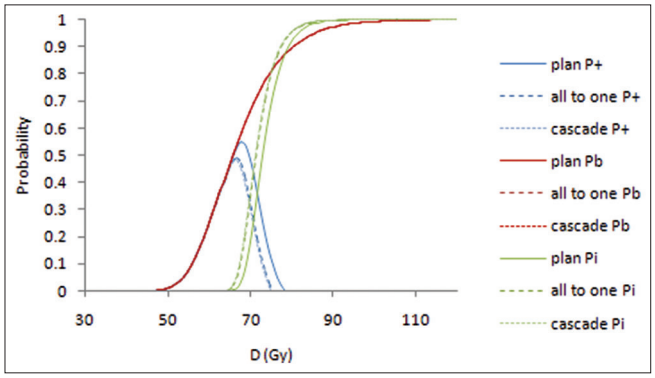

Figure 1: The curves derived from the radiobiological evaluation of the dose distributions are plotted, with the on the $\bar{\bar{D}}_B$ dose axis. The solid line indicates the planned dose distribution, while the dashed line refers to the one-to-all case and the dotted line to the cascade case. These results correspond to patient 9

Table 5 lists the differences in P_B, P_I, and P_+ between each case and the planned values. The higher the value of the P_I difference, the higher is the P_I for the particular case (same goes for the P_+ and P_B comparison). The cascade case shows higher P_I values in 70% of the cases compared to the one-to-all case. The P_I plan values are lower than either of the cases in three patients out of ten.

The dose variations in the PTV are listed in Table 6. The average percentage differences in minimum values were 3.23% and 3.11% for the one-to-all versus plan and cascade versus plan cases, respectively, and 0.49% and 0.57% in the maximum values, respectively.

For both analyzed cases, PTV coverage at the prescription dose and mean/maximum doses to the OAR are the same or slightly worse than it was in the plan [Appendix Table 1]. Average difference for the dosimetric values comparison of the "one-to-all" case to the planned values is 0.6 ± 1.8 Gy and for the "cascade" case to plan is 0.5 ± 1.8 Gy. When the patients are grouped in three groups based on the tumor location, the variation is 0.2 ± 0.4 Gy for both the "one-to-all" and "cascade" cases for the first group, 1.3 ± 3.3 Gy and 1.2 ± 3.4 Gy for the second group, respectively, and 0.2 ± 0.3 Gy for the third group, respectively. Table 6 shows that plans are not very homogeneous with some of the homogeneity actually improving with the one-to-all or cascade cases.

In Appendix Table 2, the clinical column indicates the biological effect calculated based on the prescribed dose delivered in the cases compared. The optimal column shows the corresponding highest achievable P_+ after dose escalation. Since the probability of achieving tumor control without causing severe damage to normal tissues is the pure benefit from the treatment (tumor control probability − normal tissue complication probability), in the case where the values of P_B are comparable, P_+ is going to be lower mainly due to the higher P_I. For the 10 patients, P_+ is lowest for the cascade case in the clinical column (in the 80% of cases total). Clinical standard for the overall P_I is usually set at 5%. Only for one patient, patient 4, P_I is at this acceptable level. Overall, the lowest P_I is present in the one-to-all cases. Higher overall P_I for the rest of cases stems from the significantly higher $P(D)$ of the OAR for those cases, i.e., left parotid at 27.24% for cascade case versus 16.91% for the one-to-all case (patient 2), right parotid at 60.40% for the plan versus 55.61% for the one-to-all-case (patient 5), left eye at 37.28% for cascade case versus 33.57 for the one-to-all case (patient 6), brainstem at 5.79% for the plan versus 4.81% for the one-to-all case (patient 7), and left orbit at 7.40% for the plan versus 6.96% for the one-to-all case (patient 8). The $P(D)$ of the other OARs is also higher in either cascade or plan cases versus the one-to-all case, contributing to the higher P_I in those cases.

Statistical analysis

The Mann–Whitney U-test was performed with a 95% degree of uncertainty ($\alpha = 0.05$). The result is significant if

Table 5: *P* values comparison (difference) of the "clinical" values between the two cases and the planned values

Patient#	P_I difference (case-plan)		P_+ difference (case-plan)		P_B difference (case-plan)	
	One-to-all	Cascade	One-to-all	Cascade	One-to-all	Cascade
1	2.48	2.60	−2.52	−2.62	−0.03	−0.02
2	−0.43	7.91	0.43	−7.9	0.00	0.00
3	−4.32	−10.35	4.32	10.35	0.00	0.00
4	−0.51	−0.55	0.51	0.55	0.00	0.00
5	−4.80	−2.51	4.52	1.85	−0.28	−0.66
6	−1.26	1.31	1.21	−1.43	−0.05	−0.12
7	−0.15	−0.14	0.16	0.15	0.01	0.01
8	−1.58	−1.56	1.62	1.58	0.03	0.02
9	13.23	14.64	−13.52	−14.99	−0.29	−0.36
10	9.55	3.95	−10.02	−4.22	−0.47	−0.28
Average±SD	1.22±5.81	1.53±6.61	−1.33±5.92	−1.67±6.66	−0.11±0.17	−0.14±0.23

SD: Standard deviation

Table 6: Planning target volume dose variations per patient (Gy) with the deviations of the two cases from the plan

Patient#	Plan					Plan-one-to-all					Plan-cascade				
	D_{mean}	SD	D_{95}	D_{min}	D_{max}	D_{mean}	SD	D_{95}	D_{min}	D_{max}	D_{mean}	SD	D_{95}	D_{min}	D_{max}
1	64.61	6.17	68.22	53.92	75.28	0.17	0.09	0.09	0.00	0.33	0.18	0.02	0.08	0.12	0.22
2	72.2	3.48	73.69	66.17	78.22	−0.05	0.22	0.14	−0.44	0.34	−0.19	0.26	0.17	−0.64	0.27
3	69.03	5.78	72.68	59.03	79.01	0.29	0.12	0.05	0.1	0.48	0.43	0.18	0.07	0.12	0.74
4	69.44	2.72	68.79	64.74	74.03	0.31	−0.05	0.12	0.39	0.12	0.29	−0.03	0.14	0.35	0.13
5	52.93	6.34	57.81	41.96	63.88	0.17	0.01	0.13	0.17	0.18	0.53	−0.20	0.15	0.88	0.19
6	61.7	3.97	57.34	52.48	64.76	0.28	0.14	0.14	−0.04	0.39	0.35	0.17	0.15	−0.04	0.48
7	73.35	16.63	58.08	34.71	86.18	0.14	0.32	−0.06	−0.62	0.39	0.29	0.42	0.00	−0.69	0.61
8	52.32	2.45	54.12	48.07	56.55	0.04	0.00	−0.19	0.03	0.03	0.17	−0.08	−0.19	0.31	0.03
9	58	12.23	69.46	36.82	79.14	−4.59	2.96	0.19	−9.72	0.53	−3.89	2.77	0.24	−8.70	0.91
10	58.06	12.73	70.88	36.02	80.05	−0.48	0.85	0.37	−1.95	0.98	−0.19	0.57	0.21	−1.17	0.79

SD: Standard deviation

calculated | Z score| > |Z critical|. For all three examined group pairs, |Z score| = 0.076. Since for the two-tailed test, |Z critical| = 1.960, and for one-tailed test, |Z critical| = 1.645, it is obvious that, in our case, the result is not statistically significant, and we cannot state with 95% certainty that there is a difference between the two groups for either a one-tailed test or a two-tailed test.

For the sign test, the result is significant if $P < \alpha$. The 95% certainty required $\alpha = 0.05$. For the comparison between the one-to-all and planned data, the calculated P is 0.344, and between the cascade and planned data, $P = 1.246$. This test showed that the result is not significant, and we can state that there is no difference between the planned and the CT-on-rails P_+ values.

In the Wilcoxon signed-rank test, the critical value of W for $n = 10$ and for a one-tailed test in which alpha = 0.05 equals 11. The null hypothesis can be rejected if test statistics W is greater than or equal to W critical. In our case, when the one-to-all data were compared with the planned data statistics, W was 25, and for the cascade versus planned data comparison, W was 31. Given that the test statistics W is greater than the critical W for both cases, null hypothesis is rejected, i.e., dosimetrically (at least when comparing P_+ values), CT-on-rails data are not worse or better than the planned data.

The calculated Kendall tau rank correlation coefficient value for the one-to-all versus planned data was 0.911, for the cascade versus planned data was 0.867, and for the one-to-all versus cascade data was 0.956. High tau values indicate high degree of correspondence between the each group's rankings.

Discussion

In the physical analysis of the different dose distributions, criteria such as the mean and minimum target doses, mean and maximum normal tissue doses, isodose levels, and DVHs are mostly used.[27,28] The plans tried to achieve adequate PTV coverage while respecting the tolerance doses of the involved OAR. However, when comparing different dose distributions, the differences that are observed on the DVHs and isodose lines are not always reflected in the radiobiological evaluation. This is due to the fact that radiobiological evaluation is more sensitive to small changes in dose distribution that may often not be observed in the DVH-based evaluations.

The expected complication-free tumor control for the "planned," "one-to-all," and "cascade" dose distributions

varies from case to case. For most of the studied cases, the planned dose distribution is better than the delivered dose distributions against either the one-to-all or cascade cases. The reason for this is the more effective irradiation of the PTV in the treatment plan, while normal tissue sparing is similar between the three compared distributions. However, even though in some cases the planned dose distribution may deliver lower mean doses to a given OAR, it may also show higher complication probability because of the greater maximum doses and higher seriality value of that OAR (e.g., spinal cord). Furthermore, the expected complication-free tumor control for the planned dose distributions is not always better than the delivered dose distributions for either cascade or one-to-all cases. The reason is that the different plans were not optimized using radiobiological objectives, which means that the planned dose distributions do not correspond to the maximum expected complication-free tumor control. It is observed that for normal tissues, the classification of the different dose distributions over the different cases seems to be more sensitive. In all the cases, the PTV is irradiated almost iso-effectively by the delivered dose distributions in one-to-all and the cascade cases. This is supported by the tumor control probabilities, P_B. On the other hand, the setup uncertainties produce higher normal tissue complications when the OARs move into the high-dose region (patients 3, 5, 6, and 8) or lower expected responses when the OARs move away from the high-dose region (patients 1, 2, 4, 7, 9, and 10).

The findings of this study indicate that for a fraction of the patients, the difference in expected outcome between the delivered against the planned doses can vary from 5% to 10%. For individual OARs, those values are even larger (up to 21%) [Appendix Table 3]. These results are in line with a recent study, which utilized head-and-neck cancer patients with daily CT-on-rails, where they report that, without altering patient setup, DVH analysis showed an increase in dose of 3%, 12%, and 16% to the tumor, cord, and parotids, respectively. With patient shifts to correct for setup errors, accurate dose delivery to the tumor was achieved. However, even with shifts, the cord and parotids were still overdosed by 10%.[29] Another study, using the IGRT results of five head-and-neck patients, reported that the impact of residual setup error, tumor shrinkage, organ deformation, or patient weight loss would result in a considerable change (up to 20%) in the dose received by the OARs.[30]

The statistical analysis of the P_+ values was done by means of various statistical tests, which showed that there is no statistically significant difference between the planned and the CT-on-rails P_+ values. This confirms the belief that if appropriate setup corrections are done on the patient, before each treatment, the delivered dose distribution is comparable to the planned dose distribution, regardless of how the CT-on-rail data from every fraction are grouped and analyzed.

It has to be stated that the determination of the model parameters expressing the effective radiosensitivity of the tissues is subject to uncertainties imposed by the inaccuracies in the patient setup during RT, lack of knowledge of the inter-patient and intra-patient radiosensitivity, and inconsistencies in treatment methodology. Consequently, the determined model parameters (such as the D_{50}, γ, and s) and the corresponding dose–response curves are characterized by confidence intervals. In the present study, most of the tissue response parameters have been taken from recently published clinical studies.[12,14,15]

Conclusion

In this study, the clinical effectiveness of planned and delivered dose distributions of IMRT treatments for head-and-neck cancer was evaluated using both physical and biological criteria. The difference between the "one-to-all" and "cascade" dose distributions was small, statistically insignificant, and very close to the values of the corresponding treatment plans. However, for a fraction of the patients and given OAR, the differences between the delivered and planned doses were particularly large. These findings support the necessity of the accurate patient setup before the treatment using IGRT, thus minimizing dose delivery errors.

Acknowledgment

This research is supported by the Andrew Sabin Family Foundation; Dr. Fuller is a Sabin Family Foundation Fellow. Dr. Fuller receives funding and salary support from the National Institutes of Health (NIH), including: the National Institute for Dental and Craniofacial Research Award (1R01DE025248-01/R56DE025248-01); a National Science Foundation (NSF), Division of Mathematical Sciences, Joint NIH/NSF Initiative on Quantitative Approaches to Biomedical Big Data (QuBBD) Grant (NSF 1557679); the NIH Big Data to Knowledge (BD2K) Program of the National Cancer Institute (NCI) Early Stage Development of Technologies in Biomedical Computing, Informatics, and Big Data Science Award (1R01CA214825-01); NCI Early Phase Clinical Trials in Imaging and Image-Guided Interventions Program (1R01CA218148-01); an NIH/NCI Cancer Center Support Grant (CCSG) Pilot Research Program Award from the UT MD Anderson CCSG Radiation Oncology and Cancer Imaging Program (P30CA016672) and an NIH/NCI Head and Neck Specialized Programs of Research Excellence (SPORE) Developmental Research Program Award (P50 CA097007-10). Dr. Fuller has received direct industry grant support and travel funding from Elekta AB and served as a consultant for Philips Medical Systems.

Financial support and sponsorship

Nil.

Conflicts of interest

There are no conflicts of interest.

References

1. Bel A, van Herk M, Bartelink H, Lebesque JV. A verification procedure to improve patient set-up accuracy using portal images. Radiother Oncol 1993;29:253-60.
2. Lind BK, Källman P, Sundelin B, Brahme A. Optimal radiation beam

profiles considering uncertainties in beam patient alignment. Acta Oncol 1993;32:331-42.
3. Creutzberg CL, Althof VG, Huizenga H, Visser AG, Levendag PC. Quality assurance using portal imaging: The accuracy of patient positioning in irradiation of breast cancer. Int J Radiat Oncol Biol Phys 1993;25:529-39.
4. ACR – ASTRO Practice Parameter for Image – Guided Radiation Therapy. Revised (CSC/BOC); 2014.
5. Jensen NK, Stewart E, Lock M, Fisher B, Kozak R, Chen J, *et al.* Assessment of contrast enhanced respiration managed cone-beam CT for image guided radiotherapy of intrahepatic tumors. Med Phys 2014;41:051905.
6. Sutton MW, Fontenot JD, Matthews KL 2nd, Parker BC, King ML, Gibbons JP, *et al.* Accuracy and precision of cone-beam computed tomography guided intensity modulated radiation therapy. Pract Radiat Oncol 2014;4:e67-73.
7. Yip C, Thomas C, Michaelidou A, James D, Lynn R, Lei M, *et al.* Co-registration of cone beam CT and planning CT in head and neck IMRT dose estimation: A feasible adaptive radiotherapy strategy. Br J Radiol 2014;87:20130532.
8. Källman P, Lind BK, Brahme A. An algorithm for maximizing the probability of complication-free tumor control in radiation therapy. Phys Med Biol 1992;37:871-90.
9. Mavroidis P, Stathakis S, Gutierrez A, Esquivel C, Shi C, Papanikolaou N, *et al.* Expected clinical impact of the differences between planned and delivered dose distributions in helical tomotherapy for treating head and neck cancer using helical megavoltage CT images. J Appl Clin Med Phys 2009;10:2969.
10. Mavroidis P, Lind BK, Brahme A. Biologically effective uniform dose (D) for specification, report and comparison of dose response relations and treatment plans. Phys Med Biol 2001;46:2607-30.
11. Brahme A. Which parameters of the dose distribution are best related to the radiation response of tumours and normal tissues? In: Interregional Seminars for Europe, the Middle East and Africa Organized by the IAEA: Proceedings. Leuven; 1994. p. 37-58.
12. Emami B, Lyman J, Brown A, Coia L, Goitein M, Munzenrider JE, *et al.* Tolerance of normal tissue to therapeutic irradiation. Int J Radiat Oncol Biol Phys 1991;21:109-22.
13. Ågren AK. Quantification of the Response of Heterogeneous Tumors and Organized Normal Tissues to Fractionated Radiotherapy. Ph.D. Thesis. Stockholm University; 1995.
14. Mavroidis P, Laurell G, Kraepelien T, Fernberg JO, Lind BK, Brahme A, *et al.* Determination and clinical verification of dose-response parameters for esophageal stricture from head and neck radiotherapy. Acta Oncol 2003;42:865-81.
15. Mavroidis P, al-Abany M, Helgason AR, Agren Cronqvist AK, Wersäll P, Lind H, *et al.* Dose-response relations for anal sphincter regarding fecal leakage and blood or phlegm in stools after radiotherapy for prostate cancer. Radiobiological study of 65 consecutive patients. Strahlenther Onkol 2005;181:293-306.
16. Velocity AI. Velocity Medical Solutions. Available from: www.varian.com/oncology/products/software/velocity. [Last accessed on 2018 Feb 13].
17. Kessler ML. Image registration and data fusion in radiation therapy. Br J Radiol 2006;79:S99-108.
18. Kadoya N, Fujita Y, Katsuta Y, Dobashi S, Takeda K, Kishi K, *et al.* Evaluation of various deformable image registration algorithms for thoracic images. J Radiat Res 2014;55:175-82.
19. Lyman JT. Tolerance Doses for Treatment Planning. Department of Energy, LBL-22416; 1985.
20. Bentzen SM, Constine LS, Deasy JO, Eisbruch A, Jackson A, Marks LB, *et al.* Quantitative analyses of normal tissue effects in the clinic (QUANTEC): An introduction to the scientific issues. Int J Radiat Oncol Biol Phys 2010;76:S3-9.
21. Mavroidis P, Ferreira BC, Papanikolaou N, Lopes Mdo C. Analysis of fractionation correction methodologies for multiple phase treatment plans in radiation therapy. Med Phys 2013;40:031715.
22. Ebert MA. Viability of the EUD and TCP concepts as reliable dose indicators. Phys Med Biol 2000;45:441-57.
23. Jones LC, Hoban PW. Treatment plan comparison using equivalent uniform biologically effective dose (EUBED). Phys Med Biol 2000;45:159-70.
24. Agren A, Brahme A, Turesson I. Optimization of uncomplicated control for head and neck tumors. Int J Radiat Oncol Biol Phys 1990;19:1077-85.
25. Brahme A. Dosimetric precision requirements in radiation therapy. Acta Radiol Oncol 1984;23:379-91.
26. Niemierko A. Reporting and analyzing dose distributions: A concept of equivalent uniform dose. Med Phys 1997;24:103-10.
27. Aaltonen P, Brahme A, Lax I, Levernes S, Näslund I, Reitan JB, *et al.* Specification of dose delivery in radiation therapy. Recommendations by the Nordic Association of Clinical Physics (NACP). Acta Oncol 1997;36:1-32.
28. ICRU Report 62. Prescribing, Recording and Reporting Photon Beam Therapy (Supplement to ICRU Report 50). International Commission on Radiation Units and Measurements; 1999. p. 1-52.
29. Chen CP, Wong J, Chang CW, El-Gabry M, Merrick S, Gao Z. Plan degradation in head and neck cancers. Int J Radiat Oncol Biol Phys 2008;72:S592-3.
30. Lee L, Le QT, Xing L. Retrospective IMRT dose reconstruction based on cone-beam CT and MLC log-file. Int J Radiat Oncol Biol Phys 2008;70:634-44.

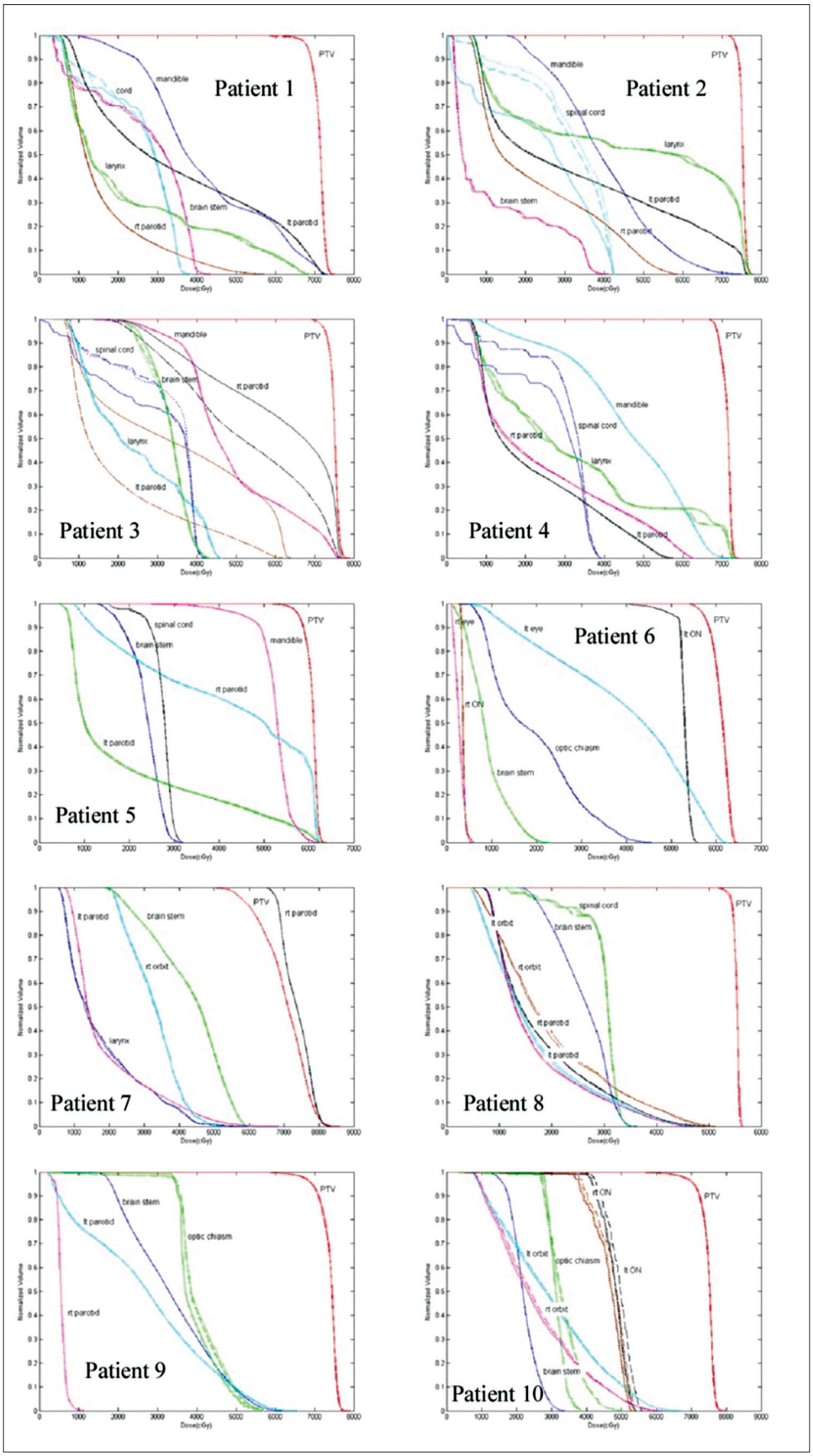

Appendix Figure 1: The dose–volume histograms of the planning target volume and the organs at risk are illustrated. The solid lines indicate the planned dose distributions, while the dashed lines correspond to the one-to-all case and the dotted lines to the cascade case

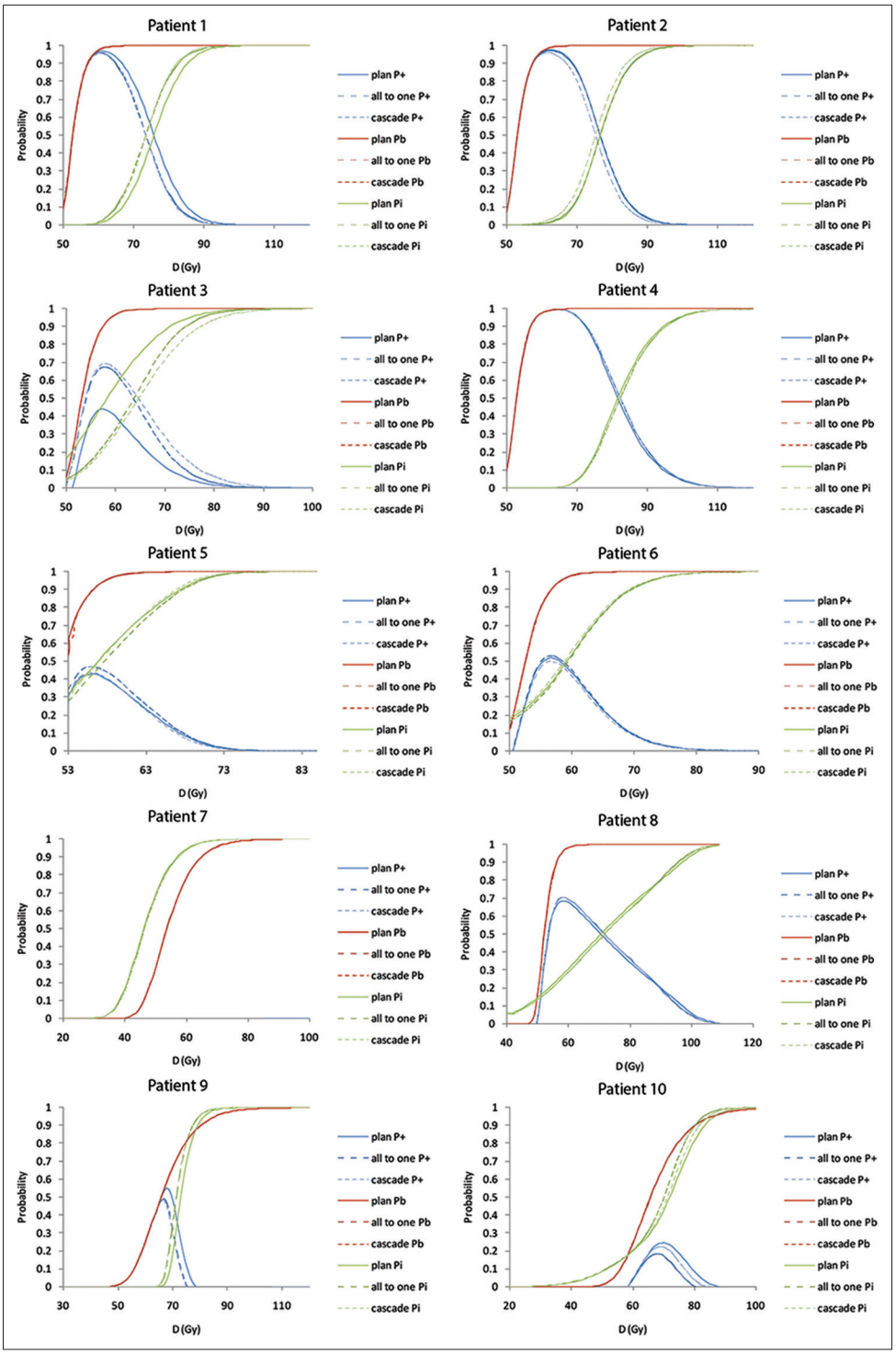

Appendix Figure 2: The curves derived from the radiobiological evaluation of the dose distributions are plotted using the $\overline{\overline{D}}$ as the unit on the dose axis. The solid lines indicate the planned dose distributions, while the dashed lines correspond to the one-to-all case and the dotted lines to the cascade case

Appendix Table 1: Dosimetric value differences per patient per case (each case compared to planed values)

Patient	Organ	Dose	Difference (Gy)		Difference percentage PTV coverage	
			A	B	A	B
Patient 1	Mandible	Maximum	−0.2	−0.1	−1.0	−1.0
	Larynx	Mean	0.0	0.0		
	Spinal cord	Maximum	0.0	−0.1		
	Brainstem	Maximum	−0.1	−0.1		
	Left parotid	Mean	−0.1	0.0		
Patient 2	Mandible	Maximum	−0.1	−0.1	0.0	0.0
	Larynx	Mean	−0.4	−0.4		
	Spinal cord	Maximum	−0.1	0.0		
	Brainstem	Maximum	−0.4	−0.8		
	Left parotid	Mean	0.0	0.0		
Patient 3	Mandible	Maximum	−0.3	−0.2	0.0	0.0
	Larynx	Mean	−0.1	0.0		
	Spinal cord	Maximum	−0.2	−0.2		
	Brainstem	Maximum	−0.1	−0.2		
	Right parotid	Mean	−1.7	−1.6		
Patient 4	Mandible	Maximum	−0.9	−0.7	−1.2	−1.4
	Larynx	Mean	−0.1	−0.1		
	Spinal cord	Maximum	0.1	0.0		
	Right parotid	Mean	0.2	0.2		
Patient 5	Mandible	Maximum	−0.2	−0.3	−0.9	−1.2
	Brainstem	Maximum	0.0	0.0		
	Spinal cord	Maximum	0.0	0.0		
	Left parotid	Mean	−0.3	−0.1		
Patient 6	Optic chiasm	Maximum	−0.2	−0.2	−1.1	−1.2
	Brainstem	Maximum	−0.2	−0.3		
	Right eye	Maximum	0.0	0.0		
	Right optic nerve	Maximum	0.0	0.0		
Patient 7	Brainstem	Maximum	−0.3	−0.1	0.0	−0.1
	Larynx	Mean	−0.5	−0.2		
	Right orbit	Maximum	−0.1	−0.3		
	Left parotid	Mean	0.0	0.0		
Patient 8	Brainstem	Maximum	0.1	0.0	0.0	0.0
	Spinal cord	Maximum	0.0	0.1		
	Left orbit	Maximum	−0.8	−0.8		
	Right parotid	Mean	0.1	0.1		
Patient 9	Optic chiasm	Maximum	1.1	1.3	−0.6	−0.7
	Brainstem	Maximum	−0.2	−0.1		
	Right parotid	Mean	0.0	0.0		
	Left parotid	Mean	−0.1	−0.1		
Patient 10	Optic chiasm	Maximum	11.7	11.8	−0.6	−0.4
	Brainstem	Maximum	−0.1	−0.1		
	Left orbit	Maximum	−0.5	−0.5		
	Left optic nerve	Maximum	2.0	0.1		

A: One-to-all, B: Cascade. PTV: Planning target volume

Appendix Table 2: Summary of the radiobiological comparison for the ten patients

Dose prescription	One-to-all		Cascade		Plan		Patient #
	Clinical delivered	Optimal delivered	Clinical delivered	Optimal delivered	Clinical planned	Optimal planned	
P_+ (%)	78.8	96.0	78.7	96.2	**81.3**	97.0	**1**
P_B (%)	99.9	97.7	100.0	97.9	100.0	98.4	
P_I (%)	21.2	1.8	21.3	1.8	**18.7**	1.4	
BEUD-b (Gy)	68.2	60.3	68.5	60.5	69.6	61.1	
BEUD-i (Gy)	42.1	35.8	42.1	35.8	41.6	35.5	
P_+ (%)	**59.7**	97.2	51.4	95.9	59.3	97.6	**2**
P_B (%)	100.0	98.7	100.0	98.7	100.0	99.2	
P_I (%)	**40.3**	1.5	48.6	2.7	40.7	1.6	
BEUD-b (Gy)	75.1	61.9	75.1	61.9	75.1	62.9	
BEUD-i (Gy)	45.7	36.0	47.0	37.1	45.8	36.0	
P_+ (%)	9.9	67.3	**15.9**	69.3	5.6	43.7	**3**
P_B (%)	100.0	91.4	100.0	91.4	100.0	91.4	
P_I (%)	90.1	24.1	**84.1**	22.1	94.4	47.7	
BEUD-b (Gy)	74.3	57.8	74.3	57.8	74.4	57.8	
BEUD-i (Gy)	55.6	43.2	53.7	42.8	57.5	46.9	
P_+ (%)	94.5	99.4	**94.5**	99.4	94.0	99.4	**4**
P_B (%)	100.0	99.7	100.0	99.7	100.0	99.7	
P_I (%)	5.5	0.3	**5.4**	0.3	6.0	0.3	
BEUD-b (Gy)	70.8	64.7	70.8	64.7	70.9	64.7	
BEUD-i (Gy)	38.1	33.0	38.1	33.0	38.3	33.1	
P_+ (%)	**41.2**	46.9	38.5	43.5	36.7	42.8	**5**
P_B (%)	97.0	87.4	96.7	90.7	97.3	88.0	
P_I (%)	**55.9**	40.5	58.2	47.2	60.7	45.3	
BEUD-b (Gy)	58.9	55.7	58.7	56.4	59.1	55.9	
BEUD-i (Gy)	46.3	44.1	46.7	45.1	47.0	44.8	
P_+ (%)	**44.6**	53.0	42.0	49.8	43.4	51.7	**6**
P_B (%)	97.7	91.0	97.7	91.2	97.8	91.1	
P_I (%)	**53.1**	38.1	55.7	41.4	54.4	39.4	
BEUD-b (Gy)	60.1	57.0	60.0	57.0	60.1	57.0	
BEUD-i (Gy)	45.4	42.5	45.9	43.2	45.7	42.7	
P_+ (%)	−6.3	0.0	−6.3	0.0	−6.5	0.0	**7**
P_B (%)	92.2	0.0	92.2	0.0	92.1	0.0	
P_I (%)	**98.5**	0.0	98.5	0.0	98.6	0.0	
BEUD-b (Gy)	66.4	0.0	66.4	0.0	66.4	0.0	
BEUD-I (Gy)	58.1	0.5	58.1	0.5	58.4	0.5	
P_+ (%)	**63.5**	70.3	63.4	70.2	61.9	68.5	**8**
P_B (%)	84.1	97.0	84.1	97.0	84.1	97.0	
P_I (%)	**20.6**	26.8	20.7	26.8	22.2	28.6	
BEUD-b (Gy)	55.2	58.9	55.2	58.9	55.2	58.9	
BEUD-i (Gy)	36.0	37.5	36.0	37.5	36.4	37.8	
P_+ (%)	8.6	49.0	7.2	48.0	**22.2**	54.9	**9**
P_B (%)	76.9	54.1	76.8	54.1	77.2	58.2	
P_I (%)	68.2	5.2	69.7	6.1	**55.0**	3.3	
BEUD-b (Gy)	73.3	66.7	73.3	66.7	73.4	67.7	
BEUD-i (Gy)	50.1	38.5	50.4	38.9	48.0	37.5	
P_+ (%)	10.1	18.4	15.9	22.3	**20.1**	24.5	**10**
P_B (%)	78.8	57.9	79.0	61.7	79.3	65.4	
P_I (%)	68.7	39.5	63.1	39.4	**59.2**	41.0	
BEUD-b (Gy)	74.0	67.6	74.1	68.6	74.2	69.6	
BEUD-i (Gy)	49.0	43.7	48.1	43.6	47.5	44.0	

BEUD: Biologically effective uniform dose

Appendix Table 3: Quantitative summary of the biological comparison for the dose distributions of the ten cases

	P-0 (%)	P-1 (%)	P-2 (%)	BEUD-0 (Gy)	BEUD-1 (Gy)	BEUD-2 (Gy)	$\bar{\bar{D}}$ -0 (Gy)	$\bar{\bar{D}}$ -1 (Gy)	$\bar{\bar{D}}$ -2 (Gy)	SD-0 (Gy)	SD-1 (Gy)	SD-2 (Gy)
Patient 1				s								
PTV	99.97	99.94	99.95	69.55	68.15	68.50	71.20	71.12	71.13	1.65	1.82	1.78
Mandible	11.04	13.75	13.79	63.65	64.15	64.15	42.57	43.32	43.32	16.21	16.68	16.69
Larynx	0.32	0.28	0.46	66.30	66.20	66.55	29.73	29.82	32.75	25.32	24.98	26.22
Cord	0.00	0.00	0.00	49.70	49.70	49.70	27.03	26.50	26.08	11.04	10.15	10.50
Brainstem	0.00	0.00	0.00	41.90	41.85	41.85	27.22	27.11	27.16	13.30	13.23	13.18
Left parotid	8.29	8.34	8.26	41.05	41.05	41.05	37.09	37.15	37.12	24.05	23.92	23.93
Right parotid	0.00	0.00	0.00	17.55	17.65	17.65	15.89	15.99	15.98	10.78	10.76	10.76
Patient 2												
PTV	100.0	100.0	100.0	75.10	75.05	75.05	75.26	75.22	75.22	0.84	0.86	0.87
Mandible	5.14	8.70	5.12	64.20	63.20	63.20	41.69	40.81	40.81	14.41	13.51	13.51
Larynx	20.99	21.80	25.52	72.95	72.85	73.40	49.94	49.96	52.44	29.64	29.31	29.09
Cord	0.00	0.00	0.00	50.45	50.45	50.45	30.78	35.32	36.08	15.15	11.03	10.16
Brainstem	0.00	0.00	0.00	38.05	39.65	39.40	11.46	13.80	13.76	12.94	14.78	14.73
Left parotid	20.29	16.91	27.24	44.30	45.15	46.75	39.21	40.10	41.68	28.14	28.24	28.63
Right parotid	0.00	0.01	0.00	29.70	28.65	27.55	26.39	25.46	24.49	19.04	18.43	17.75
Patient 3												
PTV	100.0	100.0	100.0	74.35	74.30	74.30	75.02	74.98	74.98	1.25	1.24	1.24
Cord	0.00	0.00	0.00	50.45	50.45	50.45	30.16	32.88	33.34	13.44	10.76	11.01
Brainstem	0.00	0.00	0.00	42.20	42.15	42.05	34.36	34.15	33.94	5.51	5.79	5.96
Larynx	0.00	0.00	0.00	57.15	57.15	57.15	30.13	33.04	29.35	15.10	14.82	14.88
Mandible	29.41	50.35	25.80	67.55	70.30	67.05	51.80	57.96	51.01	15.29	16.91	14.84
Right parotid	91.93	80.09	78.55	66.00	59.55	58.95	64.75	57.87	57.28	16.76	18.91	18.91
Left parotid	2.31	0.02	0.02	38.15	30.80	30.80	34.72	26.89	26.88	21.68	21.24	21.26
Patient 4												
PTV	99.98	99.98	99.98	70.90	70.80	70.80	71.29	71.22	71.21	1.23	1.24	1.24
Cord	0.00	0.00	0.00	49.70	49.70	49.70	26.20	29.94	29.95	12.16	9.10	9.04
Larynx	1.68	1.29	1.24	67.70	67.45	67.40	32.10	32.18	32.21	23.27	22.58	22.42
Mandible	4.39	4.25	4.25	61.95	61.90	61.90	46.23	46.21	46.21	15.44	15.37	15.37
Right parotid	0.00	0.00	0.00	27.35	27.35	27.35	24.03	24.07	24.10	18.38	18.21	18.13
Left parotid	0.00	0.00	0.00	24.10	24.10	24.10	21.50	21.51	21.57	15.31	15.24	15.07
Patient 5												
PTV	97.31	97.03	96.65	59.10	58.90	58.65	60.67	60.62	60.61	1.49	1.53	1.54
Brainstem	0.00	0.00	0.00	33.35	33.35	33.35	25.08	25.01	25.02	4.76	4.79	4.78
Left parotid	0.50	0.42	0.40	34.10	33.85	33.80	29.17	29.01	28.98	24.05	23.68	23.62
Right parotid	60.40	55.61	57.92	51.70	50.65	51.15	49.64	48.54	49.08	18.62	18.80	18.65
Mandible	0.15	0.14	0.13	56.85	56.75	56.75	52.49	52.47	52.46	4.24	4.17	4.20
Cord	0.00	0.00	0.00	48.50	48.50	48.50	27.89	27.88	28.28	2.90	2.94	3.04
Patient 6												
PTV	97.79	97.74	97.67	60.10	60.05	59.95	61.24	61.20	61.08	2.13	2.15	2.09
Chiasm	2.46	2.32	2.25	43.45	43.35	43.30	27.23	27.19	27.17	36.11	35.93	35.86
Brainstem	0.00	0.00	0.00	33.80	33.80	33.80	9.30	9.07	9.28	4.99	4.68	4.94
Left eye	35.70	33.57	37.28	48.35	47.55	48.90	41.20	40.46	41.97	17.50	17.14	17.45
Right eye	0.00	0.00	0.00	3.30	3.30	3.30	2.91	2.92	2.92	1.24	1.23	1.23
Left optic nerve	27.25	27.73	27.70	52.80	52.90	52.90	52.76	52.84	52.84	0.00	0.00	0.00
Right optic nerve	0.00	0.00	0.00	3.75	3.80	3.80	3.67	3.74	3.73	0.00	0.00	0.00
Patient 7												
PTV	92.14	92.15	92.15	66.40	66.40	66.40	70.48	70.44	70.46	6.52	6.48	6.49
Larynx	0.00	0.00	0.00	58.30	57.45	57.95	17.57	17.74	17.70	11.80	11.63	11.65
Brainstem	5.79	4.81	4.96	55.35	54.90	54.95	46.10	45.47	45.54	11.68	11.53	11.52
Right orbit	13.29	13.18	13.18	39.10	39.00	39.00	34.91	34.79	34.91	9.48	9.51	9.40
Left parotid	0.00	0.00	0.00	20.65	20.70	20.70	18.92	18.96	18.95	11.86	11.84	11.84

Contd...

Appendix Table 3: Contd...

	P-0 (%)	P-1 (%)	P-2 (%)	BEUD-0 (Gy)	BEUD-1 (Gy)	BEUD-2 (Gy)	$\bar{\bar{D}}$ -0 (Gy)	$\bar{\bar{D}}$ -1 (Gy)	$\bar{\bar{D}}$ -2 (Gy)	SD-0 (Gy)	SD-1 (Gy)	SD-2 (Gy)
Right parotid	98.30	98.14	98.14	74.50	74.00	74.00	74.41	73.90	73.91	4.75	4.29	4.34
Patient 8												
PTV	84.07	84.10	84.09	55.15	55.20	55.15	55.26	55.25	55.25	0.64	0.58	0.58
Brainstem	0.00	0.00	0.00	35.65	35.50	35.65	27.23	26.65	27.22	5.95	5.65	5.95
Cord	0.00	0.00	0.00	48.50	48.50	48.50	29.61	30.35	30.38	4.60	4.56	4.73
Left orbit	7.40	6.96	6.99	34.45	34.10	34.10	20.47	20.61	20.59	14.71	14.41	14.43
Left parotid	0.00	0.00	0.00	17.80	17.95	18.00	16.57	16.70	16.74	9.21	9.20	9.20
Right parotid	0.00	0.00	0.00	21.95	22.05	22.05	20.00	20.13	20.13	12.62	12.58	12.58
Right orbit	16.00	14.69	14.69	39.65	39.00	39.00	26.97	26.88	26.88	17.25	16.68	16.68
Patient 9												
PTV	77.18	76.89	76.82	73.35	73.25	73.25	73.83	73.72	73.69	2.37	2.39	2.41
Brainstem	1.55	2.51	1.52	53.30	54.25	53.25	34.88	35.87	34.85	12.39	13.17	12.34
Chiasm	54.25	67.38	69.14	55.05	56.00	56.15	52.03	53.16	53.35	11.75	11.82	11.83
Left parotid	0.12	0.12	0.12	33.15	33.15	33.15	30.15	30.20	30.20	19.34	19.23	19.20
Right parotid	0.00	0.00	0.00	6.50	6.50	6.50	6.34	6.33	6.34	2.28	2.28	2.28
Patient 10												
PTV	79.29	78.82	79.01	74.20	74.00	74.10	74.76	74.61	74.67	2.36	2.44	2.42
Brainstem	0.00	0.00	0.00	34.45	34.45	34.45	22.73	22.71	22.71	4.61	4.59	4.58
Chiasm	0.01	8.23	8.59	38.05	46.90	47.05	36.98	39.39	39.26	4.17	9.98	10.21
Left orbit	28.19	27.92	27.81	46.50	46.40	46.35	34.88	35.14	35.00	19.79	19.46	19.51
Right orbit	20.10	20.25	19.85	43.05	43.10	42.95	30.66	31.27	30.92	18.14	17.82	17.85
Left optic nerve	17.90	27.29	18.57	52.20	54.05	52.35	52.13	53.95	52.27	4.49	4.84	4.42
Right optic nerve	13.35	18.48	14.40	51.20	52.35	51.45	51.06	52.23	51.32	5.33	5.24	5.29

One-to-all case is represented by number "1," cascade by number "2," and planned values by "0." PTV: Planning target volume, SD: Standard deviation

Original Article

Expression of Bax and Bcl2 Genes in Peripheral Blood Lymphocytes of Patients with Differentiated Thyroid Cancer

Zari Hamivand[1], Gholamhassan Haddadi[2,3], Reza Fardid[1,2]

[1]Department of Radiology, School of Paramedical Sciences, [2]Ionizing and Non-Ionizing Radiation Protection Research Center (INIRPRC), Shiraz University of Medical Sciences, Shiraz, [3]Department of Medical Physics, Fasa University of Medical Sciences, Fasa, Iran

Abstract

Context: Thyroid cancer is the most common endocrine malignancy worldwide. Iodine-131 is used in the treatment of thyroid cancer with dosage of 100 mCi. In the medical applications of ionizing radiation besides the advantages such as diagnosis and treatment of diseases, the risks arising from exposure should be considered as well. **Aims:** The present study aimed to evaluate the changes in expression levels of apoptotic Bax and Bcl-2 and the ratio of Bax/Bcl-2, in the peripheral blood lymphocytes (PBLs) of patients with differentiated thyroid cancer (DTC). **Settings and Design:** This study was conducted on fifty thyroid cancer patients who had undergone surgery and were under treatment with 100 and 150 mCi doses. **Subjects and Methods:** Blood samples were taken from the patients, one before iodine treatment and another 48 h after therapy. Bax and Bcl-2 gene expression levels were measured by using real-time reverse transcriptase polymerase chain reaction. **Statistical Analysis Used:** The data were analyzed using one-way analysis of variance followed by samples *t*-test and independent samples *t*-test. **Results:** Significant changes were observed in the percentage of apoptotic cells, in groups, after radioiodine therapy compared with before treatment. The ratio of Bax/Bcl-2 in both groups showed a significant increase ($P < 0.001$). The relative expression level of Bax gene showed a significant increase in comparison with the control group. **Conclusions:** Iodine therapy reduced expression of Bcl-2 and a significant expression of Bax and finally increased the ratio of Bax/Bcl-2. Iodine therapy led to apoptosis in the PBLs of patients with DTC. Therefore, it can be suggested that this method can be useful for monitoring and detecting destructive effects of ionizing radiation in nuclear medicine patients.

Keywords: Bax, Bcl2, differentiated thyroid cancer, gene expression, peripheral blood lymphocytes

Received on: 26-08-2017 **Review completed on: 13-11-2017** **Accepted on: 14-11-2017**

Introduction

The differentiated thyroid cancer (DTC) comes for 1%–2% of malignant cancer in human. Its annual incidence is estimated 2–3.8 for women and 1.2–2.6 for men/100,000 persons. Its outbreak has increased in the recent decades.[1]

This cancer derives from either the classified epithelial follicular cells in the form of cancer with high differentiation (including papillary cancers and thyroid follicular, the thyroid cancer with low differentiation and anaplasic) or the parafollicle cells as generator of calcitonin (such as medullary cancer).[1] Generally, the differentiated forms of thyroid cancer have a slow progression trend; their treatment includes taking measures such as surgery, using radioactive iodine, and inhibiting TSH hormone.[2] Radioactive iodine-131 has been used in the treatment of malignant thyroid since 1940.[3] The radioactive 131 iodine is one of the iodine isotopes with half-life of 8 days and is released by the distribution of beta particles along with gamma radiation; and changes into stable xenon 131.[4] In the medical applications of ionizing radiation besides the advantages such as diagnosis and treatment of diseases, the risks arising from exposure should be considered too.[5]

Ionizing radiation has been known as causing oxidative stress by generating active oxygen types and free radicals in the tissues and irradiated cells.[6] These free radicals react with DNA, existing lipids in the nucleus and membrane.[6,7]

Significant changes in the structure and practice of DNA (failure of double-stranded DNA) and membrane (hard)

Address for correspondence: Dr. Reza Fardid, Department of Radiology, School of Paramedical Sciences, Shiraz University of Medical Sciences, Shiraz, Iran.
E-mail: rfardid@sums.ac.ir

Access this article online

Quick Response Code:

Website: www.jmp.org.in

DOI: 10.4103/jmp.JMP_104_17

How to cite this article: Hamivand Z, Haddadi G, Fardid R. Expression of Bax and Bcl2 genes in peripheral blood lymphocytes of patients with differentiated thyroid cancer. J Med Phys 2018;43:41-5.

lead to cell death through apoptosis.[8,9] Apoptosis is induced by a variety of toxic insults including growth factor deprivation and ionizing radiation.[10] Ionizing radiation damages DNA and is one agent that induces apoptosis in certain cells, including human lymphocytes. In the early stages of apoptosis, it is measured.[11,12] Phosphatidylinositol serine transfers from the inner surface to the outer surface of the cell membrane and the integration of cell membrane has been preserved. In the late apoptosis stages of apoptosis, the integration of cell membrane is destroyed, and the time of cell death or apoptosis depending on the type of cell has been estimated from a few hours to a few days.[13,14] The programmed cell death precisely depends on action and reaction of some gene products that activate or inhibit the process of cell suicide. Two large gene families including Caspases and Bcl-2 are involved in the path of apotheosis.[15] The Bcl-2 family has two protein groups including apoptosis promoter and inhibitor of apoptosis. The average ratio of these proteins determines a cell destiny. The Bcl-2 protein is placed in the cover of core and mitochondria; and it functions through the connection to Bax.[16] The Bax protein in terms of structural is Bcl-2 homologous, and it is considered to be a promoter of apoptosis that is placed in the cytoplasm or the cellular membrane, and hence, in terms of performance, this antagonist protein has a protective role for Bcl-2. The caspase molecules are generated in the form of prefabricate and just after receiving a death signal by cell, they are activated.[17]

Caspase 3 is an executive caspase that is activated by the starter caspases and breaks the survival and integrity of proteins. The death signals cause the setting up the apoptosis proteins family of Bcl-2, especially Bax. These proteins cause the release of cytochrome C from mitochondria to out. The release of mitochondrial cytochrome C into the cytoplasm and its subsequent association with the Apaf-1 protein is thought to be an absolute requirement for the activation of caspase-9, the apical caspase in the mitochondrial pathway of apoptosis.[18,19]

In another study in 2013, conducted by Verne Dick *et al*., apoptosis and micronuclei (MN) were investigated as the reflection of cytogenetic injury in the blood lymphocyte of 18 patients suffered from thyroid cancer under treatment with 100 and 150 mill curie doses. As apoptotic cells, using Annexin V-FITC/7-AAD kit and frequency of MN was assessed by MN assay. In this study, after radioiodine therapy in thyroid cancer patients, increase of primary apoptosis and MNs was observed.[20]

The aim of this study was to investigate the expression pattern of some inhibitors of Bcl-2 cell death and inducers of Bax cell death in patients under iodine therapy with different doses.

Subjects and Methods

This research was approved by the ethical committee of Shiraz University of Medical Sciences. The consent form was presented to patients and voluntarily read and signed. The studied population included fifty patients with thyroid cancer with the mean age of 39.08 ± 9.5; they had undergone thyroidectomy and were under treatment in the nuclear medicine department of Shiraz Namazi Hospital. Blood samples were taken before radioiodine therapy and 48 h after iodine therapy. Blood samples (2 ml of peripheral blood from patients) were collected in heparinized tubes. These samples were used for the measurement of Bax and Bcl-2 expression levels using real-time (RT) reverse transcriptase polymerase chain reaction (PCR). At first, separation of lymphocytes was made using the ficoll of innotrain, Germany, based on the standard protocol. The blood was washed with the buffer of phosphate saline with the same volume and then, 4 ml volume (blood and phosphate-buffered saline [PBS]) was added to 2 ml ficoll and centrifuged for 20 min with 3000 RPM. The separated lymphocytes after three times of washing with PBS were centrifuged for 10 min in 1400 RPM g. The surface layer was thrown out and the extracted lymphocytes were mixed with 500 PBS µl.

RNA preparation and quantification

After isolation of the lymphocytes from the peripheral blood samples, total RNA was extracted from blood samples with the RNX plus extraction kit (CinnaGene, Iran), according to the manufacturer's protocol and stored at −20°C. For extracting of RNA from chloroform and isopropanol and wash it, 75% ethanol was used. The concentration and quality of RNA were determined by measuring the absorbance by spectrophotometer system (Bekman, USA) at 260 nm (A260) and A260/A280 ratio, respectively.

cDNA synthesis and real-time quantitative polymerase chain reaction

Before cDNA synthesis, to remove pollution of RNA with DNA, the DNase I kit (Thermo Science, USA) was used. The synthesis of cDNA was done by using RevertAid First Strand cDNA Synthesis kit (Fermentase, lithuania) and based on the manufacturer's instruction. The used designed primers of Bax, Bcl-2, and B2 m gene are shown in Table 1. The B2 m gene was used as the endogenous reference. The

Table 1: Sequence-specific primers for genes BCL-2 and BAX and B2m

Gene name	Sequence of forward primers	Sequence of reverse primers	Product size (bp)
BAX	CTTCAGGGTTTCATCCAG	CTCCATGTTACTGTCCAG	169
BCL-2	ATTGATGGGATCGTTGCCTTATGCA	CCCTTGGCATGAGATGCAGGAAA	153
B2m	GTATGCCTGCCGTGTGAAC	AACCTCCATGATGCTGCTTAC	87

RT quantitative-PCR (QPCR) was done by CYBR Green kit (yekta tajhiz, Iran). The QPCR were done in cycle including: 2 min at 95°C for initial denaturation, and then, forty cycles of denaturation for 30 s in 95°C, annealing for 40 s in 57°C, with extension for 30 s in 72°C. The PCR products were separated on 2% agarose gel, and they were visible with ethidium bromide; then, they were evaluated by using trans-luminator advice UV (Uvidoc, UK). Target genes were quantified relative to the reference gene using the mathematical model described by computer tomography.

Verification polymerase chain reaction and primer design

To verify Bax, Bcl-2, and B2 m primers with 169, 153, and 87 base pair (bp) band lengths, PCR was performed with a cDNA sample. Five microliter of PCR product was loaded on 2% agarose gel. The distinctly mentioned band lengths of each gene were visible after ethidium bromide staining. Figure 1 depicts the electrophoresis image of the three primers Bcl-2 ،Bax and B2 m (Bcl-2, 153 bp, Bax, 153 bp, and B2 m 87 bp).

Statistical methods

The data were analyzed using one-way analysis of variance followed by samples *t*-test and independent samples *t*-test. The values of $P < 0.05$ were considered statistically significant.

Results

The changes in relative expression level of Bax and Bcl-2 genes Figure 2 shows the relative expression level of Bax gene 48 h after iodine therapy, at a dose of 100 and 150 mci. The relative expression level of Bax gene at a dose of 100 and 150 mci showed a significant increase in comparison with before iodine therapy ($P = 0.0001$).

As observed in Figure 3, in two groups a significant decrease was found in the expression level of Bcl-2 in comparison with the control group ($P < 0.05$). The relative expression level of Bcl2 gene at a dose of 100 and 150 mCi showed a significant reduction in comparison with before iodine therapy.

Figure 4 shows the relative expression level of Bax/Bcl-2 ratio 48 h after the iodine therapy at doses of 100 and 150 mCi). The ratio of Bax/Bcl-2 in after iodine therapy in comparison with before treatment led to a significant increase in the Bax/Bcl-2 ratio.

Figure 5 shows the relative expression level Bax, Bcl2, and Bax/Bcl-2 ratio 48 h after iodine therapy at different doses. At a dose of 150 mCi after iodine therapy, a significant increase was showed in the expression level of Bax comparison with dose 100 mci. We observed a significant increase in the ratio of Bax/Bcl-2 at a dose of 150–100 mci. It can be concluded that, at higher doses, expression of the apoptotic gene will increase and the percentage of apoptotic cells will be greater. Tables 2 and 3 show the relative expression of Bax and Bcl-2 genes and Bax/Bcl-2 ratio of two therapeutic doses 48 h after iodine therapy. The relative expression level of Bax gene in both groups showed a significant increase after radioiodine therapy compared with before treatment. Moreover, the relative decrease in gene expression of Bcl-2, after the iodine treatment in both groups was statistically significant ($P < 0.05$). The ratio of the Bax/Bcl-2 in both groups showed a significant increase ($P < 0.05$).

As shown in Table 4, we examined the effect of two different doses of the gene expression of apoptosis. At a dose of 150 mCi, there was an increase in the dose of 100 mCi of the Bax gene expression. Bcl-2 levels also significantly decreased

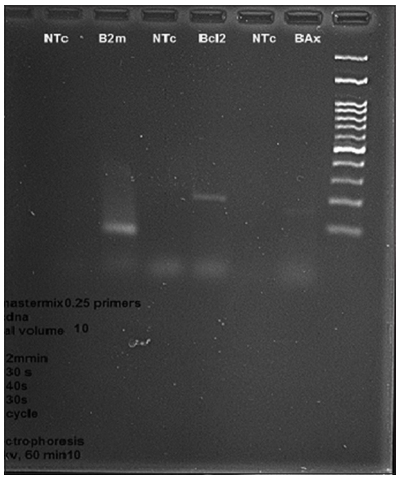

Figure 1: Electrophoresis image of the designed Bcl-2, and Bax primers (Bcl-2, 153 bp and Bax, 169, B2m 87 bp), which is visible in the image

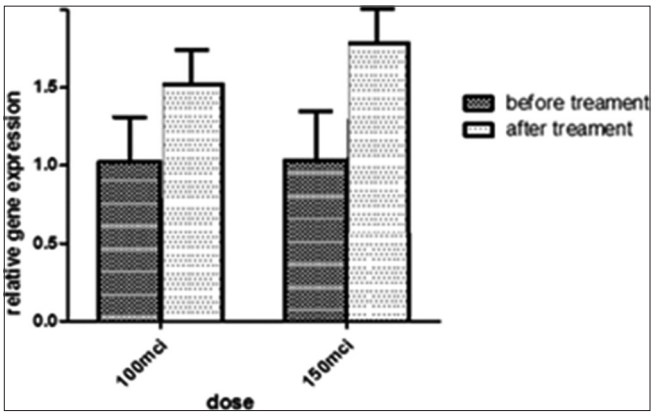

Figure 2: The relative expression level of Bax gene 48 h after the iodine therapy at doses of 100 and 150 mCi

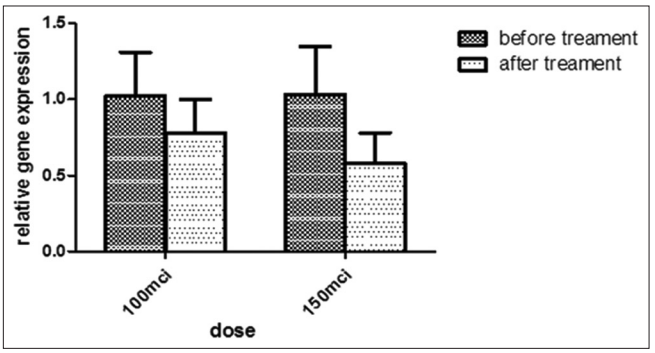

Figure 3: The relative expression level of Bcl2 gene 48 h after the iodine therapy at doses of 100 and 150 mCi

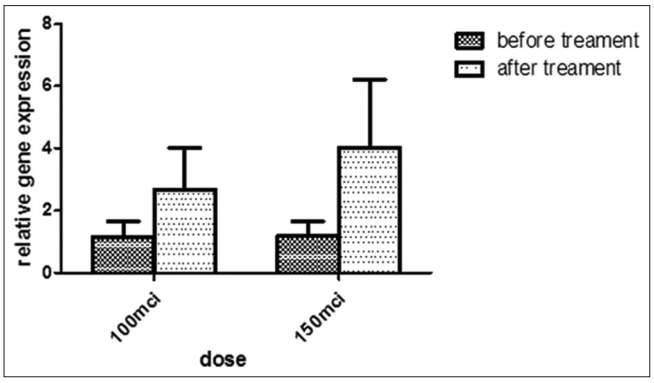

Figure 4: The relative expression level of Bax/Bcl-2 gene 48 h after the iodine therapy at doses of 100 and 150 mCi

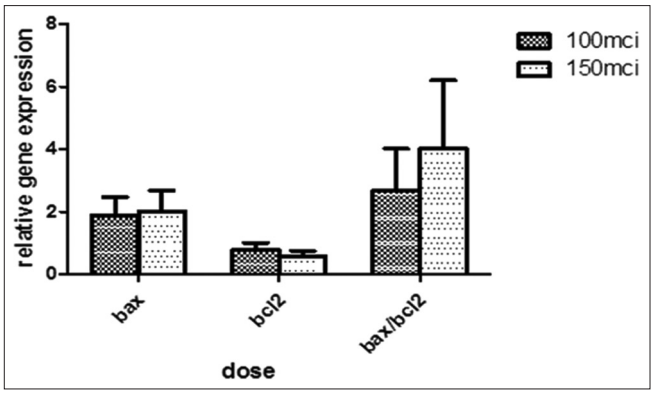

Figure 5: The relative expression level of Bax/Bcl-2 gene 48 h after the iodine therapy at doses of 100 and 150 mCi

Table 2: Comparison of gene expression BCL-2 and BAX before and 48 hours after radioiodine therapy in the dose of 100 mCi

100 mCi	Before Iodine-131	After Iodine-131	Significance (*P*)
BAX	1.07±0.24	1.89±0.59	0.0001
BCL-2	1.02±0.29	0.78±0.22	0.03
BAX/BCL-2	1.16±0.50	2.69±1.33	0.0006

Table 3: Comparison of gene expression BCL-2 and BAX before and 48 hours after radioiodine therapy in the dose of 150 mCi

150 mCi	Before Iodine-131	After Iodine-131	Significance (*P*)
BAX	1.11±0.29	2.01±0.68	0.0001
BCL-2	1.03±0.32	058±0.20	0.0001
BAX/BCL-2	1.18±0.48	4.04±2.18	0.0001

Table 4: Comparison of gene expression BCL-2 and BAX in human lymphocytes at a dose of 100 and 150 mCi

	After Iodine-131		Significance (*P*)
	100 mCi	150 mCi	
BAX	1.88±0.58	2±0.67	0.5
BCL-2	0.78±0.22	0.57±0.19	0.005
BAX/BCL-2	2.695±1.33	4.03±2.18	0.03

in a dose of 150 mCi to 100 mCi dose and this reduction was significant ($P = 0.0005$).

Furthermore, we observed a significant increase in the ratio of Bax/Bcl-2 at a dose of 150–100 mci and it can be concluded that, at higher doses, expression of the apoptotic gene will increase and the percentage of apoptotic cells will be greater.

Discussion

The 131 iodine is applicable in the thyroid cancers with a dosage higher than 100 mCi. Iodine in the patients that have undergone thyroidectomy is applied for the destruction of the remaining thyroid with probable metastases.[5] Lymphocytes are easily eliminated as high-sensitivity cells in patients treated with radioactive iodine.[21] Apoptosis is a reaction of cytogenic damage in the cells, and in this study, the expression of apoptosis genes was compared before and after iodine therapy. The purpose of this study was to investigate the effect of iodine therapy on the changes of apoptosis levels and expression of apoptosis genes.

Based on the obtained results of this study, the percent of apoptosis lymphocytes, 48 h after iodine therapy in comparison with before treatment shows that the increased level can be attributed to the increase in Bax gene expression in both groups which received 100 and 150 mCi. In addition, increase in the expression of the ratio of Bax/Bcl2 is an effective factor for incidence of apoptosis.

According to the results of a study conducted by Cui *et al*., it was shown that after 4 h exposure of all the body to 2–8 gray gamma radiation, the apoptosis lymphocytes increased rapidly, and expression of Bax gene in 24 h after radiation reached its maximum amount.[22] The Bcl-2 expression reduces after passing 3 h after radiation, and the reduction reaches its minimum amount 24 h after that.[22] This finding is consistent with the obtained results of our research; in the conducted study, the gamma arising from iodine 131 caused generation of apoptosis, increase of Bax gene expression and reduction of Bcl-2 in 48 h after prescribing iodine.

In another study done by Mehdi Mogharrabi *et al*. on patients with thyroid cancer, the injuries of radiation cytology to the peripheral blood lymphocytes (PBLs) were investigated by using the MN test.[23] The blood samples before iodine therapy and 1 week after that were taken by receiving the dosages of 100 and 150 mCi. As MN was abundant, a week after iodine therapy, it was seen that it was an indirect marker of chromosomal abnormalities and radiation injury.[23] This was similar to the obtained result of our study. MN and apoptosis are raised as cytogenic damages arising from radiation. The study results showed iodine therapy caused the effect of apoptosis, and its gene expression.

Conclusions

Iodine therapy reduces the relative expression of anti-apoptotic Bcl-2, and pro-apoptotic Bax gene expression was increased significantly. The ratio expression of Bax/Bcl-2 in doses of 100 and 150 mCi showed a significant increase. Apoptosis in PBLs after treatment with 100 or 150 mCi iodine-131 was significantly higher than before treatment. Patients with DTC have a significantly higher level of apoptosis in PBLs after iodine therapy. Based on the results of this study, radioiodine therapy in patients with thyroid cancer has led to increased apoptosis as a marker of cytogenetic damage.

Therefore, it can be suggested that this method can be useful for monitoring and detecting destructive effects of ionizing radiation in nuclear medicine patients.

Acknowledgment

The present article was financially supported by Shiraz University of Medical Sciences, Shiraz, Iran Grants No. 11087. The authors would like to thank Center for Development of Clinical Research of the Nemazee Hospital for statically analysis assistance and editing the manuscript.

Financial support and sponsorship

Shiraz University of Medical Sciences.

Conflicts of interest

There are no conflicts of interest.

References

1. Agate L, Lorusso L, Elisei R. New and old knowledge on differentiated thyroid cancer epidemiology and risk factors. J Endocrinol Invest 2012;35:3-9.
2. Patel KN, Shaha AR. Poorly differentiated and anaplastic thyroid cancer. Cancer Control 2006;13:119-28.
3. Saha GB.) Quality control of radiopharmaceuticals. In: Fundamentals of nuclear pharmacy. 5th ed. New York: Springer; 1998. p. 151-74.
4. Chilton HM, Witcofski RL. Nuclear Pharmacy: An Introduction to the Clinical Application of Radiopharmaceuticals. Philadelphia, PA: Lea and Febiger; 1986.
5. Li LB, Wang JP, Yu XR, He SS, Yu FH, Ding CH, *et al.* Medical radiation usage and exposures from medical X ray diagnosis in Shandong province of China. Radiat Prot Dosimetry 2001;93:261-6.
6. Mikkelsen RB, Wardman P. Biological chemistry of reactive oxygen and nitrogen and radiation-induced signal transduction mechanisms. Oncogene 2003;22:5734-54.
7. Tominaga H, Kodama S, Matsuda N, Suzuki K, Watanabe M. Involvement of reactive oxygen species (ROS) in the induction of genetic instability by radiation. J Radiat Res 2004;45:181-8.
8. Verma SP, Sonwalkar N. Structural changes in plasma membranes prepared from irradiated Chinese hamster V79 cells as revealed by Raman spectroscopy. Radiat Res 1991;126:27-35.
9. Elia MC, DeLuca JG, Bradley MO. Significance and measurement of DNA double strand breaks in mammalian cells. Pharmacol Ther 1991;51:291-327.
10. Lizard G, Fournel S, Genestier L, Dhedin N, Chaput C, Flacher M, *et al.* Kinetics of plasma membrane and mitochondrial alterations in cells undergoing apoptosis. Cytometry 1995;21:275-83.
11. Azimian H, Bahreyni-Toossi MT, Rezaei AR, Rafatpanah H, Hamzehloei T, Fardid R, *et al.* Up-regulation of bcl-2 expression in cultured human lymphocytes after exposure to low doses of gamma radiation. J Med Phys 2015;40:38-44.
12. Bahreyni-Toossi MT, Fardid R, Rezaee A, Sadr-nabavi A, Rafatpanah H, Bolbolian M. Expression of apoptotic genes can distinguish radiation workers from normal population. Int J Low Radiat 2011;8:388-99.
13. Vandaele L, Mateusen B, Maes DG, de Kruif A, Van Soom A. Temporal detection of caspase-3 and -7 in bovine *in vitro* produced embryos of different developmental capacity. Reproduction 2007;133:709-18.
14. Jousan FD, de Castro E Paula LA, Brad AM, Roth Z, Hansen PJ. Relationship between group II caspase activity of bovine preimplantation embryos and capacity for hatching. J Reprod Dev 2008;54:217-20.
15. Opiela J. Apoptosis in preimplantation bovine embryos and methods used for its detection. Ann Anim Sci 2009;9:3-16.
16. Gopisetty G, Ramachandran K, Singal R. DNA methylation and apoptosis. Mol Immunol 2006;43:1729-40.
17. Tsujimoto Y, Shimizu S. Bcl-2 family: Life-or-death switch. FEBS Lett 2000;466:6-10.
18. Spanos S, Rice S, Karagiannis P, Taylor D, Becker DL, Winston RM, *et al.* Caspase activity and expression of cell death genes during development of human preimplantation embryos. Reproduction 2002;124:353-63.
19. Nagata S. Apoptotic DNA fragmentation. Exp Cell Res 2000;256:12-8.
20. Vrndic O, Milosevic-Djordjevic O, Djurdjevic P, Jovanovic D, Mijatovic L, Jeftic I, *et al.* Radioiodine therapy accelerates apoptosis in peripheral blood lymphocytes of patients with differentiated thyroid cancer. Neoplasma 2013;60:568-75.
21. Lowe SW, Lin AW. Apoptosis in cancer. Carcinogenesis 2000;21:485-95.
22. Cui YF, Ding YQ, Xu H, Jiang ZJ, Liu XL, Dong B, *et al.* Relationship between apoptosis of mouse thymic lymphocytes and expressions of BAX, BCL-2 and BCL-XL after gamma-ray radiation with lethal dose. Xi Bao Yu Fen Zi Mian Yi Xue Za Zhi 2004;20:750-3.
23. Hooman A, Mogharrabi M, Solooki M, Mosaffa N, Tabeie F, Shafiee B, *et al*. Radioiodine therapy induced cytotoxicity in patients with differentiated thyroid carcinoma. Int J Endocrinol Metab 2008;2008:135-9.

Technical Note

Dosimetric Comparison of Treatment Plans Using Physical Wedge and Enhanced Dynamic Wedge for the Planning of Breast Radiotherapy

Zhenia Gopalakrishnan, Raghuram K. Nair, P. Raghukumar, B. Sarin
Division of Radiation Physics, Regional Cancer Centre, Trivandrum, Kerala, India

Abstract

The aim of this study is to compare the physical wedge (PW) with enhanced dynamic wedge (EDW) to determine the difference in the dose distribution affecting the treated breast and the contralateral breast, lungs, heart, esophagus, spine, and surrounding skin in the radiotherapy of breast cancer. Computed tomography (CT) data sets of 30 breast cancer patients were selected from the database for the study. The treatment plans which were executed with PW were re-planned with EDW without changing the beam parameters. Keeping the wedge angles same, the analytic anisotropic algorithm (AAA) with heterogeneity correction was used for dose calculation in all plans. The prescription was 50 Gy in 25 fractions. The dose- volume histogram (DVH) of the planning target volume (PTV) and critical structures of both PW and EDW plans were analyzed. The analysis showed that the maximum dose within the target volume is higher in EDW plan compared to PW plan. However the PTV conformity index (CI) remained the same in both plans. For all the critical structures, the EDW technique offered less dose compared to PW technique. The effect of volume of the contralateral breast on the dose to contralateral breast and the effect of volume of PTV breast for patients with carcinoma left breast on the dose to heart were studied and analyzed for the two wedges. No correlation between volumes and dose parameters was found for the two techniques. The number of monitor units to deliver a particular dose with EDW field is less than that of PW field due to change in wedge factor. As EDW produces less scattered dose to structures outside the treatment field, the risk of a second malignancy can be reduced with this technique.

Keywords: Contralateral breast, dose-volume histogram, enhanced dynamic wedge, physical wedge

Received on: 23-03-2017 **Review completed on: 10-11-2017** **Accepted on: 14-11-2017**

Introduction

There are various studies that prove breast conservation surgery (BCS) followed by radiotherapy to the whole breast is the preferred mode of treatment in early breast cancer.[1,2] In conventional radiotherapy, the wedge filter technique is the most commonly used. In three-dimensional conformal radiotherapy, a multileaf collimator (MLC) is used to confirm the shape of the radiation beam to avoid the nearby critical structures.[3] In Varian Clinac-600C machine, two types of wedges are available. One is a physical wedge (PW) filter which is made of an alloy of steel and lead. It is available in 4 angles (15°, 30°, 45°, and 60°) and 4 orientations (in, out, right, and left). The other is an enhanced dynamic wedge (EDW), in which wedging effect is created by moving the Y-jaws while the beam is on. It is possible to create wedge distributions for wedge angles 10°, 15°, 20°, 25°, 30°, 45°, and 60° by selecting the appropriate segmented treatment tables (STTs) called golden STT.[4] Dosimetric characteristics of PW and EDW and the clinical differences have been described elsewhere.[4,5] Several studies have shown that there is a possibility of the patient developing radiation-induced cancer following the treatment of malignancy of breast cancer. Many investigators have quantified the risk of second primary breast cancer in the contralateral breast after radiotherapy for the first breast cancer.[6] According to their study, women <40 years of age with follow-up periods more

Access this article online

Quick Response Code:

Website: www.jmp.org.in

DOI: 10.4103/jmp.JMP_40_17

Address for correspondence: Ms. Zhenia Gopalakrishnan, Division of Radiation Physics, Regional Cancer Centre, Medical College Campus, Trivandrum - 695 011, Kerala, India.
E-mail: zhenia.rcc@gmail.com

How to cite this article: Gopalakrishnan Z, Nair RK, Raghukumar P, Sarin B. Dosimetric comparison of treatment plans using physical wedge and enhanced dynamic wedge for the planning of breast radiotherapy. J Med Phys 2018;43:46-51.

than 5 years had a radiation risk of 3.0% and the dose response was significant. Women <40 years of age who received a radiation dose more than 1.0 Gy to the contralateral breast had an elevated, long-term risk of developing a second primary contralateral breast cancer. The risk is inversely related to age at exposure and is dose-dependent. Certain studies have mentioned that the risk increases with the use of wedges in the medial beam.[7,8] Some have compared the dose to the contralateral breast, ipsilateral lung, and the whole lung in tangential field radiotherapy for primary breast cancer using "dynamic wedge" and PW.[9,10] They reported that the dose to normal structures is reduced using the dynamic wedge, thereby reducing the normal tissue complication probability. The aim of the study was to investigate the effect of using PW and EDW on planning target volume (PTV) and all the critical structures during primary breast irradiation using radiotherapy treatment planning system (TPS) Eclipse v-13.

Materials and Methods

The treatment plan of thirty patients who underwent BCS for infiltrating duct carcinoma breast and stage ($T_{(1-2)}$ N_0 M_0) and who already underwent radiotherapy in the period 2012–2013 were selected for the study from the database. Twelve patients were treated for disease of right breast and 18 for left breast. For actual patient treatment, the plans were generated with PW for a dose of 50 Gy in 25 fractions. The same computed tomography (CT) data sets, target volumes, and organs at risk (OAR) were used for the study. All the patients were treated in the supine position with both the arms abducted and immobilized with breast board to reproduce daily setup and minimize setup errors. All the CT simulation images were acquired in a 16 slice CT simulator (GE Optima 580W). Scans of 5-mm slice thickness were acquired for each patient covering just below the mandible and extending 5–6 cm below the inframammary fold. A radiopaque wire was placed around the breast to be treated, to define the field borders. For each patient, PTV and OARs such as ipsilateral lung, contralateral lung, heart, contralateral breast, esophagus, and spine were contoured by the radiation oncologist. Skin was contoured as a thin strip of 5 mm extending from patient outline to the anterior surface of PTV and 2 cm equally in craniocaudal and medial and lateral directions.

Treatment planning

For each patient, plans that were already generated using PW were recalculated with EDW in "Eclipse" TPS v13 without changing the beam parameters. Varian's Clinac 600C machine with 6 MV photon beam was used for treatment. Two opposing tangential half beams were placed to cover the whole breast. The medial field border was placed near the midline of the patient. The superior border was placed just below the level of clavicle. The inferior border was placed 1 cm inferior to the inframammary fold. Gantry angles varying from 300° to 310° were used for medial tangent beam and angles ranging from 120° to 130° were used for lateral tangent for left breast cases. Similarly, gantry angles varying from 50° to 60° were used for medial beam and angles ranging from 230° to 240° were used for lateral tangent for right breast cases. For plans using PW, collimator angles of 8°–10° were given to reduce the volume of ipsilateral lung coming in the path of the beam. As PW can be inserted in any of the four orientations, this collimation was sufficient to produce the wedging in the required orientation. But with EDW, as wedging effect is produced by the movement of Y-jaws, a collimation of 90° or 270° was mandatory to produce the wedging in the required direction. Additional collimation of 8°–10° was given to reduce the volume of ipsilateral lung coming in the radiation field. Both EDW and PW plans did not use MLC as collimator rotation was different for both. The wedge angles varied from 15° to 30°. Same wedge angles were used for both plans without changing other beam parameters.

Using Beams Eye View option in Eclipse TPS, fields were placed to minimize the dose to heart, contralateral breast, ipsilateral lung, and maximize the PTV coverage. The dose was normalized to 100% at midplane where a reference point called weight point was put to normalize the prescription dose. This point was placed 2–3 cm anterior to the ipsilateral lung on the central axial slice of the treated breast PTV. The same weight point was used for both PW and EDW.

The analytical anisotropic algorithm (AAA Version 13), a photon dose calculation algorithm (grid size 2.5 mm) with heterogeneity correction was used for dose calculation in all plans. For all patients, dose was given in 25 fractions of 200 cGy to deliver a total dose of 50 Gy to the whole breast. The plans were compared using dose-volume histogram (DVH) tool. The DVH of the PTV and critical structures of both PW and EDW plans were analyzed. The criterion for PTV coverage was to deliver 95% of prescription dose to 95% of PTV and also not to exceed 110% of the prescribed dose in more than 1 cc of the PTV.

Conformity index

Conformity index (CI) was used to evaluate the plan quality in terms of PTV conformity which is defined as:

- CI = reference isodose volume/target volume.[11]

Here, reference isodose volume was taken as 95% isodose volume of the PTV. Target volume is the total volume of the PTV. CI was calculated for both sets of plans and compared.

Dose-volume constraints and toxicity

During breast radiotherapy, the critical organs such as contralateral breast, heart, lungs, and skin receive substantial amount of radiation due to their proximity to treated breast. Various groups have defined dose- volume constraints for the radiotherapy planning of breast cancer.[12-15] Dosimetric predictors of radiation (RT)-induced lung injury (pneumonitis) are mean lung dose and percentage of the total lung volume exposed to a dose of 5, 10, and 20 Gy (V_5, V_{10}, and V_{20}).[16] As per RTOG protocol, the acceptable criteria for ipsilateral lung are V_{20} <20%, V_{10} <40%, and V_5 <55%. The V_5 of the contralateral lung should be <10%–15%.[14]

RT-induced heart injury may manifest as acute or late toxicity. Pericarditis is an acute injury often transient but may be chronic. Late injury includes congestive heart failure, ischemia, coronary artery disease, and myocardial infarction.[17,18] RTOG protocols have defined heart dose-volume constraints for left-sided breast cancer as, V_{20} <5%, V_{10} <30% and mean dose <4 Gy as ideal. However, V_{25} ≤5% and V_{10} ≤35% and mean dose <5 Gy are also acceptable.[14] Dose-volume constraints of the heart for right side breast cancer were defined to keep V_{20} = 0 and V_{10} <10% as ideal, but V_{25} = 0 and V_{10} <15% are also acceptable. Some of the cardiac parameters were chosen to reflect available data regarding the risk of cardiac toxicity.[19] In the patient group selected for the study, the volume of PTV of carcinoma left breast patients ranged from 784 cc to 2260 cc. An analysis was also done to find a correlation between volume of PTV of left breast and dose parameters like D_{mean}, D_{max}, D_{30}, V_{20}, and V_{10} for heart for the two techniques.

The dose to the contralateral breast is because of the medial tangent beam, and the result of collimator scatter, leakage, scatter from wedges, etc. The RTOG breast study protocol recommends keeping the D_{max} of the contralateral breast <3.3 Gy.[14] In this study, volume of contralateral breast ranged from 358 cc to 1629 cc for 30 patients. Here also, an analysis was done to find any correlation between volume of contralateral breast and dose parameters such as D_{max}, D_5, and V_5 for the two techniques.

Emami *et al*. defined the tolerance dose of the spinal cord based on the irradiated length of the cord as follows: 47 Gy to 20 cm, 50 Gy to 10 cm, and 50 Gy to 5 cm.[13] In RTOG protocols, the maximum dose to the spinal cord is limited to 45–50 Gy.[14] In this study, we have compared the maximum cord dose between the two plans (PW and EDW). During the treatment of whole breast after BCS, the esophagus seldom comes in the path of radiation. However, we also tried to estimate the mean esophagus dose from the two plans. For skin, toxicity includes erythema, hyperpigmentation, and skin desquamation. Late toxicities include skin fibrosis, telangiectasia, contracture, and even necrosis.[20,21] For patients treated with BCS, where the skin is not at risk, the selection of adequate beam energy, careful contouring, and plan evaluation (reviewing the D_{max} and hot spot regions) may help to spare skin (4–5 mm thickness to include the epidermis, dermis, and hypodermis) to reduce acute and late toxicity and subsequently maintain cosmesis.[20] Emami *et al*. estimated tolerance doses of skin (TD5/5) as 50 Gy for 100 cm^2, 60 Gy to 30 cm^2, and 70 Gy to 10 cm^2.[13] In the present study, the maximum dose and mean dose received by skin in both plans using PW and EDW have been compared.

The data obtained was statistically analyzed using two-tailed paired Student's *t*-test.

Results

Table 1 shows the comparison of PTV and critical structures between PW and EDW techniques using dosimetric parameters. There was a significant difference between dose to 2% volume of PTV for PW and EDW ($P < 0.001$). However, there was no statistical difference in the PTV CI of plans calculated using both wedges. Figure 1 shows the dose distribution of a representative case (left breast) in transverse, sagittal, and coronal slices using PW and EDW. From the figure, it can be seen that the isodose distributions are almost similar for both PW and EDW.

The dose to all the critical structures were less for plans calculated with EDW when compared to PW ($P < 0.001$). The number of monitor units required to deliver dose with EDW is less compared to PW due to the difference in the wedge factors. This might be the reason for the reduced dose to the critical structures outside the treatment field. The DVH for PTV and

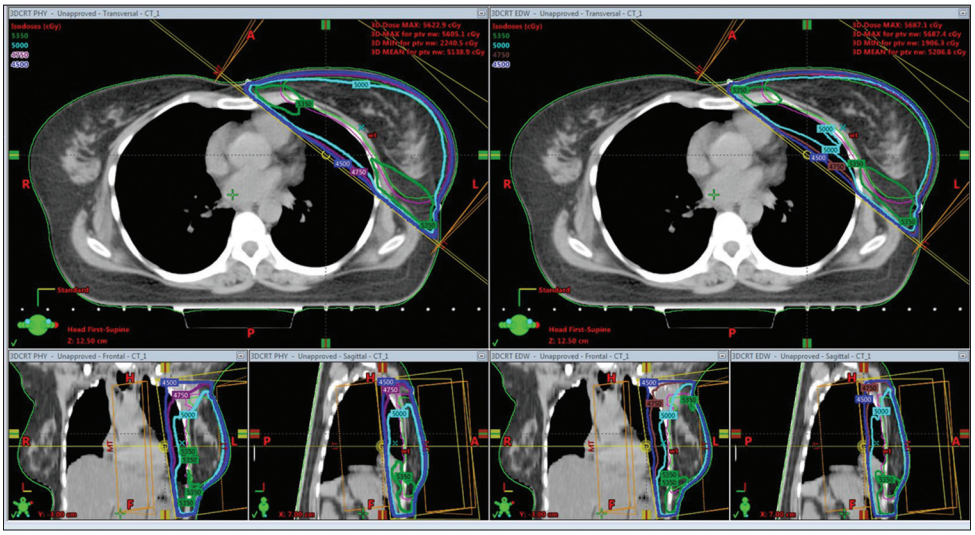

Figure 1: Dose distribution of a planned case (left breast) in transverse, sagittal, and coronal slices using physical wedge and enhanced dynamic wedge (Varian Eclipse treatment planning system V-13)

Table 1: Comparison of planning target volume and critical structures between physical wedge and enhanced dynamic wedge techniques using dosimetric parameters

Variable	Mean±SD (range)		*P*
	PW	EDW	
PTV (mean volume=1328 cc; median=1402 cc; range=417-2260 cc)			
D_{max} (cGy)	5591±143.3 (5305-5882)	5692±142.46 (5371-5945)	<0.001
D_{min} (cGy)	3914±485.08 (2434-4649.5)	3889.5±458.96 (2462-4714)	0.64
D_{mean} (cGy)	5102.0±59.7 (4985-5236)	5138±69.3 (4999-5272)	<0.001
D_{2} (cGy)	5443±102.4 (5234-5585)	5508.0±108.5 (5298-5705)	<0.001
D_{95} (cGy)	4839.0±45.4 (4780-4958)	4848.5±53.2 (4760-4987)	0.146
TV_{95} (cc)	1310.5±397.94 (409.8-2225)	1304.2±395.55 (412-2186)	0.006
Monitor units	431.7±40.25 (337-496)	253.4±9.87 (237-275)	<0.001
CI	1.06±0845 (1.00-1.29)	1.07±0.0813 (1.00-1.33)	0.347
Ipsilateral lung (mean volume=848 cc; median=860 cc; range=580-1103 cc)			
D_{mean} (cGy)	986±324 (359-1631)	820.0±303 (227-1378)	<0.001
D_{max} (cGy)	5139.0±199 (4678-5511.3)	5131.0±193 (4690-5406)	0.5
V_{20} (%)	13.9±6.44 (3.53-25.2)	13.3±6.25 (2.55-24.5)	<0.001
V_{10} (%)	19.9±7.869 (7.2-29.9)	17.1±7.08 (4.35-26.2)	<0.001
V_{5} (%)	39.3±13.7 (12.7-70.2)	25.24±8.32 (6.2-38.3)	<0.001
Contralateral lung (mean volume=889 cc; median=859 cc; range=549-1131 cc)			
D_{max} (cGy)	418±179 (169.7-1136.7)	149.6±121 (63-319)	<0.001
D_{5} (cGy)	244±78 (165.78-426)	45±15 (26.8-73)	<0.001
Heart-right lesion (mean volume=437.4 cc; median=450 cc; range=240-666 cc)			
D_{mean} (cGy)	255±51 (184.3-332)	79±13.9 (59-99)	<0.001
D_{max} (cGy)	996±545 (520-2389)	742±564 (303-2225)	<0.001
D_{30} (cGy)	288±60.0 (217-359)	94±16.4 (71-111)	<0.001
D_{5} (cGy)	450±86 (352-529)	217±42 (171-284)	<0.001
Heart-left lesion (mean volume=437.4 cc; median=450 cc; range=240-666 cc)			
D_{mean} (cGy)	667.116±267 (380-1155)	472.0±260 (188-1025)	<0.001
D_{max} (cGy)	5128.0±224 (4555-5475)	5134±245 (4367-5405)	0.71
D_{30} (cGy)	466.7±108 (315-677)	241.0±61 (180-350)	<0.001
V_{20}%	6.74±5.29 (0.87-18.8)	6.41±5.2 (0.39-18.4)	<0.001
V_{10}%	8.9±6.00 (2.3-21)	7.7±5.6 (0.89-20)	<0.001
Esophagus (mean volume=21.8 cc; median=20cc; range=6-43 cc)			
D_{mean} (cGy)	196.0±62 (115.3-347)	61.5±15 (45-102)	<0.001
Spine (mean volume=40.92 cc; median=40 cc; range=24-58 cc)			
D_{max} (cGy)	177.0±55 (110-302)	64.2±16 (41-98)	<0.001
Contralateral breast (mean volume=889.0 cc; median=869 cc; range=358-1629 cc)			
D_{max} (cGy)	734±430.2 (335-1762)	463±422 (112-1537)	<0.001
D_{5} (cGy)	352±101 (171-524)	78±26 (42-147)	<0.001
V_{5} (%)	1.71±3.36 (0-14.5)	0.004±0.018 (0-1.05)	0.01
Skin (mean volume=218 cc; median=218 cc; range=101-373 cc)			
D_{max} (cGy)	5454±147 (5224-5697)	5638.0±156 (5343-5878)	<0.001
D_{mean} (cGy)	3485±192 (3237-3758)	3455.4±183 (3217-3727)	0.1118
NTID (Gy.Lt)	45.50±12.05 (26.07-71.25)	27.08±8.13 (14.59-45.29)	<0.001

CI: Conformity index, PTV: Planning target volume, PW: Physical wedge, EDW: Enhanced dynamic wedge, NTID: Normal tissue integral dose, TV: Target volume

critical structures using PW and EDW for a representative patient is shown in Figure 2.

There was no correlation between the volume of contralateral breast and the dose to contralateral breast for both wedges. Similarly, there was no correlation between volume of PTV breast and dose to heart. Volume alone may not be the deciding factor as other parameters such as beam orientation, wedge angles, beam weights, etc., may also influence the dose to the nearby critical organs.

Discussion

The studies have shown that the scatter radiation to contralateral breast may play a large part in the induction of secondary breast cancer.[8-10,22,23] In the studies by Warlick *et al.*[23] and Akram *et al.*,[9] a comparison of the dose to the contralateral breast was made between EDW and the standard physical wedge plans. The measurements revealed a significant reduction in the contralateral breast dose (CBD) with EDW compared to the standard physical wedges. The average dose with EDW

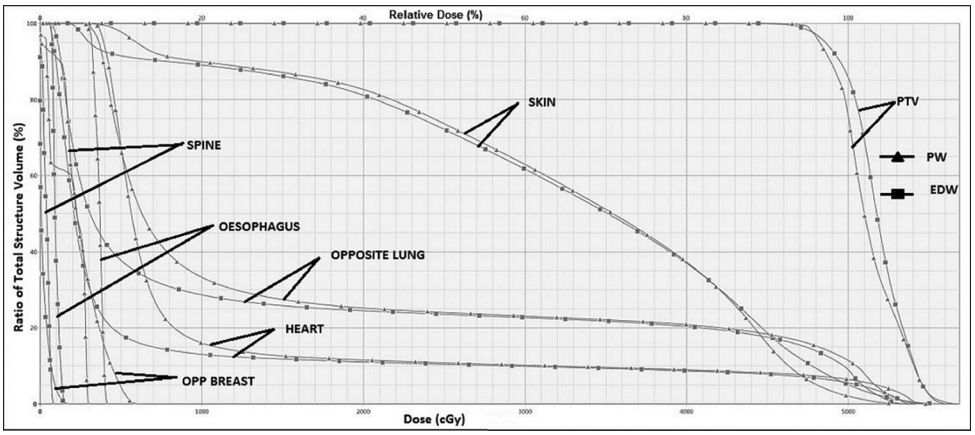

Figure 2: Dose-volume histogram of planning target volume and critical structures for enhanced dynamic wedge and physical wedge for a representative case (left breast) (Varian Eclipse treatment planning system V-13)

was 2.7%–2.8%, whereas with the standard wedge, it was 4.0%–4.7% in the study by Warlick *et al.* Comparable results are seen in the present study too where the average of dose to 5% volume of contralateral breast reduced from 7.0% in PW plans to 1.5% in EDW plans. Akram *et al.* concluded that EDW is a practical clinical advance which improves the dose distribution in patients undergoing breast conservation while minimizing dose to the contralateral breast, thereby reducing the potential carcinogenic effects. The DVH analysis of the present study also showed that the critical organ sparing is better with EDW plan compared to that of the PW plan.

The dose to heart using PW and EDW for 12 right breast patients and 18 left breast patients was compared. For the right breast cases, the mean dose, the maximum dose, and D_{30} and D_5 values of heart were significantly less for EDW plans ($P < 0.001$). For left breast plans, all the above parameters (D_{mean}, D_{30}, V_{20}, and V_{10}) except the maximum dose to heart were significantly less for the EDW plans than the PW plans ($P < 0.001$).

Wang Dan *et al.*[10] also recommended EDW compared to PW due to the reduced dose to contralateral breast. They compared the dose to the contralateral breast, ipsilateral lung, and the whole lung in tangential field radiotherapy for primary breast cancer using "dynamic wedge" which has limited wedge angles compared to EDW and PW. The mean dose to contralateral breast reduced for dynamic wedge when compared to PW. The values of V_{20} were equal. Their study verified that the dose to normal structures was reduced using the dynamic wedge, thereby reducing the normal tissue complication probability. Similar results are seen in the present study also where all the critical structures including ipsilateral lung, heart, esophagus, and spine received less dose for EDW plans compared to plans calculated with PW. Kelly *et al*. measured the CBD by comparing four primary breast irradiation techniques and recommends EDW compared to PW.[24]

For skin, the mean dose calculated with both the wedges gave comparable results. These results are similar to those reported by Li and Klein.[5] They reported that dynamic wedge and upper wedge systems deliver surface and peripheral doses similar to those of open fields in addition to maintaining wedge-shaped dose profiles that are independent of field size, in contrast to PW. They concluded that complete knowledge of the dosimetric characteristics, including the surface and peripheral doses, is critical in proper choice of a particular wedge system in clinical use. For the same prescribed dose, EDW plan required less monitor units than that of PW plan due to difference in wedge factor, which could probably reduce the scatter dose to structures outside the treatment field. Manickam and Sathyan analyzed treatment plans generated using PW and EDW for head and neck patients.[25] Their results validated that the EDW plans are comparable with that of the PW plan, and the DVH analysis showed that the critical organ sparing is slightly better with EDW plan compared to that of the PW plan. One of the disadvantages of using EDW is its reduced conformity with MLC-shaped fields due to a change in collimator rotation. This will increase the volume of ipsilateral lung coming in the radiation fields in the case of breast plans. But even then, the mean lung dose will be less with EDW plans than PW plans due to reduced monitor units. Furthermore, the normal tissue integral dose (NTID) (dose to the structure body minus PTV) was much less for EDW plans compared to PW plans. Hence, a proper choice of wedge is definitely important while planning the treatment of breast to reduce the dose to critical structures outside the treatment field, thereby reducing the chances of a second breast malignancy.

The technologist needs to re-enter the treatment room during treatment to manually place the PW in the proper orientation, thereby delaying the total execution time. Thus, the EDW technique offers reduction of time over PW by reducing the total beam ON time and overall setup time. For EDW, dose versus jaw position data are saved as dynalog files in the machine for each treatment field as the beam is delivered. Hence, a verification of dose delivery with EDW is also possible as a part of quality assurance of EDW.

Conclusion

There is no significant difference in the CI of PTV for plans calculated with PWs and EDW plans. No difference in the

average of plan normalization values were seen when PWs were replaced by EDW. Critical organ sparing is good with plans using EDW. There is a significant reduction in the dose to opposite breast, ipsilateral lung, and contralateral lung in plans calculated with EDW. The risk of a second malignancy can be reduced with EDW as it produces less scattered dose to structures outside the treatment field. The number of monitor units required to deliver the same dose is less with EDW plans, thereby reducing the overall treatment time. Furthermore, the treatment time could be reduced for EDW by more than 50% compared to PW as the technologist has to re-enter the treatment room for the insertion of the PW into the gantry head. This results in treating more number of patients in the machine.

Acknowledgment

The authors would like to thank Dr. Saju B, additional professor, Mrs. Sarika V Menon, assistant professor, Radiation Physics Division, Regional Cancer Centre, for their valuable advice.

Financial support and sponsorship

Nil.

Conflicts of interest

There are no conflicts of interest.

References

1. Veronesi U, Marubini E, Mariani L, Galimberti V, Luini A, Veronesi P, *et al*. Radiotherapy after breast conserving surgery in breast cancer: Long term result of randomized trial. Ann Oncol 2001;12:997-1003.
2. Blichert-Toft M, Nielsen M, Düring M, Møller S, Rank F, Overgaard M, *et al.* Long-term results of breast conserving surgery vs. mastectomy for early stage invasive breast cancer: 20-year follow-up of the Danish randomized DBCG-82TM protocol. Acta Oncol 2008;47:672-81.
3. Khan FM. The Physics of Radiation Therapy. 4th ed. Philadelphia: Lippincott Williams & Wilkins; 2010.
4. Saminathan S, Manickam R, Supe SS. Comparison of dosimetric characteristics of physical and enhanced dynamic wedges. Rep Pract Oncol Radiother 2011;17:4-12.
5. Li Z, Klein EE. Surface and peripheral doses of dynamic wedges. Int J Radiat Oncol Biol Phys 1997;37:921-5.
6. Stovall M, Smith SA, Langholz BM, Boice JD Jr., Shore RE, Andersson M, *et al.* Dose to the contralateral breast from radiotherapy and risk of second primary breast cancer in the WECARE study. Int J Radiat Oncol Biol Phys 2008;72:1021-30.
7. Boice JD, Elizabeth B, Harvey EB, Blettner M, Stovall M, Flannery JT. Cancer in the breast after radiotherapy for breast cancer. N Engl J Med 1992;326:781-5.
8. Heydari F, Sardari D. How Radiotherapy for Cancerous Breast may put the Opposite non-Cancerous Breast at Risk? International Conference on Earth, Environment and Life sciences (EELS-2014) December 23-24, 2014, Dubai (UAE); 2014.
9. Akram M. Optimum reckoning of contra lateral breast dose using physical wedge and enhanced dynamic wedge in radiotherapy treatment planning system. Int J Radiat Res 2014;12:295-302.
10. Dan W. Comparison between dynamic wedge and physical wedge in the influence of dose to the contralateral breast and lung in radiotherapy for primary breast cancer. Chin J Radiat Oncol 2005;38:295-7.
11. Feuvret L, Noël G, Mazeron JJ, Bey P. Conformity index: A review. Int J Radiat Oncol Biol Phys 2006;64:333-42.
12. A Randomized Phase III Study of Conventional Whole Breast Irradiation (WBI) Versus Partial Breast Irradiation (PBI) for Women with Stage 0, I, or II Breast Cancer NSABP PROTOCOL B-39/RTOG 0413: March 2011.
13. Emami B, Lyman J, Brown A, Coia L, Goitein M, Munzenrider JE, *et al.* Tolerance of normal tissue to therapeutic irradiation. Int J Radiat Oncol Biol Phys 1991;21:109-22.
14. Available from: http://www.rtog.org/ClinicalTrials/ProtocolTable.aspx. [Last accessed on 2011 Nov 20].
15. Bentzen SM, Constine LS, Deasy JO, Eisbruch A, Jackson A, Marks LB, *et al.* Quantitative analyses of normal tissue effects in the clinic (QUANTEC): An introduction to the scientific issues. Int J Radiat Oncol Biol Phys 2010;76:S3-9.
16. Demirci S, Ceylan N, Haydaroglu A. The organs at risk and radiation tolerance doses. Principles and Practice of Modern Radiotherapy Techniques in Breast Cancer. Ch. 12. New York: Springer Science+Business Media; 2013.
17. Demirci S, Nam J, Hubbs JL, Nguyen T, Marks LB. Radiation-induced cardiac toxicity after therapy for breast cancer: Interaction between treatment era and follow-up duration. Int J Radiat Oncol Biol Phys 2009;73:980-7.
18. Gagliardi G, Constine LS, Moiseenko V, Correa C, Pierce LJ, Allen AM, *et al.* Radiation dose-volume effects in the heart. Int J Radiat Oncol Biol Phys 2010;76:S77-85.
19. Qiu JJ, Chang Z, Horton JK, Wu QR, Yoo S, Yin FF, *et al.* Dosimetric comparison of 3D conformal, IMRT, and V-MAT techniques for accelerated partial-breast irradiation (APBI). Med Dosim 2014;39:152-8.
20. Halperin EC, Perez CA, Brady LW. Principles and Practice of Radiation Oncology. 5th ed. Philadelphia: Lippincott Williams & Wilkins; 2008. p. 321-50.
21. Saibishkumar EP, MacKenzie MA, Severin D, Mihai A, Hanson J, Daly H, *et al.* Skin-sparing radiation using intensity-modulated radiotherapy after conservative surgery in early-stage breast cancer: A planning study. Int J Radiat Oncol Biol Phys 2008;70:485-91.
22. McParland BJ. The effect of a dynamic wedge in the medial tangential field upon the contralateral breast dose. Int J Radiat Oncol Biol Phys 1990;19:1515-20.
23. Warlick WB, O'Rear JH, Earley L, Moeller JH, Gaffney DK, Leavitt DD, *et al.* Dose to the contralateral breast: A comparison of two techniques using the enhanced dynamic wedge versus a standard wedge. Med Dosim 1997;22:185-91.
24. Kelly C, Wang X, Chu J, Hartselle W. Dose to contralateral breast: Comparison of four primary breast irradiation techniques. Int J Radiat Oncol Biol Phys 1996;34:727-32.
25. Manickam R, Saminathan S. Evaluation of 3-D treatment plans using physical and motorized enhanced dynamic wedges. Med Phys 2009;36:2672-3.

Technical Note

Dosimetric Effect of Jaw Tracking in Volumetric-Modulated Arc Therapy

Sangutid Thongsawad, Chirasak Khamfongkhruea, Chirapha Tannanonta
Department of Radiation Oncology, Chulabhorn Hospital, Bangkok, Thailand

Abstract

The aim of this study was to investigate the potential of jaw tracking with the volumetric-modulated arc therapy (VMAT) to reduce the normal tissue dose. Plans of nasopharynx, lung, and prostate cancers (10 plans for each) were used to perform VMAT with and without jaw tracking. The dose reduction was evaluated in terms of organ doses and integral doses. Organ-dose reduction with jaw tracking was statistically significant in the volume receiving a dose of 5 Gy (V_5) of bladder, rectum, and lung, the volume receiving a dose of 10 Gy (V_{10}) of bladder, rectum, and lung, and the mean dose of lung ($P < 0.05$). Integral-dose reduction with jaw tracking was statistically significant in almost all the treatment plans ($P < 0.05$). For organ-dose reduction, jaw tracking in VMAT plan was effective in reducing V_5 and V_{10}. For integral-dose reduction, jaw tracking in VMAT plan is an efficient method for decreasing V_5.

Keywords: Integral-dose reduction, jaw tracking, organ-dose reduction, volumetric-modulated arc therapy

Received on: 06-07-2017 **Review completed on: 11-12-2017** **Accepted on: 06-01-2018**

Introduction

The purpose of radiation therapy is to deliver a prescribed dose to a tumor while minimizing doses to normal organs and surrounding tissues. Advanced radiation delivery techniques have been developed to optimize this purpose, such as intensity-modulated radiation therapy (IMRT) and volumetric-modulated arc therapy (VMAT).[1-5] However, IMRT and VMAT still deliver a low dose to normal organs because of interleaf leakage of multileaf collimators (MLCs).[6-11] Movement of collimator jaw in addition to MLCs during treatment was developed to decrease interleaf leakage to the patient.[12] VMAT with jaw tracking was developed in a recent model of linear accelerator (TrueBeam, Varian, Palo Alto, CA), as well as its corresponding commercial treatment planning system (TPS), Eclipse V.10.0, and newer versions. Collimator scattering during jaw moving was taken into account in the dose calculation algorithm at each control point for the Eclipse TPS.[13]

Many studies have shown the potential of jaw tracking in reducing radiation doses to normal organs by using different radiation delivery techniques. Joy *et al*.[14] evaluated the dosimetric effect of jaw tracking in step-and-shoot IMRT. Schmidhalter *et al*.[15] showed that dynamic IMRT with jaw tracking can decrease the integral dose. Kim *et al*.[16] evaluated the potential of VMAT with jaw tracking for reducing the dose to normal organs for nasopharynx plans. Snyder *et al*.[17] studied the advantage of jaw tracking in reducing doses to normal organs in IMRT and VMAT for spine stereotactic radiosurgery.

The purpose of this study was to investigate the potential of jaw tracking with the VMAT to reduce the normal tissue dose in nasopharynx, prostate, and lung treatment plans. In addition, this study provided a method for verifying an accuracy of TPS calculation for VMAT with jaw tracking by contouring a rectangular shape target volume to generate jaw tracking.

Subjects and Methods

The study was performed on a TrueBeam linear accelerator (Varian Medical Systems, Palo Alto, CA) equipped

Access this article online

Quick Response Code:

Website: www.jmp.org.in

DOI: 10.4103/jmp.JMP_75_17

Address for correspondence: Dr. Sangutid Thongsawad, Department of Radiation Oncology, Chulabhorn Hospital, 54 Kamphaengphet 6 Road, Laksi, Bangkok 10210, Thailand.
E-mail: sangutid.th@gmail.com

How to cite this article: Thongsawad S, Khamfongkhruea C, Tannanonta C. Dosimetric effect of jaw tracking in volumetric-modulated arc therapy. J Med Phys 2018;43:52-7.

with a millennium 120 MLC and was planned on Eclipse TPS V.10.0 (Varian Medical Systems, Palo Alto, USA).

Dose verification for jaw tracking

The accuracy of dose calculation for jaw tracking in the TPS was verified in terms of point dose and dose distribution before using the TPS to determine the reduction of the normal organ doses. Computed tomography (CT) images of an IMRT phantom (IMRT phantom, IBA Dosimetry, Germany) was acquired with a slice thickness of 3 mm, and then, the dose distribution was calculated on the CT images. For this purpose, we created rectangular shape of target volume in the IMRT phantom with a size of 16 cm × 17 cm × 4 cm (width × length × depth), as shown in Figure 1a. In the dose calculation, we used the rectangular shape target volume to generate the maximum jaw-tracking distance in the x-jaws and y-jaws of the collimator. The investigation was performed by using 10 MV photon with VMAT beam delivery with and without jaw-tracking methods. RapidArc plans were optimized by using two full arcs for each plan (Plan#1 and Plan#2) to verify the effect of collimator scattering in different jaw positions (x-jaw and y-jaw). A summary of the x-jaw and y-jaw moving distances for each plan are listed in Table 1. Figure 1b shows a collimator rotation to generate jaw tracking in x-jaw and y-jaw directions. For x-jaw tracking (Plan#1), the collimator was rotated to 30° and 330° for the first and second arc, respectively. For y-jaw tracking (Plan#2), the collimator was rotated to 70° and 300° for the first and second arc, respectively.

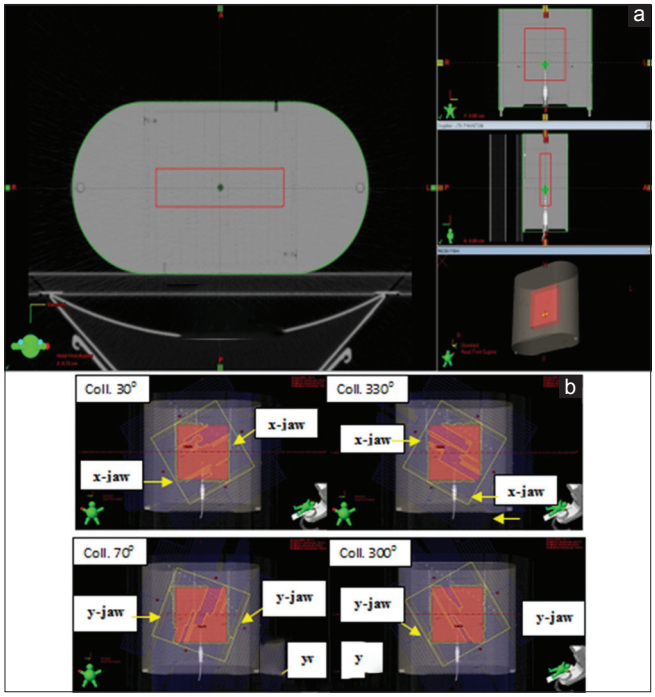

Figure 1: (a) The rectangular shape target volume for volumetric-modulated arc therapy with jaw tracking to generate the x-jaw and y-jaw traveling, (b) Collimator rotations of 30°/330° for x-jaw tracking and 70°/300°for y-jaw tracking

Point-dose measurement

A 0.6 cm^3 ionization chamber (PTW Freiburg GMBH, Germany) was inserted in the IMRT phantom for the measurement of point doses. The dose measurement was compared with the TPS calculation to determine the difference.

Dose distribution measurement

The dose distribution verification was performed by using portal dose image prediction (PDIP) (Varian Medical Systems, Pala alto, USA). Dose agreement between the portal dosimetry measurement and PDIP was analyzed by using gamma index[18] criteria of 2% and 2 mm. The portal dosimetry measurement was calibrated for darkfield, flood field, and dose normalization prior to use following manufacturer's recommendations.[19]

Determination of dose reduction from jaw tracking

Thirty plans were used for the organ-dose reduction evaluation: 10 nasopharyngeal cancers, 10 lung cancers, and 10 prostate cancers; plan information is listed in Table 2. In this study, we also evaluated the effect of tumor shape on dose reduction with jaw tracking by observing the jaw-tracking distance. To control the same parameters, VMAT planning was performed with and without jaw tracking using the same constraints and priorities. In addition, MU objective function was used to control the similar MU during optimization with the strength parameter of 90 (maximum 100). The dose constraints used to evaluate normal organs are listed in Table 3. The dose was normalized as 95% isodose to cover the planning target volume (PTV) for all plans.

Dose reduction was evaluated in terms of organ and integral doses. Organ-dose reduction was measured as the volume receiving a dose of 5 Gy (V_5), the volume receiving a dose of 10 Gy (V_{10}), the volume receiving a dose of 20 Gy (V_{20}), and mean dose. Organ-dose reduction was determined in the parotids for nasopharyngeal treatment plans, normal lung for lung treatment plans, and bladder and rectum for prostate treatment plans. To determine the radiation-induced secondary malignancies, the integral dose volume was calculated as the body subtracted from the PTV for each plan.[20] The integral-dose reduction was measured in terms of V_5, V_{10}, and mean dose. The data were presented as the averages of all patients followed by the standard deviation . According to the normal distribution of data, the paired *t*-test was used in this study to determine statistically dose reduction of jaw tracking compared with no jaw tracking. $P < 0.05$ is considered to be statistically significant.

Results

Dose verification for jaw tracking

Point-dose measurement

The percent difference between the point-dose measurement and TPS calculation was <0.5% for x-jaw and y-jaw tracking.

Dose distribution measurement

Dose agreement between the portal dosimetry measurement and PDIP was more than 96% gamma index passing rates with gamma index criteria of 2% and 2 mm for x-jaw and y-jaw tracking.

Table 1: Summary of x-jaw and y-jaw moving distance of jaw tracking plans for dose verification

Collimator rotation (°)	Jaw moving distance (cm)	
	x-jaw	y-jaw
Plan #1		
30	10.0	0.4
330	9.8	0.4
Plan #2		
70	5.0	9.6
300	3.2	11.3

Table 2: Summary of plan information for 30 patients in nasopharynx, lung, and prostate cancers

Plans	Energy (MV)	Jaw moving distance in cm, range (average)	
		x-jaw	y-jaw
Nasopharynx	6	0-8.5 (2.73)	0-6.3 (2.26)
Prostate	10	0.7-4.8 (2.23)	0-3.6 (1.11)
Lung	6 (5 plans) 10 (5 plans)	0-5.7 (2.04)	0-4.1 (1.22)

Table 3: Dose constraints for plan evaluation

Organ	Dose constraint
Parotids	D_{mean} <26 Gy
	$D_{50\%}$ <30 Gy
Rectum	$D_{50\%}$ <50 Gy
	$D_{35\%}$ <60 Gy
	$D_{25\%}$ <65 Gy
	$D_{20\%}$ <70 Gy
	$D_{15\%}$ <75 Gy
Bladder	$D_{50\%}$ <65 Gy
	$D_{35\%}$ <70 Gy
	$D_{25\%}$ <75 Gy
	$D_{15\%}$ <80 Gy
Lung	D_{mean} <20 Gy
	V_5 <65%
	$D_{35\%}$ <20 Gy (for radiation + chemo)
	$D_{40\%}$ <20 Gy (for radiation alone)
	$D_{30\%}$ <20 Gy

V_5: Volume receiving a dose of 5 Gy

Determination of dose reduction from jaw tracking

Figure 2 shows organ-dose reduction by using jaw tracking in various normal organs.

The most prominent reduction was found in V_5 of bladder with −1.52% of the volume. For both parotids, V_5 had similar values between jaw tracking and no jaw tracking with 100% volume receiving a dose of 5 Gy. Normal lung was the only organ that had reduction for all the categories with −0.85% for V_5, −0.82% for V_{10}, −0.59% for V_{20}, and −0.23 Gy for mean dose. Table 4 shows the *P* value of organ-dose reduction by using jaw tracking in various normal organs. Dose reduction with jaw tracking was statistically significant in V_5 of the bladder, rectum, and lung, V_{10} of the bladder, rectum, and lung, and mean dose of lung ($P < 0.05$). For right and left parotid, there was no significant difference in V_5, V_{10}, V_{20}, and mean dose ($P > 0.05$).

Figure 3 shows the integral-dose reduction by using jaw tracking in nasopharynx, prostate, and lung cancer plans. The most distinct reduction was found in the V_5 of nasopharynx cancer with −1.13% of the volume, while the smallest reduction was found in the mean dose of prostate cancer plans with −0.09% of the volume. Table 5 shows the *P* value of integral-dose reduction by using jaw tracking in nasopharynx, prostate, and lung cancer plans. Integral-dose reduction with jaw tracking was statistically significant in almost all the treatment plans ($P < 0.05$); only the V_{10} of prostate plan showed no significant difference ($P > 0.05$).

In addition, the advantage of jaw tracking over no jaw tracking in y-jaw collimator was also observed. The result was found that the jaw tracking could reduce low doses at the upper and lower regions of the PTV, as shown in Figure 4.

Discussion

For verification of the TPS calculation, a 10 MV photon was used to determine the accuracy of the dose calculation because higher energy has a greater effect on the scattered-dose calculation.[21] In this study, the method to generate the maximum jaw-tracking distance was developed by using the rectangular shape target volume which can generate jaw moving by 10 cm and 11.3 cm for x-jaw and y-jaw tracking, respectively. Jaw-tracking distances were generated in TPS verification to be as large as possible to verify the accuracy of jaw-tracking calculation in the worst scenario. The accuracy of the dose calculation for RapidArc with jaw tracking in Eclipse TPS was sufficient for our study, with a point-dose difference of <0.5% and dose-distribution agreement of more than 96% gamma index passing rates (2%/2 mm gamma index criteria).

Schmidhalter *et al.*[15] suggested that the backscattered radiation of the y-jaw would increase because the y-jaws are closer to the monitor chamber than the x-jaws. Our study showed that no significant differences were observed between x-jaw travelling and y-jaw travelling with gamma passing rates of 99.6% and 99.9% for x-jaw and y-jaw tracking, respectively. This result indicated that the collimator backscatter changes during jaw tracking were taken into account in the dose calculation.

For sensitive organs, such as lung, rectum, and bladder, a large reduction of organ dose was found in the V_5 and V_{10}; this may decrease the chance of radiation-induced secondary malignancies. For integral-dose reduction, a large reduction was found in the low-dose regions (V_5) because jaw tracking can reduce the effects of leaf transmission. The maximum jaw moving had an average distance of 2.73 cm and range

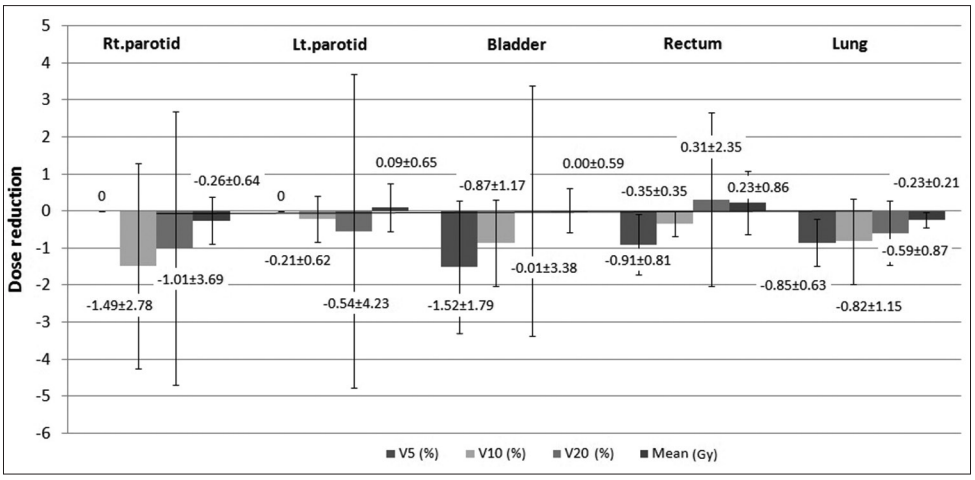

Figure 2: Organ-dose reduction for both sides of the parotid, rectum, bladder, and normal lung

Table 4: Comparison of organ dose between volumetric-modulated arc therapy with jaw tracking and volumetric-modulated arc therapy without jaw tracking

Plans	Organ	$\bar{x}\pm$SD		Difference	*P*
		JT	No JT		
Nasopharynx	Right parotid				
	V_5 (%)	100±0	100±0	0	0.5
	V_{10} (%)	97.93±3.28	99.43±0.80	−1.49	0.06
	V_{20} (%)	68.94±15.17	69.95±14.77	−1.01	0.21
	Mean dose (Gy)	37.93±8.54	38.20±8.26	−0.26	0.11
	Left parotid				
	V_5 (%)	100±0	100±0	0	0.5
	V_{10} (%)	97.22±5.77	97.43±5.23	−0.21	0.16
	V_{20} (%)	74.67±12.57	75.21±13.30	−0.54	0.35
	Mean dose (Gy)	40.40±9.54	40.31±9.30	0.09	0.34
Prostate	Rectum				
	V_5 (%)	87.38±18.39	88.28±18.65	−0.91	<0.05
	V_{10} (%)	78.42±17.73	78.77±17.82	−0.35	<0.05
	V_{20} (%)	59.49±21.64	59.18±22.55	0.31	0.34
	Mean dose (Gy)	31.42±8.0	31.18±8.11	0.23	0.20
	Bladder				
	V_5 (%)	82.42±21.76	83.95±21.69	−1.52	<0.05
	V_{10} (%)	75.41±24.46	76.28±24.55	−0.87	<0.05
	V_{20} (%)	60.62±22.55	60.63±23.67	−0.01	0.50
	Mean dose (Gy)	29.61±9.58	29.61±9.69	0.01	0.49
Lung	Normal lung				
	V_5 (%)	55.07±24.05	55.92±23.93	−0.85	<0.05
	V_{10} (%)	45.48±24.72	46.30±25.51	−0.82	<0.05
	V_{20} (%)	27.05±18.29	27.64±19.03	−0.59	0.053
	Mean dose (Gy)	13.72±7.97	13.95±8.17	−0.23	<0.05

V_5: Volume receiving a dose of 5 Gy, V_{10}: Volume receiving a dose of 10 Gy, V_{20}: Volume receiving a dose of 20 Gy, SD: Standard deviation, JT: Jaw tracking

from 0 to 8.5 cm [Table 2]. This was found in nasopharynx treatment plans which could reduce the maximum integral dose reduction in the V_5 by 1.13% of the volume. This indicated that integral-dose reduction depends on the tumor shape; for example, a large size difference between the anterior and lateral views in the nasopharynx tumor can create larger jaw moving.

Our study found that jaw tracking can reduce organ dose and integral dose as shown in Figures 2 and 3, which were comparable with the other study. Joy *et al.*[14] found that V_5, V_{10}, and V_{20} of normal organs can be reduced by 2% by using jaw tracking, and a large dose decrease was found in V_5. Schmidhalter *et al.*[15] found that dynamic IMRT with jaw tracking can decrease the integral dose by 1.5% and 1.8%

Table 5: Comparison of integral dose between volumetric-modulated arc therapy with jaw tracking and volumetric modulated arc therapy without jaw tracking

Plans	Integral dose	$\bar{x}\pm$SD		Difference	*P*
		JT	No JT		
Nasopharynx	V_5 (%)	47.24±6.78	48.37±6.91	−1.13	<0.05
	V_{10} (%)	37.51±4.85	38.19±5.08	−0.69	<0.05
	Mean dose (Gy)	13.34±1.41	13.47±1.44	−0.13	<0.05
Prostate	V_5 (%)	22.39±6.20	22.76±6.29	−0.38	<0.05
	V_{10} (%)	16.55±5.09	17±5.06	−0.45	0.07
	Mean dose (Gy)	4.31±1.33	4.41±1.35	−0.09	<0.05
Lung	V_5 (%)	24.48±12.89	24.99±13.11	−0.51	<0.05
	V_{10} (%)	15.94±9.0	16.18±10.11	−0.24	<0.05
	Mean dose (Gy)	4.81±2.83	4.90±2.88	−0.09	<0.05

V_5: Volume receiving a dose of 5 Gy, V_{10}: Volume receiving a dose of 10 Gy, SD: Standard deviation, JT: Jaw tracking

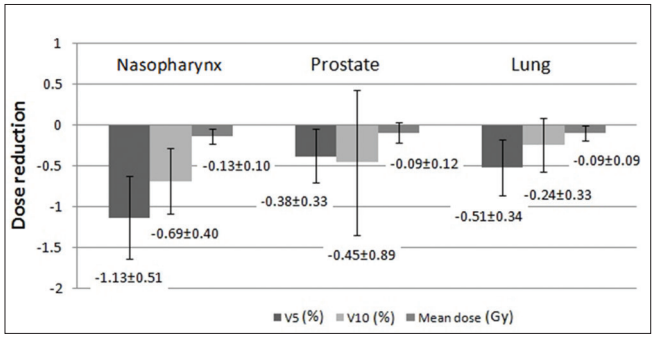

Figure 3: Integral-dose reduction in Nasopharynx, prostate, and lung plans

in nasopharynx and prostate treatment plans, respectively. They also evaluated a decrease in leaf transmission with jaw tracking in academic cases (sliding gap and chair pattern) and found decreases of 9% and 4% for the sliding gap and chair pattern, respectively. Kim *et al*.[16] showed that VMAT with jaw tracking decreased the dose to normal organs ranging from 3.7% to 8.1% for prostate plans and 4.3% to 11.9% for the nasopharynx plans. The dose reduction was more pronounced in the dose received by 80% of volume ($D_{80\%}$), the dose received by 90% of volume ($D_{90\%}$), the dose received by 95% of volume ($D_{95\%}$) than in the dose received by 5% of volume ($D_{5\%}$), the dose received by 10% of volume ($D_{10\%}$), and the dose received by 20% of volume ($D_{20\%}$) for all patients. Snyder *et al*.[17] found jaw tracking can reduce doses to normal organs in IMRT and VMAT for spine stereotactic radiosurgery. They suggested that jaw tracking can be used for decreasing the dose to the spinal cord in both IMRT and VMAT.

Conclusions

For organ-dose reduction, jaw tracking in VMAT plan was superior to no jaw tracking in reducing of low-dose regions (V_5 and V_{10}) for radiosensitive organs such as bladder, rectum, and normal lung. For integral-dose reduction, jaw tracking in VMAT plan is an efficient method for decreasing low-dose regions (V_5).

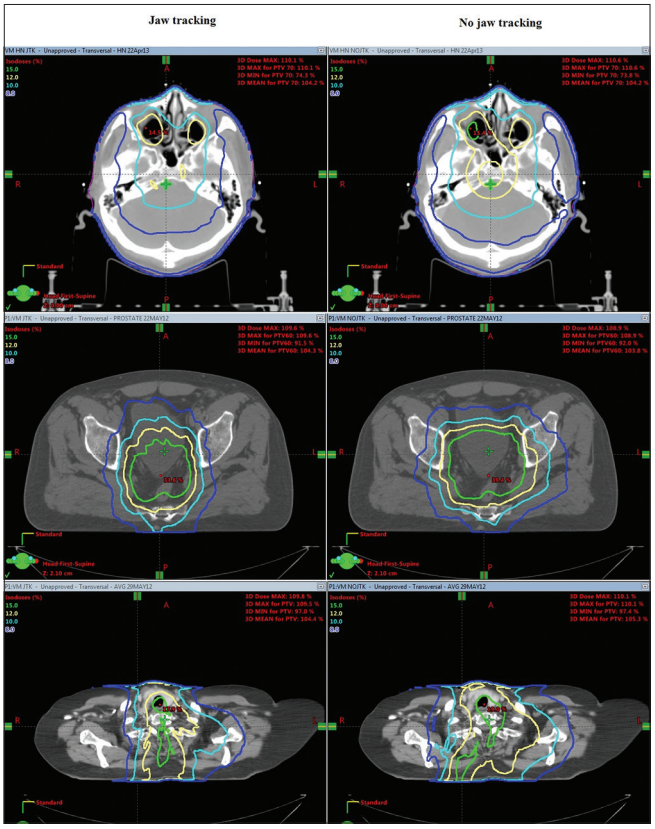

Figure 4: Comparison of low-dose distribution at upper and lower regions of planning target volume between jaw tracking and no jaw tracking in nasopharynx, prostate, and lung plans. Blue line = 8% of doses, cyan line = 10% of doses, yellow line = 12% of doses, and green line = 15% of doses

Acknowledgment

The authors would like to thank Dr. Danupon Nantajit for his assistance in reviewing the manuscript.

Financial support and sponsorship

Nil.

Conflicts of interest

There are no conflicts of interest.

References

1. Verhey LJ. Comparison of three-dimensional conformal radiation therapy and intensity-modulated radiation therapy systems. Semin Radiat Oncol 1999;9:78-98.
2. Veldeman L, Madani I, Hulstaert F, De Meerleer G, Mareel M, De Neve W, *et al.* Evidence behind use of intensity-modulated radiotherapy: A systematic review of comparative clinical studies. Lancet Oncol 2008;9:367-75.
3. Staffurth J, Radiotherapy Development Board. A review of the clinical evidence for intensity-modulated radiotherapy. Clin Oncol (R Coll Radiol) 2010;22:643-57.
4. Guerrero Urbano MT, Nutting CM. Clinical use of intensity-modulated radiotherapy: Part I. Br J Radiol 2004;77:88-96.
5. Guerrero Urbano MT, Nutting CM. Clinical use of intensity-modulated radiotherapy: Part II. Br J Radiol 2004;77:177-82.
6. Deng J, Pawlicki T, Chen Y, Li J, Jiang SB, Ma CM, *et al.* The MLC tongue-and-groove effect on IMRT dose distributions. Phys Med Biol 2001;46:1039-60.
7. Balog JP, Mackie TR, Wenman DL, Glass M, Fang G, Pearson D, *et al.* Multileaf collimator interleaf transmission. Med Phys 1999;26:176-86.
8. Agnew CE, Irvine DM, Hounsell AR, McGarry CK. Improvement in clinical step and shoot intensity modulated radiation therapy delivery accuracy on an integrated linear accelerator control system. Pract Radiat Oncol 2014;4:43-9.
9. Klein EE, Low DA. Interleaf leakage for 5 and 10 mm dynamic multileaf collimation systems incorporating patient motion. Med Phys 2001;28:1703-10.
10. Arnfield MR, Siebers JV, Kim JO, Wu Q, Keall PJ, Mohan R, *et al.* A method for determining multileaf collimator transmission and scatter for dynamic intensity modulated radiotherapy. Med Phys 2000;27:2231-41.
11. Chow JC, Seguin M, Alexander A. Dosimetric effect of collimating jaws for small multileaf collimated fields. Med Phys 2005;32:759-65.
12. Feng Z, Wu H, Zhang Y, Zhang Y, Cheng J, Su X, *et al.* Dosimetric comparison between jaw tracking and static jaw techniques in intensity-modulated radiotherapy. Radiat Oncol 2015;10:28.
13. Varian Medical Systems. Eclipse Algorithm Reference Guide Version 10.0. Palo Alto, CA: Varian Medical Systems; 2010.
14. Joy S, Starkschall G, Kry S, Salehpour M, White RA, Lin SH, *et al.* Dosimetric effects of jaw tracking in step-and-shoot intensity-modulated radiation therapy. J Appl Clin Med Phys 2012;13:3707.
15. Schmidhalter D, Fix MK, Niederer P, Mini R, Manser P. Leaf transmission reduction using moving jaws for dynamic MLC IMRT. Med Phys 2007;34:3674-87.
16. Kim JI, Park JM, Park SY, Choi CH, Wu HG, Ye SJ, *et al.* Assessment of potential jaw-tracking advantage using control point sequences of VMAT planning. J Appl Clin Med Phys 2014;15:4625.
17. Snyder KC, Wen N, Huang Y, Kim J, Zhao B, Siddiqui S, *et al.* Use of jaw tracking in intensity modulated and volumetric modulated arc radiation therapy for spine stereotactic radiosurgery. Pract Radiat Oncol 2015;5:e155-62.
18. Low DA, Harms WB, Mutic S, Purdy JA. A technique for the quantitative evaluation of dose distributions. Med Phys 1998;25:656-61.
19. Varian Medical Systems. Vision Documentation: Portal Vision & Dosimetry 6.5. Palo Alto; 2003.
20. D'Arienzo M, Masciullo SG, de Sanctis V, Osti MF, Chiacchiararelli L, Enrici RM, *et al.* Integral dose and radiation-induced secondary malignancies: Comparison between stereotactic body radiation therapy and three-dimensional conformal radiotherapy. Int J Environ Res Public Health 2012;9:4223-40.
21. Huang PH, Chu J, Bjärngard BE. The effect of collimator backscatter radiation on photon output of linear accelerators. Med Phys 1987;14:268-9.

Technical Note

Brachytherapy Localization Radiographs with Conventional Diagnostic X-Ray Machine

Ramamoorthy Ravichandran, Bandana Barman, Purnendu Deb Roy[1], Gopal Datta[2], Ravi Kannan[3]

Medical Physics Unit, [1]Departments of Radiodiagnosis, [2]Radiotherapy, [3]Surgical Oncology, Cachar Cancer Hospital and Research Centre, Silchar, Assam, India

Abstract

With conventional diagnostic X-ray machines with over couch X-ray tubes, it is not possible to obtain anteroposterior (AP) and lateral (Lat) radiographs without changing the posture of the patients. In an old 300 mA X-ray machine with a fluoroscopy screen (12.4 kg) (1995 model), by substituting the screen with suitable counterweight and making provision to take the hoist pillar up to the edge of the wall, we could get isocentric setup for a hospital stretcher kept near the chest stand. This setup provided acceptable AP–Lat radiographs for brachytherapy localization using "Perspex jig" (Nucletron, Netherlands) and field check radiographs in head and neck, esophagus patients for treatment planning.

Keywords: Diagnostic X-ray machines, high-dose rate brachytherapy, localization, treatment planning

Received on: 08-08-2017 **Review completed on: 27-11-2017** **Accepted on: 29-11-2017**

Introduction

Brachytherapy treatments using remote-controlled high-dose rate (HDR) machines are offered only in major centers. In recent days, conventional radiotherapy simulators (Sim) are being replaced by computed tomography Sims (CT Sim). HDR brachytherapy is carried out with multiple fractionations, and taking X-ray CT scans on all days becomes difficult. This will also impart additional radiation dose to patients by repeat scans. Two-dimensional (2D) localization methods achievable in low-dose orthogonal and nonorthogonal methods (using special Perspex jig[1,2]) give equivalent accuracy. Mobile X-ray machines provide unsatisfactory radiographs preventing their usage after brachy applications in theater. An earlier study[3] has highlighted a possibility to provide satisfactory orthogonal radiographs with a hospital stretcher using a 500 mA diagnostic machine, but this technique was not standardized then.[3] In the absence of dedicated radiotherapy simulator for HDR brachytherapy treatment planning, and to conserve resources of a CT Sim, our attempt to obtain solution with an old radiography/fluoroscopy 300 mA diagnostic X-ray machine is illustrated.

Materials and Methods

In our cancer hospital, about 3000 new patients are seen per year and about 400 of them receive radiotherapy with a Theratron 780E (M/s Theratronix) cobalt machine[4] and microSelectron HDR (M/s Elekta). The hospital faces many resource constraints since it is non-governmental voluntary organization. A diagnostic X-ray machine (PleophosD, Siemens, 120 KV, 300 mA) installed in 1995 available in this hospital is modified for our work. This X-ray machine had a "direct fluoroscopy image receptor" (2.5 mm lead equivalent screen), weighing 12 kg mounted as a counterweight to X-ray tube arm [Figure 1]. To substitute this counterweight, the "L-arm" carrying the X-ray tube is mounted with suitable weight [Figure 2]. With X-ray tube, assembly having one-head swivel movement and "L-arm" rotation movements can bring exposure positions for vertical and lateral (Lat) projections [Figures 3 and 4]. It could be seen that for brachytherapy applicator localizations, the patient is positioned in the gap area between the X-ray tube and chest stand wall for obtaining this anteroposterior (AP) and Lat radiography.

Results

The modification of the diagnostic X-Ray machine facilitated the possibility to use the Nucletron jig and to

Address for correspondence: Dr. Ramamoorthy Ravichandran, Department of Radiotherapy, Cachar Cancer Hospital and Research Centre, Medical Physics Unit, Silchar - 788 015, Assam, India.
E-mail: ravichandranrama@rediffmail.com

Access this article online

Quick Response Code:

Website: www.jmp.org.in

DOI: 10.4103/jmp.JMP_97_17

How to cite this article: Ravichandran R, Barman B, Roy PD, Datta G, Kannan R. Brachytherapy localization radiographs with conventional diagnostic X-ray machine. J Med Phys 2018;43:58-60.

Figure 1: Fluoroscopic Screen mount detached

Figure 2: L Arm with new counterweight

Figure 3: X-ray tube for anteroposterior film

Figure 4: X-ray tube for lateral film

take AP and Lat projected radiographs without disturbing the patient's geometry [Figure 3]. The Lat projection is possible, by bringing the X-ray tube to the orientation shown in Figure 4. Furthermore, it is now feasible to obtain Lat radiographs to check field margins and matching of centers of the fields for head and neck radiotherapy portals. Figures 5 and 6 show the localization radiographs obtained for an intrauterine/intravaginal microSelectron application. The radiographs to localize a breast interstitial implant for an HDR treatment, with custom-made copper wire markers inserted into plastic catheter tubes, are shown in Figures 7 and 8.

Discussion

We have highlighted a method to use existing diagnostic X-ray machine for obtaining brachytherapy localization radiographs. This also enables us to obtain verification radiographs for radiotherapy portals planned for the patient, before they are taken up for treatment. This work appears to be important especially in places where there are no dedicated therapy simulators and no CT simulator available for brachytherapy localization or when an alternative method is required in exigent situations. In olden days, the X-Ray machines were designed for conventional radiography as well as for direct fluoroscopy for barium meal or barium enema with multiformat films. Such X-ray machines have problems because this arrangement was designed to act as counterweight on the L-Arm. The presence of counterweight could not allow the vertical stand to travel near the edge of the wall and also to obtain the desired focus film distance, which were overcome by the present modification. With adaptation of this properly designed counterweight, the usage efficiency of our x-ray machine is now increased. This method makes it feasible to diagnostic X-ray machine. There may be an apprehension, why there is a need of old 2D localization method, in the era of 3D planning introduced as standard protocol for HDR brachytherapy. An earlier report[2] compared that jig radiography method gave equal localization results. Standardization of this technique will provide a dependable alternative to quality dose delivery even in paucity of facilities. The jig [Figure 3] has embedded cross wire marks both in the entry portals of X-ray beam along with

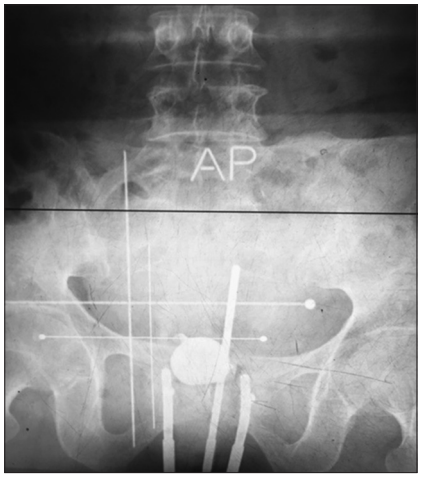

Figure 5: Radiograph anteroposterior view

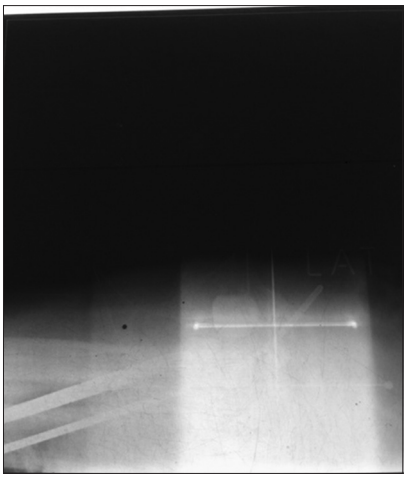

Figure 6: Lateral X-ray of pelvis

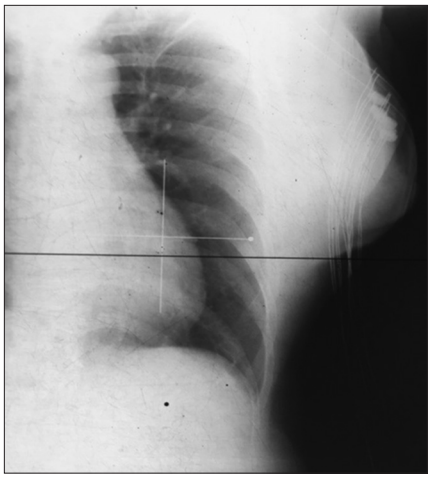

Figure 7: Breast implant (anteroposterior view)

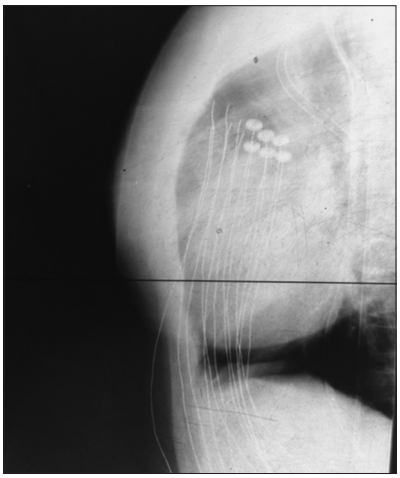

Figure 8: Breast implant (lateral view)

lead shots to correct for slight differences in orthogonality as a quality assurance measure. If focus-to-axis distance of 100 cm or 80 cm is obtained, this X-ray machine could serve as a simulator in principle. The jig also has "insert slots" for the "film cassette" or "computed radiography (CR) phosphor cassette" in perpendicular to the X-ray beam. In this hospital, lateral radiographs are not in the radiotherapy process, because of the use of CT Sim, but for the work of head and neck radiotherapy for large number of patients, which could be found in a report,[4] there is a need for standardized radiography protocol, and this method therefore has applications. We are in the process of 2D dose planning method in our Oncentra treatment planning system for our brachy plans in intracavitary, interstitial, and intraluminal treatments.

Declaration of patient consent

The authors certify that they have obtained all appropriate patient consent forms. In the form the patient(s) has/have given his/her/their consent for his/her/their images and other clinical information to be reported in the journal. The patients understand that their names and initials will not be published and due efforts will be made to conceal their identity, but anonymity cannot be guaranteed.

Acknowledgments

The authors thank the Director, Cachar Cancer Hospital and Research Centre, for the support in achieving modifications in X-ray machine. The authors would also like to thank Sri. Jantai, Electrician for the fabrication of mechanical structure.

Financial support and sponsorship

Nil.

Conflicts of interest

There are no conflicts of interest.

References

1. Orthogonal localization of applicators. 'Oncentra' Nucletron Treatment Planning Manual, 2000.
2. Tyagi K, Mukundan H, Mukherjee D, Semwal M, Sarin A. Non isocentric film-based intracavitary brachytherapy planning in cervical cancer: A retrospective dosimetric analysis with CT planning. J Contemp Brachytherapy 2012;4:129-34.
3. Ravichandran R. Localization Radiographs from Conventional Diagnostic X-ray Machine for Intracavitary and Implant Brachytherapy Applications. International Conference on Medical Physics. 6-9 November, AIIMS, New Delhi; 1998.
4. Ravichandran R, Manimegalai C. Head and neck radiotherapy with telecobalt machine-efficacy and need for tissue compensation. Int J Radiol Radiat Ther 2017;2:25.

Technical Note

Bismuth-Silicon and Bismuth-Polyurethane Composite Shields for Breast Protection in Chest Computed Tomography Examinations

Parinaz Mehnati[1,2], Mehran Arash[2], Parisa Akhlaghi[1,2]

[1]Medical Radiation Sciences Research Team, [2]Department of Medical Physics, School of Medicine, Tabriz University of Medical Sciences, Tabriz, Iran

Abstract

The article aims at constructing protective composite shields for breasts in chest computed tomography and investigating the effects of applying these new bismuth composites on dose and image quality. Polyurethane and silicon with 5% of bismuth were fabricated as a protective shield. At first, their efficiency in attenuating the X-ray beam was investigated by calculating the total attenuation coefficients at diagnostic energy range. Then, a physical chest phantom was scanned without and with these shields at tube voltage of 120 kVp, and image parameters together with dose values were studied. The results showed that these two shields have great effects on attenuating the X-ray beam, especially for lower energies (<40 kV), and in average, the attenuation coefficients of bismuth-polyurethane composite are higher in this energy range. The maximum relative differences between the average Hounsfield units (HUs) and noises of images without and with shield for both composites in 13 regions of interest were 4.5% and 15.7%, respectively. Moreover, primary investigation confirmed the ability of both shields (especially polyurethane-bismuth composite) in dose reduction. Comparing these two composites regarding the amount of dose reduction, the changes in HU and noise, and attenuation coefficients in diagnostic energy range, it seems that polyurethane composite is more useful for dose reduction, especially for higher tube voltages.

Keywords: Bismuth composites, breast shielding, computed tomography, dose reduction, Hounsfield unit, noise

Received on: 28-06-2017 **Review completed on: 22-12-2017** **Accepted on: 02-01-2018**

Introduction

Chest computed tomography (CT) scan is used as a valuable and precise diagnostic imaging tool for the noninvasive assessment of lungs, heart, and mediastinum diseases. The major disadvantage of this imaging is the radiation exposure to superficial organs (i.e., breasts in chest scan), which are not usually the target of examinations. The risk of cancer increases linearly with increasing dose, with higher risks for females,[1] and exposures to young girls around the age of menarche and breast bud carry a high risk.

A common method for dose reduction during CT examinations is the use of shielding to protect superficial organs.[2,3] Shields could remove the lower energies in the X-ray spectrum, and materials with higher attenuation coefficients in diagnostic energy range eliminate the lower energies with smaller required thickness and therefore reduce the image artifacts.[4] Numerous investigations have reported the use of high atomic number (Z) shielding materials such as lead and bismuth to attenuate X-rays and γ-rays.[5,6]

Despite the advantages of using protective shields in decreasing the dose values, concerns are being raised regarding their impacts on image quality.[7] Some statements are discouraging about applying shields,[8] while in some reports, it was stated that using this technique reduces the surface dose to patients with no appreciable loss in diagnostic quality.[9,10]

As reported in the literature, bismuth is an appropriate in-plane shield for protecting superficial organs. The study of Kim *et al*.[11] on the amount of breast dose reduction using bismuth

Address for correspondence: Dr. Parisa Akhlaghi, Department of Medical Physics, Faculty of Medicine, Tabriz University of Medical Sciences, Golgasht Av., Tabriz, Iran.
E-mail: parissa_akhlaghi@yahoo.com

Access this article online

Quick Response Code:

Website: www.jmp.org.in

DOI: 10.4103/jmp.JMP_74_17

How to cite this article: Mehnati P, Arash M, Akhlaghi P. Bismuth-Silicon and bismuth-polyurethane composite shields for breast protection in chest computed tomography examinations. J Med Phys 2018;43:61-5.

shielding indicated that shield enabled a 16%–37.5% dose reduction in the breast, while it increased CT images' noise up to 40%. Tappouni and Mathers[12] assessed the effects of bismuth breast shield on dose and image quality. They showed that breast shield decreased dose to the anterior chest by 38% and caused a reduction in noise by a factor of 1.86 in the anterior compared to posterior regions.

It should be mentioned that besides the effectiveness of a protective shield on dose reduction and not degrading the image quality, additional factors such as conformability, cost-effectiveness, weight factor, toxicity, and durability are important in selecting shields. In the past decades, several investigations have reported application of nano- and micro-polymer composite materials to attenuate high energy radiation. Because of their favorable properties, these materials have great potential to be used as radiation protective shields.[13]

Based on the mentioned points, for the first time, two different homemade composites of polyurethane and silicon with 5% of bismuth were constructed and their impacts on image quality and dose were investigated. To verify their effects on dose reduction due to the presence of bismuth composite shields, thermoluminescence dosimeters (TLDs) were inserted in breasts and dose values were measured without and with both shields.

Materials and Methods

Appropriate shield

In this study, to construct bismuth composites, silicon and polyurethane were used as matrices for bismuth particles. Bismuth powder (metal beads with maximum sizes of 150 μm provided from Merck Group) was poured gently by a pipette on a silicon or polyurethane flat surface with a thickness of 1.1 mm and an area of 30 cm × 40 cm. These shields were left in the oven at 60°C and humidity of 90% for 10–15 days. This method gently and continuously dries the composite mixtures with no air bubbles. On exiting the oven, they were left for 1 day at room temperature (25°C) to adapt with the normal situations, and then, they were used for the experiments. To compare the shields, attenuation coefficient of each element of both bismuth composites was obtained from XCOM program,[14] and then, total mass attenuation coefficients of composites in CT energy range (<120 kVp) were calculated by compiling a FORTRAN program.

Chest physical phantom

A physical chest phantom of a female was designed and built based on the recommendation of ICRP publication 23,[15] ICRU report 48, and also the available anatomical data of lung and breasts in Tabriz University of Medical Sciences. The initial plan of the chest phantom was drawn using AutoCAD 2012. Based on the plan and by a waterjet cutter, phantom was cut into slices with thickness of 1 cm. Breasts and chest were made of polyethylene, and the lung was fabricated by cork. Two different breasts sizes were considered for female phantom to mimic different women physically and radiographically.[16] Figure 1 displays the designed physical female chest phantom with two different breasts sizes.

Computed tomography examinations

The female phantom was placed in a supine posture at the isocenter of a Siemens Somatom Sensation 16 scanner. The conventional chest scanning parameters for adults considered by the machine automatically (tube voltage of 120 kVp, tube current of 80 mA, slice thickness of 10 mm, pitch of 1.3, and pixel size of 2 mm × 2 mm) were used for phantom imaging. The shields were placed on foam with thickness of 1 cm, and then, they were made to cover the anterior surface of the breasts. To avoid increasing the scan parameters after placing shields were placed after acquiring the CT topogram.

Image-quality analysis

To investigate the effects of shield on image quality, CT scans were performed without and with shields and the image quality was evaluated. Bismuth-silicon and bismuth-polyurethane composites were placed on small breast and big breast, respectively. The quantitative assessments of image quality include determining the differences between HU and noise of shielded and unshielded images. For this purpose, five circular regions of interest (ROIs) in the trunk and four ROIs in each breast, with area of 1.9 cm^2, were selected to measure both the average HU and the standard deviation (SD) in each region. The measures of SD can be used as a quantitative assess of noise within CT images, and collecting the average HU will check for variations caused by the presence of shields.[17] ROIs were selected in the trunk and breast of phantom (in anterior, in lateral, in middle, and in posterior) on consecutive slices. Moreover, statistical analysis was performed using Statistical Package for the Social Sciences (SPSS) software developed by IBM Corporation and $P < 0.05$ was considered as the significance of the results.

Dosimetric evaluation

An initial assessment for the effects of these two composites on dose reduction was done using calibrated, energy-specific LiF: Mg, Cu, P (GR-200) TLDs (Hangzhou Freqcontrol Electronic Technology Ltd., China). They were placed inside the breasts

Figure 1: Physical female phantom

of the phantom for irradiation without and with the presence of shield. Readout of the TLDs was done in a 7103 model Raman Security Development Co. TLD reader[18] during the temperature of 240°C for 10–20 s.

Results

In Figure 2, the radiographic images of bismuth-silicon and bismuth-polyurethane composites at tube voltage of 40 kV are represented. The bismuth beads are noticed on the surface of composites. For these two composites, Figure 3 displays the total attenuation coefficients in cm^{-1}.[14] From figure, although two composites are similar in low energies , the attenuating property of polyurethane is more than silicon in higher energies. Considering the figure, for scans performed at lower tube voltages (i.e., 80 or 100 kVp instead of 120 kVp), these shields have more effects on beam attenuation and consequently their dose reduction rate might increase.

Figure 4 displays the ROIs selected in all five slices of CT images. Each ROI identifies with a number. For the ROI located in the middle of chest, the circular area, mean HU, and standard deviation were measured. For these selected ROIs, the average value of HU, and noise without and with the presence of bismuth composite shields on the surface of phantom are tabulated in Table 1. From Table 1, the HU values increased up to 4.5% and 1.8% for images shielded by polyurethane and silicon composites, respectively, while the increase in noises were 15.7% and 15.02%, respectively. The *P* values of the differences between HUs without and with shields were not statistically significant ($P > 0.05$).

The outcomes of dosimetric measurements with TLDs using two shields showed 9.57% and 37.6%, dose reduction by bismuth-silicon and bismuth-polyurethane composites, respectively.

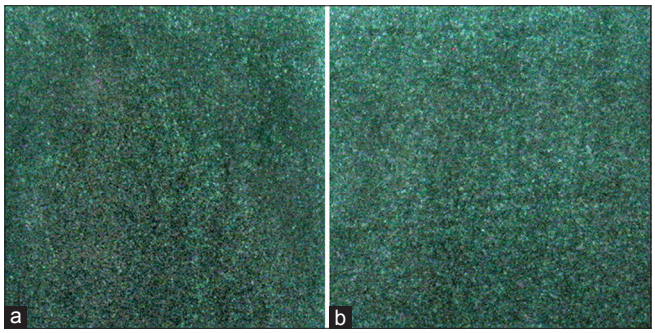

Figure 2: The radiographic images of (a) bismuth-silicon composite and (b) bismuth-polyurethane composite at tube voltage of 40 kV and tube loading of 1.6 mAs. The bismuth beads are observed as bright spots

Discussion

Despite the advantages of CT scan in diagnostic procedures, its increasing and frequent use raises concern about the radiation dose. It was reported that the value of effective dose, as a protection quantity, in chest CT scan (5.4 mSv) is almost 54 and 68 times more than that in mammography (0.1 mSv) and chest radiography (0.08 mSv), respectively.[19] Therefore, it seems that reducing radiation dose, especially for superficial radiosensitive organs, which are not usually the target of imaging, is important.[17] Hitherto, the effects of shielding superficial organs by high-attenuating materials (e.g., bismuth) on radiation dose reduction are reported frequently by various investigators.[17,18,20-24] Geleijns *et al*. were concerned about the inclusion of breast shields in CT scan range, which may cause streak artifacts and diminish image quality,[7] and also the amount of unavoidable internally scattered radiation.[25] Some investigators believed that optimizing scan protocol may have a greater effect on patient radiation dose than the use of patient shields.[20,26]

In addition, it was reported that polymer-based shielding materials are lightweight and conformable, and they can be designed to include nontoxic, high Z materials that provide effective X-ray protection.[13] In Table 2, some of the investigations used conventional breast shields were tabulated.

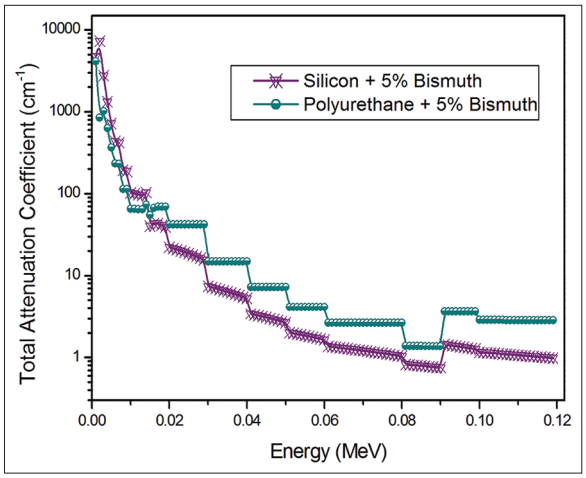

Figure 3: Total attenuation coefficients of two bismuth composites in diagnostic energy range

Table 1: Average Hounsfield unit and noise in the computed tomography images without and with shields of bismuth-polyurethane and bismuth-silicon composites

Location	Without shield				Bismuth-silicon composite				Without shield				Bismuth-polyurethane composite			
	9	10	11	12	9	10	11	12	5	6	7	8	5	6	7	8
Average HU	−62.33	−64.00	−65.00	−67.00	−61.91	−62.86	−64.16	−66.5	−61.75	−64.86	−64.00	−67.13	−59.75	−62.57	−61.13	−64.56
Noise	2.33	5.12	4.50	8.12	2.68	5.48	4.98	8.88	2.10	3.13	3.61	5.59	2.43	3.55	4.00	6.31

HU: Hounsfield unit

Table 2: Some studies conducted on the effects of shielding breast by bismuth layer on image quality in chest computed tomography scans

Authors	Method	Shield	Results
Geleijns *et al*.[7]	A RANDO phantom was scanned by a MDCT scanner at tube voltage of 120 kVp and tube loading of 100 mAs	Bismuth shield (F and L Medical Products Co., USA)	Image noise was increased by 5.5% in chest scan
Coursey *et al*.[21]	Atom pediatric 5-year-old phantom (model 705-D, CIRS) was scanned by a MDCT scanner	Bismuth shield (F and L Medical Products Co., USA)	Mean noise was not significantly different with the addition of the breast shield
Kalra *et al*.[22]	An anthropomorphic chest phantom (GmBH, Germany) was scanned by a MDCT scanner	Bismuth shield (F and L Medical Products Co., USA)	Increase in HU and noise (53.5%) was noted directly below the shield
Catuzzo *et al*.[23]	RANDO phantom was scanned by two different MDCT scanners	4 layers of 0.0085 g/cm^2 bismuth latex	There was no significant difference in noise
Wang *et al*.[24]	An anthropomorphic chest phantom (GmBH, Germany) was scanned by a MDCT scanner	A breast shield made of bismuth-impregnated latex	Shielding led to a substantial increase in HU by 10-20 HU
Einstein *et al*.[27]	Atom phantom (model 701; CIRS) was scanned by a MDCT scanner	Bismuth shield (F and L Medical Products Co., USA)	HU was decreased by 14.6 HU
Servaes and Zhu[28]	Atom pediatric 5-year-old phantom (model 705-D, CIRS) was scanned by a MDCT scanner	Bismuth shield (F and L Medical Products Co., USA)	Noise level increased by 4-6 HU
Alonso *et al*.[29]	A RANDO female phantom was scanned at tube voltage of 120 kVp and tube current of 150 mA by a MDCT scanner	1 mm thick Bismuth breast shield	Image noise increased (there was no quantitative assessment)

MDCT: Multiple detector computed tomography, HU: Hounsfield unit, CIRS: Computerized imaging reference systems

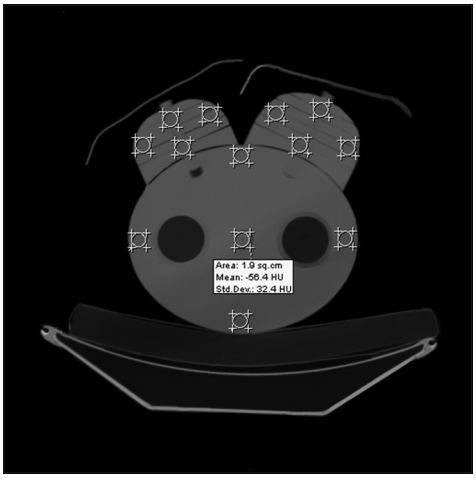

Figure 4: Thirteen regions of interest selected for image analysis. Bismuth-silicon and bismuth-polyurethane composites were placed on small breast and big breast, respectively. The average Hounsfield unit value and noise were determined for the marked places with an area of 1.9 cm^2

According to the outcomes, the relative differences between the average HUs of images without and with shield in 13 different ROIs were <4.5% for both shields. In addition, the maximum increase in noise was observed directly below the shields, which was 15.7% for polyurethane composite shield and 15.02% for silicon composite [Table 1]. Given Table 2, most of the studies reported an increase in HU and noise. The results of this study confirm this as expected. It could be said that applying shields affects the values of HU because the effective energy of X-ray is changed and HU is directly dependent on energy. In addition, the increase in image noise is likely related to the beam hardening and scattering associated with the presence of shield.[22]

Considering the assessments of image quality, it seems that these two bismuth composites have no significant impact on HU and noise in the inner body and the maximum changes in these values relate to the breast, which locates directly below the shield. As long as the breast is not the target of imaging, these shields help reducing the high level of breast dose absorbed as the byproduct of its location. Comparing these two composites, the changes in HU and noise in bismuth-polyurethane composite are more than bismuth-silicon composite, but the differences are not statistically significant ($P > 0.05$). On the other hand, considering the amount of dose reduction, bismuth-polyurethane composite is more useful in dose reduction for diagnostic procedures, especially for higher tube voltages, which is expected from its attenuation property.

Conclusions

Given the advantages of polymer composite over conventional materials for protective shields, two different bismuth composites were designed and fabricated. Polyurethane and silicon with 5% of bismuth were constructed as breast protective shield, and their effects on image quality and dose reduction in chest CT scan were investigated. According to the results, both composite shields reduce dose values and increase noises, which are most evident directly below the shield, but they do not cause distractions. However, breasts are not usually the target of CT imaging, so shields cannot interfere with diagnostic procedures.

Financial support and sponsorship

This work was supported by the office of the vice president as a novel and technical project for research at the Tabriz University of Medical Sciences in Iran.

Conflicts of interest

There are no conflicts of interest.

References

1. Committee on the Biological Effects of Ionizing Radiation. Health Risks from Exposure to Low Levels of Ionizing Radiation. BEIR VII, Phase 2. Washington: The National Academies Press; 2005. p. 21-172.
2. Hopper KD, King SH, Lobell ME, TenHave TR, Weaver JS. The breast: In-plane x-ray protection during diagnostic thoracic CT – Shielding with bismuth radioprotective garments. Radiology 1997;205:853-8.
3. Parker MS, Kelleher NM, Hoots JA, Chung JK, Fatouros PP, Benedict SH, *et al.* Absorbed radiation dose of the female breast during diagnostic multidetector chest CT and dose reduction with a tungsten-antimony composite breast shield: Preliminary results. Clin Radiol 2008;63:278-88.
4. Akhlaghi P, Miri-Hakimabad H, Rafat-Motavalli L. Effects of shielding the radiosensitive superficial organs of ORNL pediatric phantoms on dose reduction in computed tomography. J Med Phys 2014;39:238-46.
5. Szajerski P, Zaborski M, Bem H, Baryn W, Kusiak E. Optimization of the heavy metal (Bi-W-Gd-Sb) concentrations in the elastomeric shields for computer tomography (CT). J Radioanal Nucl Chem 2014;300:385-91.
6. Akhlaghi P, Hoseinian-Azghadi E, Miri-Hakimabad H, Rafat-Motavalli L. A Monte Carlo study on quantifying the amount of dose reduction by shielding the superficial organs of an Iranian 11-year-old boy. J Med Phys 2016;41:246-53.
7. Geleijns J, Salvadó Artells M, Veldkamp WJ, López Tortosa M, Calzado Cantera A. Quantitative assessment of selective in-plane shielding of tissues in computed tomography through evaluation of absorbed dose and image quality. Eur Radiol 2006;16:2334-40.
8. Halliburton SS, Abbara S, Chen MY, Gentry R, Mahesh M, Raff GL, *et al.* SCCT guidelines on radiation dose and dose-optimization strategies in cardiovascular CT. J Cardiovasc Comput Tomogr 2011;5:198-224.
9. Kim S, Frush DP, Yoshizumi TT. Bismuth shielding in CT: Support for use in children. Pediatr Radiol 2010;40:1739-43.
10. Gbelcová L, Nikodemová D, Horváthová M. Dose reduction using bismuth shielding during paediatric CT examinations in Slovakia. Radiat Prot Dosimetry 2011;147:160-3.
11. Kim YK, Sung YM, Choi JH, Kim EY, Kim HS. Reduced radiation exposure of the female breast during low-dose chest CT using organ-based tube current modulation and a bismuth shield: Comparison of image quality and radiation dose. AJR Am J Roentgenol 2013;200:537-44.
12. Tappouni R, Mathers B. Scan quality and entrance skin dose in thoracic CT: A Comparison between bismuth breast shield and posteriorly centered partial CT scans. ISRN Radiol 2013;2013:457396.
13. Nambiar S, Yeow JT. Polymer-composite materials for radiation protection. ACS Appl Mater Interfaces 2012;4:5717-26.
14. Korea Atomic Energy Research Institute. Nuclear Data Center. Available from: http://www.atom.kaeri.re.kr: 8080/cgi-bin/w3xcom. [Last accessed on 2018 Jan 23].
15. International Commission on Radiological Protection (ICRP). Report on the task group on reference man. ICRP Publication 23. Ann ICRP 1975;23:1-64.
16. Mehnati P, Ghavami M, Heidari H. Reducing radiation doses in female breast and lung during CT examinations of thorax: A new technique in two scanners. J Biomed Phys Eng 2017;7:217-24.
17. Foley SJ, McEntee MF, Rainford LA. An evaluation of in-plane shields during thoracic CT. Radiat Prot Dosimetry 2013;155:439-50.
18. Raman Security Development Co. TLD Cards and Readers. Available from: http://www.rsdco.ir/proitem?item=tld-reader-model-7103. [Last accessed on 2017 Dec 01].
19. Mettler FA Jr., Wiest PW, Locken JA, Kelsey CA. CT scanning: Patterns of use and dose. J Radiol Prot 2000;20:353-9.
20. Fricke BL, Donnelly LF, Frush DP, Yoshizumi T, Varchena V, Poe SA, *et al.* In-plane bismuth breast shields for pediatric CT: Effects on radiation dose and image quality using experimental and clinical data. AJR Am J Roentgenol 2003;180:407-11.
21. Coursey C, Frush DP, Yoshizumi T, Toncheva G, Nguyen G, Greenberg SB, *et al.* Pediatric chest MDCT using tube current modulation: Effect on radiation dose with breast shielding. AJR Am J Roentgenol 2008;190:W54-61.
22. Kalra MK, Dang P, Singh S, Saini S, Shepard JA. In-plane shielding for CT: Effect of off-centering, automatic exposure control and shield-to-surface distance. Korean J Radiol 2009;10:156-63.
23. Catuzzo P, Aimonetto S, Fanelli G, Marchisio P, Meloni T, Mistretta L, *et al.* Dose reduction in multislice CT by means of bismuth shields: Results of *in vivo* measurements and computed evaluation. Radiol Med 2010;115:152-69.
24. Wang J, Duan X, Christner JA, Leng S, Yu L, McCollough CH, *et al.* Radiation dose reduction to the breast in thoracic CT: Comparison of bismuth shielding, organ-based tube current modulation, and use of a globally decreased tube current. Med Phys 2011;38:6084-92.
25. Geleijns J, Wang J, McCollough C. The use of breast shielding for dose reduction in pediatric CT: Arguments against the proposition. Pediatr Radiol 2010;40:1744-7.
26. Hurwitz LM, Yoshizumi TT, Goodman PC, Nelson RC, Toncheva G, Nguyen GB, *et al.* Radiation dose savings for adult pulmonary embolus 64-MDCT using bismuth breast shields, lower peak kilovoltage, and automatic tube current modulation. AJR Am J Roentgenol 2009;192:244-53.
27. Einstein AJ, Elliston CD, Groves DW, Cheng B, Wolff SD, Pearson GD, *et al.* Effect of bismuth breast shielding on radiation dose and image quality in coronary CT angiography. J Nucl Cardiol 2012;19:100-8.
28. Servaes S, Zhu X. The effects of bismuth breast shields in conjunction with automatic tube current modulation in CT imaging. Pediatr Radiol 2013;43:1287-94.
29. Alonso TC, Mourão AP, Santana PC, da Silva TA. Assessment of breast absorbed doses during thoracic computed tomography scan to evaluate the effectiveness of bismuth shielding. Appl Radiat Isot 2016;117:55-7.

Safety, Security and Regulations in Handling Radiation Sources

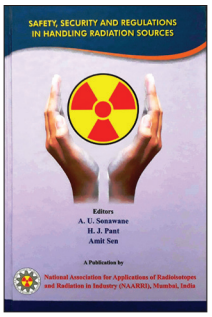

Editors: A. U. Sonawane, H. J. Pant and Amit Sen
Title: Safety, Security and Regulations in Handling Radiation Sources
Published by: National Association for Applications of Radioisotopes and Radiation in Industry, Mumbai, India, 2017
Pages: 550

National Association for Applications of Radioisotopes and Radiation in Industry (NAARRI) has published a thematic book entitled, "Safety, Security and Regulations in Handling Radiation Sources." Thirty-two articles have been contributed by different authors. The book starts with "Forewords" by Dr. Sekhar Basu, Chairman, Atomic Energy Commission and Secretary, Department of Atomic Energy, Government of India and Shri S. A. Bhardwaj, Chairman, Atomic Energy Regulatory Board (AERB), India. It is commented that the book will be useful for the understanding of various aspects for radiation source handling and will be an asset for the readers in terms of providing information on the safety and security aspects of radiation sources being used in various applications. Preface, by the President, NAARRI, ends with a note that this thematic book can be widely acclaimed as one of the best reference materials by the scientific community in the field. The articles in the book deal mostly with experiences in safety, security and regulatory aspects in handling radiation sources in different radiation practices in India.

First article gives an overview of safety, security and regulatory aspects of radiation sources in India, while discussing medical, industrial, and research applications of ionizing radiations. The legal, administrative and regulatory framework in India has the necessary provisions such that the safety and security of radioactive sources receive required supervision and regulatory coverage and ensure control over the radioactive sources throughout their life cycle. Total safety is achieved by built-in safety combined with operational safety. To meet the challenge of the steady growth in the applications of ionizing radiation technology, AERB implemented a state-of-the-art e-governance system, electronic licensing of radiation applications (e-LORA), through automation of regulatory processes associated with the use of ionizing radiation in India.

Second article deals with biological effects of radiation and their implications in radiation protection and medical management. Health effects of radiation exposure may be grouped in two general categories: (i) Deterministic effects and (ii) Stochastic effects. It is stated that deterministic effects do not occur at low doses or following chronic exposures as encountered by occupational workers who are exposed within prescribed dose limits. The article describes how radiation induces damage in human cells and how the irradiated cells undergoing division result in alterations in the structure of chromosomes, namely, chromosome aberrations. Increase in the frequency of dicentric chromosomes in human lymphocytes (white blood cell) is used as a biological dosimeter. A table depicting "significance of different levels of radiation exposures" is given at the end of the article.

Third article specifies necessity for safety standards for working with radiation. The international safety standards (e.g., IAEA Basic Safety Standards, BSS-2014) are based on considerable research work done in international research institutes and universities on effects of ionizing radiation on man and his environment and critical review and analysis of these research reports by international organizations, including UNSCEAR, ICRP, ICRU, IAEA, etc. The international safety standards are endorsed by other international organizations such as the WHO, ISO, FAO, and ILO. Thus, the safety standards have a scientific basis as well as international acceptance. It is stated that radiation protection standards are required for different situations and applications. All these standards must be consistent with one another. This is achievable only if all these standards are derived from a common set of basic safety standards, leading to harmonization of standards. In conclusion of this article, it is stated that the national standards for radiological safety developed and being implemented in India are consistent with the international safety standards.

Six articles in the book deal with regulatory control of medical applications of radiation. Article 4 deals with regulatory control of radiotherapy sources and associated safety and security aspects. In radiotherapy, potential hazard is relatively high due to involvement of high activity/intensity sources, as well as due to introduction of high-tech treatment modalities, therefore, utmost care is needed while handling such radioactive sources. In order to obtain desired level of safety and security while handling these sources, all stakeholders, including licensee, RSO, radiation oncologist, medical physicist, radiation technologist and service engineer must execute their role effectively. Article 5 describes radiation protection procedures in radiotherapy facilities using radiotherapy equipment, as well as procedures for ensuring compliance with all the regulatory requirements, including the safety and security of radiotherapy sources. Article 6 discusses experience in handling/management of therapeutic sources for cancer treatment at Tata Memorial Hospital, with particular emphasis to brachytherapy equipment. It is opined that despite advancement of intensity modulated, image guided treatments

in external beam therapy, brachytherapy remains an important modality of treatment due to its ability to deliver very high dose to the core of the tumor and rapid dose fall-off, sparing normal tissues. Article 7 describes procedures used for safety in handling of radioisotopes for therapeutics and nuclear imaging in nuclear medicine, as well as advances in the field due to the development of new radiopharmaceuticals, including cyclotron and positron emission tomography products. It is projected that the future of nuclear medicine will be dominated mostly by new radioisotopes and procedures. Article 8 summarizes steps taken by AERB toward improving regulatory control and radiation safety in the field of diagnostic radiology through the provisions of recently published safety code (AERB/SC/Med-3, 2015). Article 32 discusses radiation safety in some of the commonly used cyclotron-produced radioisotopes, including ^{18}F, and their transportation aspects to the utility. It is concluded that with appropriate design, workflow, safety interlocks, administrative controls, technical controls and radiation surveillance, radiation dose to the staff and members of the public can be maintained well below the regulatory limits.

Nine articles in the book deal with regulatory control of industrial applications of radiation. Article 9 describes general principle as well as uses of radiotracer techniques for troubleshooting and process optimization in full scale industrial reactor due to their many advantages over conventional tracers. Article also gives criteria for selection of a radiotracer, their applications in industry, as well as radiological safety, security and regulatory aspects. It is stated that specialized services are provided to Indian Industry by Bhabha Atomic Research Centre (BARC) and Board of Radiation and Isotope Technology (BRIT) leading to significant benefits to the Industry. Articles 10–12 describe the objective of radiation processing of foods. Different classes of food products and their corresponding dose limits for radiation processing are given. At present, there are 19 gamma radiation processing facilities (GRAPFs) in India. All the radiation safety and regulatory requirements for GRAPFs are discussed in the articles. As per the security requirements, GRAPF containing Category 1 radioactive source requires "Security Level A." It is stated that the volume of food irradiated in India has been steadily increasing. Article 13 discusses safety aspects in electron beam (EB) processing in the energy range up to 10 MeV, including depth dose curve characteristics for various energies. It is concluded that industrial EB accelerators incorporating proper safety features ensure reliable operation. Article 14 discusses radiation safety and regulatory aspects of particle accelerators-electron, proton and heavy ion accelerators. Accelerators in terms of energy, intensity, and technology are growing at a rapid pace, which is driven by the need of industry, scientific research, medicine, agriculture, etc. Due to the uncertainties in dose estimation prevailing in these peculiar radiation environments, one has to give importance to engineered, redundant radiation safety such as various interlocks, shielding, zoning, access control, training of personnel, and operational procedures. Article 15 describes nondestructive evaluation of welding, castings, and assemblies using industrial radiography sources. All the radiation safety, security and regulatory requirements for industrial radiography practice are nicely covered. Article 16 shares experience in handling/management of industrial radiography sources in Heavy Engineering manufacturing. Article also discusses regarding use of thermoluminescent dosimeter badge based on $CaSO_4$:Dy Teflon discs for personnel monitoring. Article 17 describes safety, security and regulatory aspects in nucleonic control system and oil well logging.

Articles 19–21 in the book deal with production and handling of radioisotopes (sealed and unsealed), as well as provide guidelines for establishing radioisotope laboratories using sealed/unsealed radioisotopes. Sealed radioactive sources (SRSs) are designed and manufactured in BRIT, DAE in accordance with national and international standards while complying with safety and security requirements for production of sealed sources. Sealed radioactive sources manufactured by BRIT are widely used in medicine, industry, and agriculture. The radioisotope production program at BARC involves several interrelated activities such as target fabrication, irradiation in a reactor or accelerator, transportation of irradiated target to the radioactive laboratory, radiochemical processing or encapsulation in the sealed source, quality control, and transportation to end users while complying with all the requirements for safety, security, and applicable regulations. Radioisotopes with activity ranging from 10^{-6} to 10^{3} TBq are supplied to end users through BRIT, DAE. Because of potentially hazardous properties of radioisotopes (sealed as well as unsealed), their use must be closely regulated so that protection of workers, public and the environment could be ensured through adherence to rules and regulations and good procedures.

Article 27 describes the interaction of ultra-high intensity (» tera-watt) laser beam with foil target, which produces electron bunches with the energy of several MeV and relatively high charge. Further these electrons, through secondary processes, produce MeV energy photons, protons, heavy ions and neutrons, which pose ionizing radiation hazard similar to a radioactive source and therefore require radiological safety. Thus, ultra-high intensity laser facility should comply with all the applicable safety and regulatory requirements similar to that for an ionizing radiation facility.

Since the consumer products, such as ICSD, GTLS/GTLD, fluorescent lamp starter, and incandescent gas mantle, involve very small amount of radioactive material in each of these devices, manufacturers/suppliers of these consumer products are only regulated by AERB; end users are not regulated (article 22). Various industrial scanning systems which are used for security and quality assurance purposes, end users are also regulated in addition to manufacturers/suppliers. Article 23 deals with the transport of radioactive material in India. The recently published (Rev. 1, 2016) code on "Safe Transport of Radioactive Material" prescribes the classification, design and test requirements for radioactive material and classification, design and test requirements for packagings, packages, and corresponding activity limits, etc. In the article the role of Emergency Control Room, DAE (ECR, DAE) in the event of any accident or emergency during transport of radioactive material is stated.

In India, Atomic Energy Act, 1962 is the primary legislation and Atomic Energy (Radiation Protection) Rules, 2004 are the regulatory rules promulgated under the Act (article 24). Chairman, AERB has been notified as competent authority to enforce these Rules. In the event of contravention of any of the provisions of these Rules by the licensee, the Rules have provisions for enforcement actions including suspension, modification, revocation or withdrawal of license issued under the Rules. For those enforcement actions calling for judiciary action and penalty, provisions of the Atomic Energy Act, 1962 are invoked. Article vividly describes all the aspects of enforcement actions as per the Act and the Rules. Article 25 describes the rules and regulations applicable for radioactive waste management, classification of waste, waste management practices in India and the role of regulatory bodies (BARC Safety Council (BSC) and AERB) for ensuring the safety of workers, the public and the environment. While BSC, constituted under the Atomic Energy Act, 1962, regulates the safety of BARC facilities, AERB regulates nuclear and radiological facilities in the public domain. Compliance with the relevant codes and guides of AERB is also followed in BARC facilities. Article 26 stresses the requirement to establish an overall nuclear security policy and a nuclear security system to prevent, detect and respond to theft, sabotage, unauthorized access, illegal transfer or other malicious acts involving nuclear and other radioactive substances. The factors which affect/influence nuclear safety culture and other security issues are also discussed.

Training in radiation protection and safety is an important means of promoting safety culture and enhancing the level of competence of personnel involved in radiation protection activities. In this context, RP and AD, BARC is conducting a number of radiation safety related training and certification programs in the field of medicine, industry and research, some of these training programs are conducted by BARC/AERB approved institutions. Syllabi of all these training courses have been approved by AERB. Articles 28 and 29 give details of the radiation safety related training courses conducted by RP and AD, BARC. These articles also give details regarding various training courses and the number of personnel certified by RP and AD till October 2016.

Article 18 provides details of requirements related to the infrastructure, regulatory consents to be obtained from AERB for setting up calibration laboratory of radiation monitoring instruments and qualified personnel required from safety and security considerations. It is stated that till date six such laboratories have been recognized by AERB. Article 31 describes uses of different types of radiation monitoring instruments in different applications of ionizing radiation in industry, medicine and research, covering uses of both dose and dose rate meters. The article also describes the procedure for tests, maintenance and calibration of monitoring instruments. However, detectors/instruments used for measuring pulsed radiation fields (e.g., pulsed X-ray beams) are not covered. Article 30 describes salient features of the e-LORA system which is a web-based information and communication technology application establishing direct communication channel between AERB and its stakeholders for exchange of information and communication transaction for delivering its regulatory services, as well as for achieving higher efficiency, reliability and transparency in dealings, while ensuring compliance with all the applicable regulatory requirements. The system is designed to automate the comprehensive business processes of radiological application of regulations targeted to a large number of facilities involved in the use of ionizing radiation.

There are some conspicuous formatting errors, typos and some other errors of minor nature in the texts of some of the articles, these are mentioned below:

i. At many places in the text, words have wrongly joined together, which affect the readability of the text.
ii. Legends of some of the figures are not legible.
iii. For some of the references cited in the articles, year of publication is neither given in the text nor in the list of references.
iv. In the article 10, title in the article is different than that given in the "Table of contents." In the article 32, there is something amiss in the title. In article 20, the order of the authors is different in the article than that given in the "Table of contents."

In conclusion, the editors and the contributors of different articles in the book have done a commendable task in bringing out this very useful compilation. Inclusion of ionizing radiation hazard of ultra-high intensity laser beams, in the books on radiation protection and safety, is probably a recent development. The book will be an asset to the readers, practitioners of radiation technology in particular, in terms of providing information on safety, security and regulatory aspects of radiation sources being used in various applications, as well as in strengthening the provisions for the same in different practices using ionizing radiation.

Bhuwan Chandra Bhatt
Ameya Co-operative Housing Society, Navi Mumbai, Maharashtra, India

Address for correspondence: Dr. Bhuwan Chandra Bhatt, B-6, Ameya Co-operative Housing Society, Sector 9-A, Vashi, Navi Mumbai, Maharashtra - 400 703, India.
E-mail: bcbhatt2003@yahoo.com

Access this article online

Quick Response Code:

Website: www.jmp.org.in

DOI: 10.4103/jmp.JMP_150_17

How to cite this article: Bhatt BC. Safety, security and regulations in handling radiation sources. J Med Phys 2018;43:66-8.

Dosimetric Studies in Image-Guided Adaptive Brachytherapy in Gynecological Cancers: A Journey to Successful Implementation

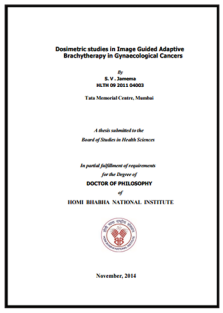
Dosimetric studies in Image Guided Adaptive Brachytherapy in Gynaecological Cancers

By

S. V. Jamema

HLTH 09 2011 04003

Tata Memorial Centre, Mumbai

A thesis submitted to the Board of Studies in Health Sciences

In partial fulfillment of requirements for the Degree of

DOCTOR OF PHILOSOPHY

of

HOMI BHABHA NATIONAL INSTITUTE

November, 2014

Author: Jamema Swamidas, Department of Medical Physcis, ACTREC, Tata Memorial Centre, Mumbai, India

Title: Dosimetric studies in Image-Guided Adaptive Brachytherapy in Gynecological Cancers: A journey to successful implementation

Pages: 203

Chief Guide: Prof. D.D. Deshpande, Department of Medical Physics, Tata Memorial Hospital, Mumbai, India

Date of award: Aug 2015

Thesis available at:: http://www.hbni.ac.in/students/dsp_ths.html?nm=hlth/HLTH09201104003.pdf

Implementation of Image-guided adaptive brachytherapy (IGABT) in India and other developing countries is a major challenge due to the resources, expertise and financial constraints. The basis of this thesis was to address various issues related to transition and successful implementation of IGABT in clinical routine.[1] Tata Memorial Hospital (TMH), Mumbai has a long tradition of being active in international collaborative research. Various fellowship programs for both clinicians and physicists have been the basis for successful collaborative research. Within many such projects, TMH is one of largest participating centers in the ongoing multi-centric collaborative international study on magnetic resonance (MR) imaging-guided brachytherapy in locally advanced cervical cancer. The study was designed to evaluate the dose-effect relationship on local control/morbidity of the tumor and toxicities of organs at risks (OAR) when MR images were used for cervical cancer brachytherapy. This thesis reiterates that, like any other advanced techniques, IGABT too requires systematic clinical implementation taking into account various technological, dosimetrical, and clinical issues. Systematic transition and appropriate implementation of IGABT for locally advanced cervical cancers may result in better outcome.

Specific Objectives of the Work Undertaken in this Thesis

1. To analyze the dosimetric difference between the standard loading, manually optimized and inverse optimized dosimetric plans using Inverse Planning Simulated Annealing (IPSA) and Hybrid Inverse Planning Optimization (HIPO) for various applications in IGABT in gynecological cancers for various types of applications:
   a. Intracavitary brachytherapy – Tandem and Ovoid and Tandem and Ring applicators
   b. Combined intracavitary and interstitial (IC + IS) Vienna applicator
   c. Interstitial template for gynecological applications – Martinez Universal Perennial Interstitial Template (MUPIT).
2. To analyze the inter application variation for
   a. Orthogonal Radiograph Image Based Brachytherapy
   b. MR image-based brachytherapy using rigid registration
   c. MR image-based brachytherapy using deformable image registration.

This thesis has been divided into five chapters; the first chapter describes about brachytherapy history, technological developments, and implantation techniques. The second chapter describes the conventional methods of treatment planning, its limitations and the newer developments such as MR-IGABT, the processes involved in the transition and its rationale. The third chapter describes the application of inverse planning for various gynecological applications. The fourth chapter addresses the uncertainties in IGABT, especially, organ motion related to inter-application variation in multi-fractionated brachytherapy in both radiograph-based and volumetric imaging-based brachytherapy environments. Finally, fifth chapter summarizes the important findings of this thesis and also discusses the future direction of research.

Inverse Planning Algorithms

The use of inverse planning algorithms in external beam therapy is an established procedure and widely accepted in the clinics, while in brachytherapy, its use is dependent on the specific application. Interstitial implants with many needles providing a high degree of freedom have a substantially different dose distribution compared to intracavitary implants. The technique has been successfully implemented in prostate brachytherapy, while its use in gynecological brachytherapy is unclear. There are certain issues with currently available inverse planning algorithms, especially for intracavitary brachytherapy, which need to be clearly understood for various clinical situations before clinical implementation. For example, the loading pattern resulting from these algorithms

has a large deviation from the conventional pattern which may not be clinically acceptable when substantially changing the spatial dose distributions and dose gradients within the target volumes, OARs and healthy tissues. The first part of this thesis addresses issues related to inverse planning for various clinical scenarios in IGABT using two commercially available inverse planning algorithms, IPSA and HIPO.[2-4] Dosimetric and clinical evidence have to be collected to obtain as much knowledge as possible which may be useful to integrate into future inverse planning tools.

The major findings of this section are summarized as follows. For intracavitary applications, inverse planning with HIPO and/or manual optimization offers improved plans in terms of OAR sparing while maintaining target coverage when compared to standard clinical plans. However, the average loading pattern was found to deviate from a traditional standard Fletcher loading. The tandem loading was decreased compared to the ovoids mainly due to high sigmoid dose. For combined intracavitary and interstitial applicators, inverse planning with IPSA resulted in plans with higher volumes of high dose regions. Without help structures, the treatment time in the needles was high resulting in highly modified spatial dose distributions, which was significantly reduced when help structures were included. For interstitial gynecological implants based on MUPIT template, IPSA resulted in significant sparing of normal tissues without compromising the target coverage as compared to geometrically and graphically optimized plans.

Uncertainties of Organ Motion

The second part of this thesis addresses the uncertainties in IGABT, which have not been adequately addressed so far.[5,6] It is essential to identify these uncertainties, their magnitude, and their impact on the overall uncertainty of dose delivery to the patient. This knowledge may provide correct dose assessment in IGABT, dose-effect modeling, and subsequently improved clinical outcome when using better planning aims with dose and volume constraints. In multi fractional brachytherapy, inter-application/fraction variations occur between different treatments/applicator insertions, both in terms of geometric and dosimetric parameters. These parameters have been identified as bladder and/or rectal filling, movements of sigmoid colon, and variation in vaginal packing among others. The current practice of determining the D_{2cm^3} cumulative dose to OARs during brachytherapy is based on what has previously been called "the worst-case scenario," which is the assumption that the D_{2cm^3} regions are located in the same anatomical part of the organ in each fraction. This assumption implies that the cumulated brachytherapy dose can be calculated by adding D_{2cm^3} values for each fraction. This approximation can lead to OAR dose overestimation when different organ parts are exposed to a high dose in different fractions. This question has been addressed systematically for orthogonal radiograph based dosimetry and IGABT using MR images with rigid and deformable image registration in this thesis.

The major findings of this section are as follows. For orthogonal radiograph image-based dosimetry, the inter application dose variation for the International Commission on Radiation Units and Measurement (ICRU) rectum and bladder was found to be 10%. ICRU rectal point was more stable as compared to the ICRU bladder point. Similarly, in MR image-based dosimetry using rigid registration, the inter application variation of the spatial location of D_{2cm^3} volumes was found to be most stable for rectum and to a large extent for the bladder. Minimal to moderate geometric changes in sigmoid are seen in the majority of the patients resulting in maximal variation in the spatial location of D_{2cm^3} volumes which may lead to over estimation of doses during the direct Dose Volume Histogram (DVH) addition. The results of dose accumulation using deformable image registration indicate that the current DIR algorithms are not robust enough to handle large deformations in rectum and bladder. For the sigmoid, it was, in general, not feasible to perform DIR due to significant deformations. DIR based dose accumulation based on different DIR algorithms resulted in large discrepancies on the accumulated dose for bladder and rectum. It is, therefore, recommended to use direct DVH addition for estimation of total dose, while DIR is not recommended for dose accumulation.

Summary and Conclusion

IGABT has evolved into a high-technology modality of radiotherapy incorporating modern imaging, advanced brachytherapy applications using newer applicators and advanced computational algorithms. Various processes involved in the implementation of IGABT have been established while some concerns about uncertainties related to imaging, treatment planning, dose delivery, and anatomical variations have been raised. These are current areas of research by various groups. This thesis is a hallmark for addressing few of the issues enumerated above and has provided some insight into the IGABT processes. The significant findings of the thesis are as follows: (1) Manual dose optimization significantly improves the dose as compared to standard point A prescription. (2) Application of inverse dose optimization has major pitfalls; hence, inverse planning is not recommended for IGABT for cervical cancers. (3) Dose accumulation across fractions can be done with a good precision for bladder and rectum by direct DVH additions. However, the sigmoid dose may be overestimated with direct DVH addition, and special care should be taken during plan evaluation depending on imaging findings for sigmoid. Image-guided adaptive brachytherapy is a high technology modality within radiotherapy which can be performed with the promising outcome and economical gain in India.[7-10]

Dissemination of this promising technique should be addressed systematically for a smooth transition from conventional to IGABT approach in cervical cancer. This can be achieved through continuing teaching and training

efforts through national/regional and hospital based hands-on workshops as well as teaching courses in collaboration with various national (AMPI/AROI/IBS) and International societies (ESTRO). This thesis supports the implementation of high-quality treatment planning and dose reporting for IGABT in cervical cancer.

References

1. Available from: http://www.hbni.ac.in/students/dsp_ths.html?nm=hlth/HLTH09201104003.pdf. [Last accessed on 2018 Feb 11].
2. Jamema SV, Kirisits C, Mahantshetty U, Trnkova P, Deshpande DD, Shrivastava SK, *et al.* Comparison of DVH parameters and loading patterns of standard loading, manual and inverse optimization for intracavitary brachytherapy on a subset of tandem/ovoid cases. Radiother Oncol 2010;97:501-6.
3. Jamema SV, Sharma S, Mahantshetty U, Engineer R, Shrivastava SK, Deshpande DD, *et al.* Comparison of IPSA with dose-point optimization and manual optimization for interstitial template brachytherapy for gynecologic cancers. Brachytherapy 2011;10:306-12.
4. Jamema SV, Mahantshetty U, Deshpande D, Sharma S, Shrivastava S. Does help structures play a role in reducing the variation of dwell time in IPSA planning for gynecological brachytherapy application? J Contemp Brachytherapy 2011;3:142-9.
5. Jamema SV, Mahantshetty U, Andersen E, Noe KØ, Sørensen TS, Kallehauge JF, *et al.* Uncertainties of deformable image registration for dose accumulation of high-dose regions in bladder and rectum in locally advanced cervical cancer. Brachytherapy 2015;14:953-62.
6. Jamema SV, Mahantshetty U, Tanderup K, Malvankar D, Sharma S, Engineer R, *et al.* Inter-application variation of dose and spatial location of D(2cm(3)) volumes of OARs during MR image based cervix brachytherapy. Radiother Oncol 2013;107:58-62.
7. Mahantshetty U, Swamidas J, Shrivastava SK, Institutional experiences, practical approaches to image guided brachytherapy. In: Viswanathan AN, Kirisits C, Erickson B, Potter R, editors. Gynaecologic Radiation Therapy, Novel Approaches to Image-Guidance and Management. India: Tata Memorial Hospital Mumbai, Springer; 2010. p. 207-15.
8. Swamidas JV, Kirisits C. IMRT, IGRT, and other high technology becomes standard in external beam radiotherapy: But is image-guided brachytherapy for cervical cancer too expensive? J Med Phys 2015;40:1-4.
9. Mahantshetty U, Krishnatry R, Hande V, Jamima S, Gadi Y, Engineer R, *et al*. Magnetic resonance image guided adaptive brachytherapy in locally advanced cervical cancer: an experience from a tertiary cancer center in a low and middle income countries setting. Int J Radiat Oncol Biol Phys 2017;99:608-17.
10. Chakraborty S, Mahantshetty U, Chopra S, Lewis S, Hande V, Gudi S, *et al.* Income generated by women treated with magnetic resonance imaging-based brachytherapy: A simulation study evaluating the macroeconomic benefits of implementing a high-end technology in a public sector healthcare setting. Brachytherapy 2017;16:981-7.

Christian Kirisits, Umesh Mahantshetty[1], Kari Tanderup[2]

Department of Radiation Oncology, Medical University of Vienna, Vienna, Austria, [1]Department of Radiation Oncology, Tata Memorial Hospital, Mumbai, Maharashtra, India, [2]Department of Oncology, Aarhus University Hospital, Aarhus, Denmark

Address for correspondence: Dr. Christian Kirisits, Comprehensive Cancer Center, Department of Radiotherapy, Medical University of Vienna, Vienna, Austria.
E-mail: christian.kirisits@meduniwien.ac.at

Access this article online	
Quick Response Code:	Website: www.jmp.org.in
	DOI: 10.4103/jmp.JMP_146_17

How to cite this article: Kirisits C, Mahantshetty U, Tanderup K. Dosimetric studies in image-guided adaptive brachytherapy in gynecological cancers: A journey to successful implementation. J Med Phys 2018;43:69-71.

Dosimetric Evaluation and Optimization of Fractionated Stereotactic Radio-Surgery

Author: Raj Kishor Bisht, Department of Neuro-Surgery, AIIMS, New Delhi
Title: Dosimetric evaluation and optimization of fractionated stereotactic radio-surgery
Chief Guide: Prof. S. S. Kale, Department of Neuro-Surgery, AIIMS, New Delhi
Date of award: 29th July 2017

In recent years, stereotactic radiosurgery (SRS) has evolved as the major radiotherapy modality for brain tumors and requires very precise radiation dose delivery using state of the art treatment planning systems. SRS can be delivered by Gamma Knife, CyberKnife, or XKnife; however, Gamma Knife offers an efficient treatment to a number of neurological disorders in the brain, with relatively lower radiation dose fractions, have a radiobiological advantage on tumor and/or adjacent normal structures. In this study, RK Bisht under the guidance of neurosurgeon, medical physicist, and radiation oncologist has investigated and evaluated the accuracy of the system with the help of newly developed multipurpose human shaped phantom and physics support for the patients treated with custom-made Extend System (ES) on Gamma Knife Perfexion for various clinical indications.

The work is planned meticulously, executed accurately, the results obtained are analyzed wisely and presented in very elaborate and in a well-structured manner in the present thesis. I enjoyed the reading the thesis as the language used is simple, and the matter is discussed very extensively with relevant references. The thesis consists of eight main chapters.

The first chapter deals with historical development and physics approach of stereotactic irradiation using various stereotactic radiosurgical machines. Further, the Gamma Knife methodology for single and multiple fractions with ES is at the core of this thesis segment. Chapter 2 is devoted to review of literature, highlighting the background clinical and experimental work done so far using ES of Gamma Knife technology. The study believes that the single fraction SRS of small tumor volumes with cumulative higher radiation dose may carry additional risks of radiation damage to close proximal critical structures such as the brain stem, facial nerves or the optic nerve in the brain. In these cases, hypofractionated radiosurgery delivered in 3–5 fractions over consecutive days is an alternative treatment option. With appropriate references cited in the present study, it is understood that the multiple fraction SRS has a radiobiological advantage of effectively killing of distinguished rapidly dividing cells, whereas the single fraction radiosurgery do not explain the mitotic activity or inherent radiosensitivity. The repeated session of relatively lower dose fractions in hypofractions regimen significantly lowers the dose to adjacent normal tissue.

Chapter 3 of the thesis is dedicated to the description of research materials, equipment and methods followed by the candidate for this work. The use and preparation of individual ES is adequately described with associated tools such as frame, mouthpiece, patient control unit, the extend indicator, digital measurement probe, and repositioning tool in this chapter. Stereotactic imaging was acquired using latest X-ray computed tomography machine and the DICOM images were transferred through PACS system to the treatment planning system for preparation of precise treatment plan. Consistency in repeated reference positioning is an important factor during multi-fraction SRS which is described in an immobilization methodology section of this chapter.

Chapter 4 describes the initial study on evaluation of fractionated SRS with ES of Gamma Knife technology. The treatment preparation and clinical outcome of the patient treated with various clinical indications are discussed in this chapter. With the suggested approach on patient positioning technique, reference position recording, and treatment planning showed an improved clinical outcome. The study includes positional reproducibility check and dosimetric evaluation of ten patients treated with ES. In this study, RK Bisht has shown the improved planning indices, reduced neighboring structure doses and finally commendable clinical outcome demonstrating the efficacy of ES for fractionated SRS.

The most remarkable achievement of this work is the design and development of patient simulating phantom with capability for dosimetric verification of Gamma Knife ES based fractionated SRS. The candidate has meticulously and articulately fabricated a human upper body shaped phantom with thorax part to simulate fractionated SRS in a real patient. The phantom has been designed in such a way that it may also be used as a quality assurance tool for imaging modalities and verification mold with futuristic equipment and devices in addition to the traditional treatment verification gadgets such as ion chamber, thermoluminescent dosimeters/optically stimulated luminescent (TLDs/OSLs), and films. A patient treatment plan with fractionated regimen was delivered and identical fractions were compared using EBT3 films and in-house MATLAB codes. Gamma index analysis across fractions exhibited close agreement between LGP and film measured dose with >90% (max 93%) pixel pass rate at 1mm of spatial

and 1% of dosimetric tolerances. The study finally concludes that the fractionated SRS with ES of Gamma Knife provided substantial treatment accuracy and the designed patient simulating phantom was highly versatile for the dosimetric verification of hypofractionated regimen.[1-3]

The chapter 6 of the thesis is focused on statistical optimization of SRS treatment. The purpose of this study was to estimate technical treatment accuracy in fractionated SRS using ES of Gamma Knife. The study concluded that the quality assurance of tools such as reposition check tool (RCT), digital probe, and vacuum supported patient head cushion integrity is essential for reliable patient positioning using ES. The study predicts the technical treatment uncertainty in the clinic, whereas combining the results with explicit medical uncertainties such as having knowledge of neurological abnormality and radiation response will be in the scope of future research for the determination of the treatment accuracy.

The work presented in the form of this thesis covers various practical approaches in the routine clinic to improvise the quality of highly conformal SRS. A newly designed head-neck phantom is a "comprehensive treatment setup simulation model" for SRS. The phantom is not just limited to performing film dosimetry, but the provision of placing various other dosimetric devices such as ion chamber, TLD/OSLs, chemical gels, and online dosimetry systems makes it an ideal dosimetric tool for treatment verification. The superior part of this phantom was designed to establish a link between Hounsfield unit and physical parameter of materials with varied density. The imaging information of this segment with various known/unknown materials with different physical density and/or dosimetric tools will be useful in modeling the "planning documents" for various TPS computation or model/factor based algorithms. In routine fractionated SRS treatments, the determination of positional shift with radial difference vector calculations is the only available "mathematical quality parameter" to quantify the treatment precision. In this study, the procedural uncertainty of the treatment was evaluated at calibration, imaging, and measurement stage. An "absence of medical uncertainties" in experiments, depends on imaging resolution (AAPM report no 54) and was believed to be within clinical tolerances.

In conclusion, the present study evaluates similar treatment regimen with comparable clinical results, however, a modified dose regimen like a dose per fraction, number of fractions and cumulative dose might be a clinical advancement in future research. Tangible future studies of the radiobiological effect in tumor volume and/or surrounding structures following routine or improvised hypofractionated regimen will be more realistic in determining the best possible clinical outcome. The research material and sequential methods, chosen in this thesis justify a procedural verification of fractionated treatment with ES. A statistical study with newly designed head-and-neck phantom certainly leads a mathematical optimization on the estimation of optimal uncertainty in routine fractionated treatment. Although the phantom was designed to investigate fractionated SRS procedures with ES of Gamma Knife, however, the model certainly helps in standardizing other immobilization techniques (using a thermoplastic mask, skeleton marker) and popular radiotherapy treatments.

Arun Chougule

Department of Radiological Physics, S.M.S. Medical College and Hospitals, Jaipur, Rajasthan, India

Address for correspondence: Prof. Arun Chougule, Department of Radiological Physics, S.M.S. Medical College and Hospitals, Jaipur, Rajasthan, India.
E-mail: arunchougule11@gmail.com

References

1. Natanasabapathi G, Bisht RK. Verification of gamma knife extend system based fractionated treatment planning using EBT2 film. Med Phys 2013;40:122104.
2. Bisht RK, Kale SS, Gopishankar N, Kumar P, Singh MJ, Agarwal D, *et al.* Preliminary experience of fractionated stereotactic radiosurgery with extend system of Gamma Knife. Int J Cancer Ther Oncol 2016;4:1414.
3. Bisht RK, Kale SS, Gopishankar N, Singh MJ, Agarwal D, Garg A, *et al*. Verification of Gamma Knife based fractionated radiosurgery with newly developed head-thorax phantom. Radiat Meas 2016;91:65-74.

Access this article online

Quick Response Code:

Website: www.jmp.org.in

DOI: 10.4103/jmp.JMP_145_17

How to cite this article: Chougule A. Dosimetric evaluation and optimization of fractionated stereotactic radio-surgery. J Med Phys 2018;43:72-3.

EXPLORER: A Full-Body Positron Emission Tomography Scanner in Making

Researchers at University of California, Davis, are working to build a 2-m long total body positron emission tomography (PET) scanner which could be the first full-body scanner in making.

The project is under development by a multi-institutional EXPLORER consortium and likely to provide a whole-body fast PET scanner which may scan the whole body in single breath-hold with about 30–40 times more sensitivity than the current PET scanner despite giving very low dose of 10 MBq (which is about 50 times lower dose than the current scanning system imparts). The device may have 560,000 scintillator crystals and 90 billion lines of response which is about 100 times more than the current technology. In place of sinogram-based reconstruction, EXPLORER uses list-mode data processing for image construction. The scientists have tried to reduce the parallax effect between crystal pair in rings in the long axial field of view (FOV). The first prototype of the EXPLORER is expected to be available next year.

(Taken from www.medicalphysicsweb.org dated March 7, 2017)

Carbon Ion Dosimetry Accuracy: The Heidelberg Ion Beam Therapy Centre on Work

Carbon ion therapy is a treatment modality which has certain advantages over conventional radiotherapy, especially for radiation-resistant and deep-seated tumors. Despite being in existence for the last 20 years or so, carbon ion beam dosimetry needed improvement. The researchers from HIT and Physikalisch-Technische Bundesanstalt used water calorimeter for the measurement of absorbed dose from the carbon ion beam to quantify the accuracy (or uncertainty) in the dosimetry of the carbon ion beam at the entrance channel by scanning a 6 cm × 6 cm radiation field of 429 MeV per nucleon carbon ion. This led to the experimental measurement of beam quality-dependent K_Q factor of the chamber. Until now, this factor was calculated. The researchers could achieve a relative standard measurement uncertainty of 0.8% which is about three-fold reduction in uncertainty in the result from the value arrived at by the calculation method.

(Taken from www.ioppublishing.org dated February 18, 2017)

AAPM TG 158: Measurement and Calculation of Doses Outside the Treated Volume from External Beam Radiation Therapy

The introduction of advanced techniques and technology in radiotherapy has greatly improved our ability to deliver highly conformal tumor doses while minimizing the dose to adjacent organs at risk. Despite these tremendous improvements, there remains a general concern about doses to normal tissues that are not the target of the radiation treatment; any "nontarget" radiation should be minimized as it offers no therapeutic benefit. As patients live longer after treatment, there is increased opportunity for late effects including second cancers and cardiac toxicity to manifest. Complicating the management of these issues, there are unique challenges with measuring, calculating, reducing, and reporting nontarget doses that many medical physicists may have limited experience with. Treatment Planning Systems (TPS) become dramatically inaccurate outside the treatment field, necessitating a measurement or some other means of assessing the dose. However, measurements are challenging because outside the treatment field, the radiation energy spectrum, dose rate, and general shape of the dose distribution (particularly the percent depth dose) are very different and often require special consideration. Neutron dosimetry is also particularly challenging, and common errors in methodology can easily manifest as errors of several orders of magnitude. Task Group 158 was, therefore, formed to provide guidance for physicists in terms of assessing and managing nontarget doses. In particular, the report: (a) highlights the major concerns with nontarget radiation; (b) provides a rough estimate of doses associated with different treatment approaches in clinical practice; (c) discusses the uses of dosimeters for measuring photon, electron, and neutron doses; (d) discusses the use of calculation techniques for dosimetric evaluations; (e) highlights techniques that may be considered for reducing nontarget doses; (f) discusses dose reporting; and (g) makes recommendations for both clinical and research practice.

(The above-written abstract and full-length report has been published on August 20, 2017, in Medical Physics, Vol. 44, e391-e429, DOI: 10.1002/mp.12462).

TreatSafely Foundation Shares Practical Learning Videos and Documents

The TreatSafely Foundation runs a website, https://i.treatsafely.org, which provides free practical learning videos apt for radiation therapy professionals. It is a peer-to-peer learning site and it means that videos are shared by the professionals working in the clinical scenario and about the practical stuff cropping up in our daily life. The site has a vast arrays of topics. For example, a video entitled "Setting the isocenter-Breast field-in-field" by Beth Bottani occupies the label of most-viewed video. "Intro to Quality and Safety-Overview" by Derek Brown is another interesting video. Some newer videos have titles "IMRT Planning in Eclipse" and "Plan Analysis in Eclipse." The site also has downloadable documents and quality assurance (QA)/Safety series. "Monthly TPS QA" is the most-downloaded document at present, while "Introduction to quality and safety" is the most-viewed QA/Safety series.

Comparison of Computed Tomography Scanners among Various Models of Different Vendors

Imaging Technology News has launched an online chart for comparison of various models of computed tomography (CT) scanners across the vendors in terms of technology, specifications, and other information. According to the site, the chart is sponsored by Philips. The site provides facility for the customized search as well. It lists 43 models of CT scanners spread over six manufacturers and includes even mobile CT scanners. The user has to register with the site before getting the help in comparison of the CT scanners. One may check the following site: https://www.itnonline.com/content/computed-tomography-systems?eid=402709264andbid=1945973.

Guidance on Three-Dimensional Printing of Medical Devices from the Food and Drug Administration

The US Food and Drug Administration (FDA) has issued a new set of guidelines for creating medical products using three-dimensional (3D) printers. The FDA enumerates its recommendation regarding design of the devices, their testing, and the requirements for the quality system. 3D printing has recently caught the attention of the researchers and has great potential for the wide range of clinical applications such as creating accurate replicas of complex anatomical structures, facilitating surgery simulations for addressing hearing loss, stroke clot, and hip disorders. Such policy framework from the FDA would help the manufacturers to bring 3D-printed models to the market more efficiently. The FDA conducted a joint workshop with the RSNA's 3D Printing Special Interest Group and came up with the recommendations which have three topics. The first one is design and manufacturing process which covers the technical aspects of 3D printing process such as image quality, resolution, image processing algorithm, and clarity of anatomic landmark during acquiring imaging data which helps in creating patient-specific models. The second topic is device testing which deals with testing, characterization, measurement, biocompatibility, sterilization, etc., of the 3D-printed devices. Labeling is the third part which looks after the patient identifier, device use, and final design and survey of the patient for any bodily changes before applying the device. Details are available at https://www.fda.gov/MedicalDevices/ProductsandMedicalProcedures/3DPrintingofMedicalDevices/default.htm.

(Based on the publication at AuntMinnie.com)

The US Food and Drug Administration Approves First 7 Tesla Magnetic Resonance Imaging

The Magnetom Terra from Siemens Healthineers has become the first 7 tesla magnetic resonance imaging (MRI) machine approved by the US FDA for its clinical use. So far, 3T MRI is used in clinical practice. A report emanating from the US FDA Centre for Devices and Radiological Health says that increasing magnetic field strength more than double will add to the image quality. The US FDA undertook 510(k) premarket clearance pathway for clearing Magnetom Terra. It also reviewed the safety aspect of its radiofrequency subsystem using simulation, modeling, and experimental measurements. Such high magnetic strength MRI is indicated for the patient who weighs more than 66 pounds and is limited to imaging of extremities. Siemens has informed that such machine has good potential for neurological and musculoskeletal imaging with finer details not available earlier at 3T machine. Detail is available at https://www.itnonline.com/content/fda-clears-first-7t-mri-system-magnetom-terra?eid=402307001andbid=1900080

ICRP Publication 135: Diagnostic Reference Level in Medical Imaging

ICRP Publication 135 details comprehensively about the diagnostic reference level (DRL) in medical imaging. It addresses the issues connected with definition, determination of DRL values, interval for re-evaluation of DRL values, methods to be adopted, application of DRL concept to newer modalities, etc. The report has been authored by E Vano, DL Miller, CJ Martin, MM Rehani, K Kang, M Rosenstein, P Ortiz-Lopez, S Mattsson, R Padovani, and A Rogers and has been published in Ann. ICRP 46(1), 2017.

Calendar of Events

- Hands-on Fluoroscopy Testing Workshop, February 24–25, 2018, Wichita, Kansas, US. For details: https://www.mtmi.net/course/hands-fluoroscopy-testing-workshop
- European Artificial Intelligence Innovation Summit, London, UK, March 5–6, 2018. Details are available at http://exlevents. com/euro-artificial-intelligence
- Webinar on Diagnostic and Nuclear Medicine Radiation Shielding. Three-part webinar of 1.5 h each during March 6–8, 2018. For details, visit https://www.mtmi.net/webinar/diagnostic-and-nuclear-medicine-radiation-shielding
- The 3rd International Conference on Medical Physics in Radiation Oncology and Imaging, Dhaka, Bangladesh, March 10–12, 2018. Details are available at http://www.bmpsbd-icmproi.org
- National Symposium on High Precision Radiation Oncology, AIIMS, New Delhi, India, March 24–25, 2018. Details are available at http://www.ampi.org.in/?p=3322
- Society of Breast Imaging/American College of Radiology Breast Imaging Symposium 2018, The Cosmopolitan of Las Vegas, Las Vegas, Nevada, US, April 12–15, 2018. Details are available at https://www.sbionline.org/EDUCATION/CurrentandFutureCoursesMeetings/2018SBIACRBreastImagingSymposium.aspx

- World Congress on Medical Physics and Biomedical Engineering, Prague, Czech Republic, June 3–8, 2018. Details are available at http://www.iupesm2018.org
- The 39th Annual National Conference of Association of Medical Physicists of India, Chennai, Tamil Nadu, India, November 2–4, 2018. Details are available at http://ampicon2018.com.

Pratik Kumar

Professor, Medical Physics Unit, IRCH. AIIMS, New Delhi, India

Address for correspondence: Dr. Pratik Kumar, Medical Physics Unit, IRCH, AIIMS, New Delhi - 110 029, India.
E-mail: drpratikkumar@gmail.com

Access this article online

Quick Response Code:

Website: www.jmp.org.in

DOI: 10.4103/jmp.JMP_13_18

How to cite this article: Kumar P. News. J Med Phys 2018;43:74-6.

Reviewers List, 2017

We gratefully acknowledge the services of following experts who have given their valuable time and cooperation in reviewing the manuscripts

A Shukla K, *India*
Ajay Srivastava Kumar, *India*
Ali Neshasteh-riz, *Iran*
Ambika Sahai Pradhan, *India*
Archana Gautam, *USA*
Arun Chougule, *India*
Ashok Bakshi, *India*
B Satish Rao, *India*
Ben-Hua Xu China
Bhola Subhalakshmi, *India*
Bhudatt Paliwal R, *USA*
Bora Tash Turkey
BS Rao, *India*
Challapalli Srinivas, *India*
Chandra Joshi Prakash, *Canada*
D Datta, *India*
D Deshpande D, *India*
David Eaton, *United_Kingdom*
David J Schlesinger, *USA*
Debashis Sen, *India*
G.C. Jagetia, *India*
Ganesan Ramanathan, *India*
Ganesh Narayanasamy, *USA*
Golam Zakaria Abu, *Germany*
Gopalkrishna Kurup, *India*
Harold DSouza, *United_Kingdom*
Hema Vaithianathan, *Australia*
Huijun Xu, *USA*
Indra Das J, *USA*
Ivana Zanella da Silva daSilva, *Brazil*
J Velmurugan, *India*
jamema swamidas, *India*
James CL Chow, *Canada*
Jessica Bahari Kashani, *USA*
John Schreiner, *Canada*
K J MariaDas, *India*
K Ram Das, *Australia*
K.M. Ganesh, *India*
K.N. Govindrajan, *India*
Kai Niu, *USA*
Kamal el Ghamrawy, *Egypt*
Katsuyuki Karasawa, *Japan*
Kevin Jordan, *Canada*
kirisits christian Austria
Komanduri Ayyangar, *USA*
L Nithya, *India*
Lalit M Aggarwal, *India*
Lisa Karam, *USA*
M Ravi Kumar, *India*
Ma Jiasen, *USA*
Manoj Semwal, *India*
Maria Mania Aspradakis, *Switzerland*
Marimuthu Sankaralingam, *United_Kingdom*
Masaru Wakatsuk, *Japan*
Moses Arunsingh, *United_Kingdom*
Murugan Appasamy, *India*
Mutian Zhang China
N Gopishankar, *India*
Nagesh N Bhat, *India*
Oinam Arun Singh, *India*
P K Dash Sharma, *India*
P Venkatachalam, *India*
Palani Selvam, *India*
Panayiotis Mavroidis, *USA*
Pankaj Tandon, *India*
Paul Ravindran B, *India*
Pratik Kumar, *India*
Pushkar T Desai, *USA*
Raghavendra Holla, *India*
Raghuram K Nair, *India*
Rajesh Kinikar, *India*
rajesh kumar, *India*
Rakesh Joshi, *Australia*
Ramamoorthy Ravichandran, *India*
Ramesh Desai, *India*
Ramkrushn S Vishwakarma, *India*
Ravi Teja Seethamraju, *USA*
Rima Pathak, *India*
Rituraj Upreti Rituraj Upreti, *India*
Roshan Livingstone Samuel, *India*
S Mahalakshmi, *India*
S Sathiyan, *India*
Salahuddin Ahmad, *USA*
Sekaran Sureka, *India*
Shaleen Kumar, *India*
Shanta Appukutan, *India*
Shokouhozaman Soleymanifard, *Iran*
SK Shrivastava, *India*
Slav Yartsev, *Canada*
Sreedevi Balakrishnan, *India*
Sriram Padmanaban, *United_Kingdom*
Stephen McMahon, *United_Kingdom*
Subhash Kheruka, *India*
Sudesh Deshpande, *India*
Surendra Rustgi, *USA*
Suresh Chaudhari, *India*
T. S. Kehwar, *USA*
Tabassum Wadasadawala, *India*
Tejpal Gupta, *India*
Tim Olding, *Canada*
Tomas Kron, *Australia*
Umakanta Tripathy, *India*
V Sathiyanarayanan, *India*
Vandana Srivastava V, *India*
YB Cihan Turkey
Yujie Chi, *USA*

The fastest and easiest way to keep track of your QA data

Track-it

The New QA Data Management Solution by PTW

Tracking. Trending. Reporting.
On one single platform.

Anytime. Anywhere. Your way.

PTW DOSIMETRY INDIA PVT.LTD
ACE Towers, 2nd Floor, 73/75, Dr. Radhakrishnan Road, Mylapore, Chennai - 600 004.
Ph : 044 - 4207 9999 Telefax : 044 - 4207 2299 E-mail : info@ptw-india.in Web : www.ptw-india.in

PTW
Knowing what responsibility means

Klarity
BETTER PRODUCTS FOR BETTER CARE

MEDITRONIX

PATIENT POSITIONING

KLARITY AIO SYSTEM

- Versatile system for whole body immobilization.
- Full Carbon Fiber structure. No use of high attenuation polyurethane cushion in treatment area.

Arm Support

Thorax & Pelvic Base Plate

Klarity AIO Base Plate

KLARITY SBRT SYSTEM

FRAMELESS SRS/SRT TREATMENT SOLUTION

Optek™ Overlay Board

Klarity AccuCushion™

Shell Moulds

Patient with Shell Mould

Radimage HEALTHCARE INDIA Pvt. Ltd.

Radimage Healthcare India Pvt. Ltd.
(An ISO 9001 : 2015 Certified Company)
G-236, Sector-63, Noida - 201 303 (INDIA)
Tel.: +91 120 4263270 Fax: +91 120 2406097
www.radimageindia.com; radimagehealthcare@gmail.com
(A Meditronix Corporation Group Company)

RADIATION ONCOLOGY

MEDITRONIX

PRODUCTS & SERVICES

Having representing the best technologies for over 35 years, we have understood the treatment needs which changes with the newer challenges everyday. Today, we represent world's premium brands for different modalities of cancer diagnosis and treatment.

Radimage Dosimeter

A2J Moving & Fixed Lasers

Precisis Cobalt MLC

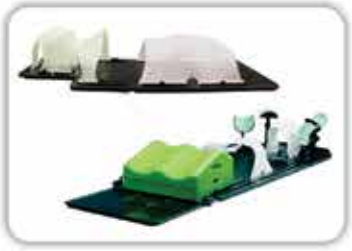

Klarity AIO Baseplate

Klarity SBRT System

Klarity Thermoplastics

Ludlum 9DP Pressurised
Ion Chamber Survey Meter

Rexon TLD Reader

Par Scientific Block Cutter

CIRS Dynamic Thorax Phantom

Quartz QA Kit

AERB Recognized Calibration Facility
For Radiation Measuring Instruments

Radimage HEALTHCARE INDIA Pvt. Ltd.

Radimage Healthcare India Pvt. Ltd.

(An ISO 9001 : 2015 Certified Company)

G-236, Sector-63, Noida - 201 303 (INDIA)

Tel.: +91 120 4263270 Fax: +91 120 2406097

www.radimageindia.com; radimagehealthcare@gmail.com

(A Meditronix Corporation Group Company)

Klarity
BETTER PRODUCTS FOR BETTER CARE

MEDITRONIX

THERMOPLASTIC SHEETS

Klarity Masks are a new higher standard for thermoplastic immobilization. Klarity masks are non-stick, stronger, with lower shrinkage than all other standard masks. IMRT AccuPerf™ pattern offer enhanced perforation designes for higher fixation strength, minimal bolus effect and better patient comfort. Klarity offer masks for S-Type, U-Frame, O-Type, E-Type, V-Type, P-Type, Stereotactic, BoS and various frame types.

RD105-2022N

RD206-2022N

RDLG-207-24AF

Klarity® O-Type Mask (Orfit Design)

Klarity O-Type masks fit all standard O-Type baseplates (Orfit-Type) from Klarity, Orfit (Standard and AIO) and others. Klarity O-Type masks feature exclusive EZ-Grip™ clamps and are available in standard white and Klarity Green™.

Klarity® S-Type Mask (CIVCO Design)

Klarity S-type masks fit all standard S-Type baseplates from Klarity, CIVCO and others. Klarity S-Type masks are available in standard white and Klarity Green™. Both white and green masks offer strong, rigid immobilization and easy moldability.

RDLG-207-24AF

R461-8STF

R-PRTS-2415

R-PRT3-2415

R-PRTL-2415

Klarity® P-Type Mask (Macromedics Design)

Klarity P-Type masks fit all standard P-Type baseplates (Posifix-Type) from Klarity, Civco and others, and offer the highest quality of thermoplastic masks.

R-406-1

Klarity® 'Brainlab Mask' (Stereotactic Design)

- Two-part masking system
- Economical stereotactic mask option
- Non-invasive and flexible immobilization

R-408-1

Klarity® E-Type Mask (Elekta)

RLG-ESH3-2412CN

RLG-ELS-2412CN

Klarity Green™ masks for Elekta's Leksell Gamma Knife® Icon™ System, Fraxion™, and HeadSTEP™

Proton therapy BoS Masks

RGBSH-2436

RGBLS-2436

Radimage HEALTHCARE INDIA Pvt. Ltd.

Radimage Healthcare India Pvt. Ltd.
(An ISO 9001 : 2015 Certified Company)
G-236, Sector-63, Noida - 201 303 (INDIA)
Tel.: +91 120 4263270 Fax: +91 120 2406097
www.radimageindia.com; radimagehealthcare@gmail.com
(A Meditronix Corporation Group Company)

AERB Recognised Calibration Laboratory

- **AERB recognised calibration laboratory vide letter no. AERB/RSD/ Recog-Cal04/2014/7963 dt. 12.8.2014**
- **Facility to calibrate any brand or type of Radiation Survey Meter, Area (Zone) Monitor and Pocket Dosimeters. Either analogue or digital**
- **Pick-up and drop through courier can be arranged, if the need arise**
- **Routine turn around calibration time is 5-6 days**
- **Instrument should always be in working condition, to avoid delays**
- **Calibration validity two years**

Radimage Healthcare India Pvt. Ltd.

G-236, Sector-63, Noida - 201 303, India

Tel.: +91 120 2406096, 4263270 | Fax: +91 120 2406097

radimagehealthcare@gmail.com | www.radimageindia.com

(A MEDITRONIX CORPORATION GROUP COMPANY)

iba-dosimetry.com

myQA HALO™ solution at the University of Pennsylvania during validation & acceptance of the Varian Halcyon™ and its TPS data, Sept. 2017.

myQA HALO™

Integrated Quality Assurance for Varian Halcyon™

DOSIMETRY

PROTECT +
ENHANCE +
SAVE LIVES

ROSALINA INSTRUMENTS

ROSALINA INSTRUMENTS
127 BUSSA UDYOG BHAVAN
T.J. ROAD
SEWRI, MUMBAI 400015 INDIA
+919820627499
www.ROSALINA.in

MR3T LASER SYSTEMS IN RT

PRECISE PATIENT ALIGNMENT

REMOTE CONTROLLED LASER ADJUSTMENT

DORADOnova MR3T
ESSENTIAL AND COMFORTABLE

APOLLO MR3T
ESSENTIAL AND ELEMENTARY

LAP LASER

www.LAP-LASER.com

Efficiency, accuracy and clinical relevance at the same time

Cornerstones of ScandiDos

INSTANTLY ANALYZE AND APPROVE PLANS	The analysis starts with the Dose - Picture.
QUICKLY AND EASILY FIND THE CAUSE OF DEVIATIONS	If a deviation is noted, the user can easily zoom in on the details.
VERIFY THE DOSE DELIVERY WITHOUT COMPROMISES IN 3D	Reliable QA must be highly accurate and comprehensive. Delta 4®PT measures the dose with high density in the high gradient region with the resolution of 50nGy.
ANALYZE THE CLINICAL RELEVANCE OF A DEVIATION	The level of importance in discrepancy between delivered and planned dose is determined using patient anatomy (e.g. target and risk structures) to gauge the clinical relevance.

THE DIFFERENCE CLEAR

ROSALINA INSTRUMENTS

Registered with Registrar of Newspapers in India
Vide RNI No. MAHENG/2012/44833, Rs 20 for AMPI Members

Editor Dr. A. S. Pradhan. Printed and published by Wolters Kluwer India Private Limited on behalf of Association of Medical Physicists of India, Mumbai and printed at Dhote Offset Technokrafts Pvt. Ltd., Jogeshwari (E), Mumbai - 400 060, India, and published at A-202, 2nd Floor, The Qube, C.T.S. No.1498A/2 Village Marol, Andheri, Mumbai, India